CHEMIA

Studia Universitatis Babes-Bolyai Chemia has been selected for coverage in Thomson Reuters products and custom information services. Beginning with V. 53 (1) 2008, this publication will be indexed and abstracted in the following:

- Science Citation Index Expanded (also known as SciSearch®)
- Chemistry Citation Index®
- Journal Citation Reports/Science Edition

CUPRINS – CONTENT – SOMMAIRE – INHALT

IN MEMORIAM

Profesor Doctor Docent LIVIU ONICIU

Profesor Liviu Oniciu was born on 11th of February 1927 in Cluj. He got an excellent high school education in both, literary and scientific directions, at the Pedagogical Seminar of the Cluj University (1946). He graduated the Faculty of Science of "Victor Babeş" University in Cluj (1950), becoming an assistant at the Chair of Physical Chemistry of this faculty. He retired in 1997, at the age of 70, but he continued to work as a consulting Professor, until the last days of his life (27th of November 1999).

In his remarkable teaching period, he was: lecturer (1961), associated professor (1965), full professor (1970), Dean of the Faculty of Chemistry (11 years), Head of the Department of Physical Chemistry (14 years), member of Faculty Council (32 years), member of the University Senate (24 years). In 1984, he received the Award of the Excellence in Teaching, from the Ministry of Education.

In his outstanding scientific period, he become: PhD (1961), ScD (1971), PhD advisor (since 1969), and he received the "Nicolae Teclu" prise from the Romanian Academy of Science (1980).

Profesor Liviu Oniciu was: Director of the Cluj-section of the Institute of Chemical and Biochemical Energetics (10 years), Director of the Research Centre in Electrochemistry at the Babeş-Bolyai University (9 years), member of the International Society of Electrochemistry (I S E), the American Society of Electrochemistry, the Council of European Academy of Surface Technology, and as a proof of his recognition at the international level. I mention that I S E has elected him to be the representative of Romanian group of electrochemistry in ISE.

Professor Liviu Oniciu wrote 6 books (two of them abroad), 8 monographs (one of them translated abroad), 19 patents and more than 220 scientific papers.

Prof. Liviu Oniciu was the founder of the prestigious School of Electrochemistry from Cluj, recognized in our country as being the most important school in "Electrochemical Conversion of Energy".

As research directions I mention: anodic oxidation of methanol on various electrocatalysts, the fuel cells: hydrazine/ hydrogen peroxide, hydrogen/oxygen, the alkaline batteries Ni-Fe; Ni-Cd, as well as Na-S battery and batteries with Li anode.

One must also mention the results obtained in applied electrochemistry by the Cluj-Section of the Institute of Chemical and Biochemical Energetics (10 years), namely: organic electrosynthesis, electrodeposition of metals, and photoelectrochemical conversion of energy.

Finally, we must underline that prof. Liviu Oniciu was a visionary scientist and due to this quality he was able to orient his coworkers towards scientific directions which will become important in millennium III, as for instance: fundamentals and applications of Electrochemical (and Electrochemical –Hydrodynamical) Impedance Spectroscopy in: Chemistry, Biochemistry, Pharmacy and Biology; Biosensors; modern electrochemical methods in studying the drugs and their therapeutic effects, just to indicate some of those which are already in development at Cluj.

Prof. Liviu Oniciu died in 1999, but his name will live as much as the Electrochemical Science in our country.

May he rest in peace.

Prof. dr. ing. Nicolae Bonciocat
Prof. dr. Ionel Cătălin Popescu

In memoriam prof. dr. Liviu Oniciu

ARCHAEOMETRIC CHARACTERISATION OF THE NEOLITHIC POTTERY DISCOVERED AT ALBA IULIA-*LUMEA NOUA* ARCHAEOLOGICAL SITE (ROMANIA)

SIMONA VARVARA[a,*], BRUNO FABBRI[b], SABRINA GUALTIERI[b], PAOLA RICCIARDI[b], MIHAI GLIGOR[a]

ABSTRACT. A set of 21 Neolithic painted pottery fragments belonging to the Lumea Noua culture (5th millennium B.C.) and discovered at Alba Iulia-*Lumea Noua* (Romania) settlement were investigated in order to elucidate some aspects concerning the manufacturing technique used for the ancient pottery production. The chemical, microstructural and petrographic features of the ceramic bodies were determined by X-ray fluorescence, X-ray diffraction and optical microscopy. The preliminary obtained data were used to make inferences concerning the pottery's technology in terms of type of raw clays and firing temperatures.

Keywords: pottery, Neolithic, Romania, X-ray fluorescence, X-ray diffraction, optical microscopy

INTRODUCTION

Pottery analysis plays an important and multi-faceted role in the interpretation of an archaeological site, being the fundamental tool used by archaeologists for dating sites or for determining trading patterns, cultural exchanges between peoples and social structures.

In the last decades, an impressive range of analytical techniques (*i.e.* X-ray fluorescence, neutron activation analysis, SEM-EDS, X-ray diffraction, etc.) have been exploited with considerable success to produce detailed "fingerprints" that can be used to ascertain the provenance and to reconstruct the technologies used in the manufacture of the ancient artefacts [1].

Contrary to other European regions, in Romania only very few investigations on prehistoric pottery have been made using modern techniques [2-3]. Consequently, in spite of the large quantities of ancient ceramic material collected from archaeological excavations, there are still many unknown aspects about the origin and production techniques of the prehistoric pottery discovered on the actual Romanian territory.

---

[a] *"1 Decembrie 1918" University, Dept. of Topography, 11-13 Nicolae Iorga St., 510009 Alba Iulia, ROMANIA. *E-mail: svarvara@uab.ro*

[b] *CNR, Institute of Science and Technology for Ceramics, 64 Via Granarolo, 48018 Faenza, Italy. E-mail: bruno.fabbri@istec.cnr.it*

In the last years, one of the most controversial issues of the Romanian archaeology was related to a Neolithic painted ceramic material belonging to the "Lumea Noua" culture (first half of the 5th Millennium B. C.). "Lumea Noua" pottery was found in relatively small quantities in few settlements (Alba Iulia-*Lumea Noua*, Limba, Tartaria, Zau de Campie, Cheile Turzii) from Transylvania and the painted decoration patterns show strong analogies with the ceramic finds from Slovakia (Bükk and Raškovce cultures) [4], Hungary (Esztár and Bükk cultures) [5] and Ukraine (Diakovo culture) [6], and North-Western of Romania (Piscolt group) [7].

The present study is part of a systematic archaeometric investigation on "Lumea Noua" pottery discovered at Alba Iulia-*Lumea Noua* settlement aiming at establishing its production technology in terms of the raw materials used, forming and firing procedures. The selected pottery samples were studied by X-ray fluorescence, X-ray diffraction and optical microscopy in order to obtain chemical, mineralogical and petrographic information.

RESULTS AND DISCUSSION

Thin-sections analysis (texture and mineralogy)

The observation of the thin-section of the samples under the polarizing microscope revealed that the 21 "Lumea Noua" potsherds display aplastic inclusions of various type, abundance and grain-size. Moreover, different types of relicts of micro-fossils (*i.e.* bioclasts, bivalve, algae and foraminifera) have been identified.

According to the absence or presence of the fossil relics, the "Lumea Noua" potteries have been grouped into two main "petrographic groups". Beside bioclasts, the abundance, type and size of aplastic inclusions are other parameters used to ascertain the groups.

Group 1 consists of 9 pottery samples (LN1 – LN 9) which do not enclose bioclasts in their ceramic body (Figure 1).
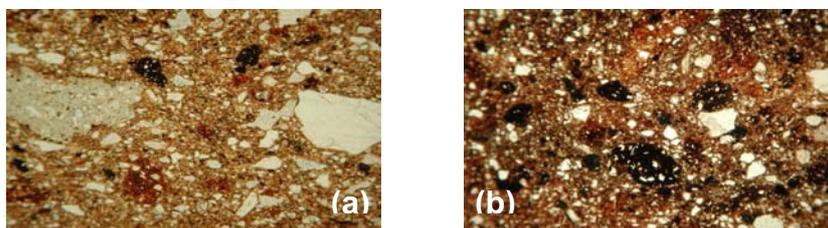
Figure 1. Thin-section of the ceramic bodies of the pottery samples belonging to group 1: (a) LN 1; (b) LN6 (40x; parallel nicol).

These samples are characterized by an inhomogeneous and mainly anisotropic matrix, which contains argillaceous rock fragments. The skeleton has a sandy texture; the aplastic inclusions are around 15-20% of the ceramic body. Their mineralogical composition is represented by quartz (mono- and polycrystalline), mica (biotite or muscovite), small amounts of K-feldspars and plagioclase.

Group 2 includes 12 samples (LN 10 - LN 21) which contain different types of relicts of fossils in their ceramic body (Figure 2).
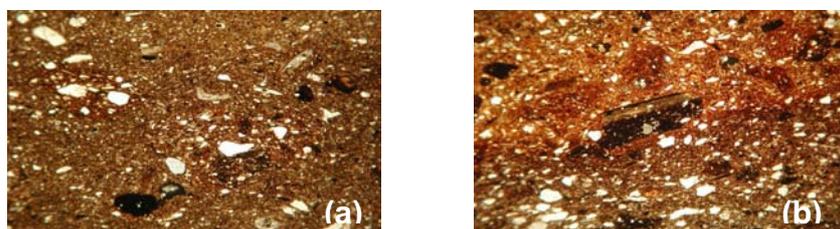
Figure 2. Thin-section of the ceramic bodies of the pottery samples belonging to the group 2: (a) LN 18; (b) LN19 (40x; parallel nicol)

The samples in group 2 have a semi-isotropic to isotropic groundmass, orange-yellow to reddish-brown in colour. Many samples have a sandwich-like structure from the colour point of view, which suggests that the firing atmosphere was not sufficiently oxidizing. A characteristic of the samples belonging to the group 2 is represented by the presence of a relatively high macro-porosity. The pores are rounded, have big dimensions and are seldom filled with secondary calcite. The rounded pores suggest that the artefacts were shaped by hands. The mineral composition of the temper is given by quartz (mono- and polycrystalline), micas, plagioclase, K-feldspars and rare and partially decomposed carbonatic rock fragments.

Under the polarizing microscope the white or light yellow slips observed on all "Lumea Noua" pottery appear as thin layers with thicknesses varying mostly between 100 and 120 μm. The thickness of the decoration layer varies between 10 and 20 μm.

Chemical composition of the ceramic bodies

The chemical composition of the ceramic bodies was determined by XRF analysis and the measured elements were Na, Mg, Al, Si, K, Ca, Ti, Fe, Mn and P expressed as oxide percentages (w/w). The P_2O_5 concentration exhibits values in a restricted range (0.18-0.50 %), except for samples LN 10 (0.95%) and LN 16 (1.37%), suggesting a possible post-depositional contamination with phosphorous during burial [8].

7

The IL values vary over a not very wide range, mainly between 1 and 3%, approximately. Only three samples show higher values, LN 1 (4.56%), LN 16 (6.63%) and LN 15 (6.57%), probably due to the fact that they were partially rehydrated during burial.

In order to make accurate comparisons between the chemical composition of different pottery and raw clays, the analytical data were normalised by excluding the IL and P_2O_5 values (Table 1). The silica content of the ceramic bodies is situated in the range of 61 to 73%, while the amount of alumina and iron oxide varies from 14.7 to 20% for Al_2O_3 and from 4.9 to 8% for Fe_2O_3. Most of the samples are characterized by a relatively low content of CaO (1.26 – 3.47%) and MgO (around 2%). In three samples (LN 2, LN 8, LN 11) the amount of CaO is around 4.8%, while sample LN 18 shows the highest concentration of calcium oxide (6.2%). All the samples present a low content of sodium (<1% Na_2O), while the concentration of potassium is higher and varies between 1.8 and 3.8% K_2O. The low contents in CaO are compatible with the scarcity of the calcareous micro-fossils in the ceramic paste.

Table 1.

Chemical composition of the "Lumea Noua" pottery samples and of the raw materials (wt% after normalization)

	Sample	SiO_2	Al_2O_3	TiO_2	Fe_2O_3	MnO	MgO	CaO	Na_2O	K_2O
Group 1	LN 1	70.95	16.22	0.87	4.93	0.07	1.94	2.16	0.84	2.01
	LN 2	63.00	18.76	0.84	6.73	0.12	2.19	4.47	0.68	3.21
	LN 4	61.97	19.20	0.80	7.62	0.15	2.60	3.47	0.91	3.19
	LN 6	67.34	17.21	0.83	6.23	0.12	2.30	1.55	1.02	3.40
	LN 7	64.41	18.81	0.86	7.08	0.08	2.47	1.92	0.98	3.38
	LN 8	61.67	18.49	0.84	6.68	0.13	2.69	4.88	1.03	3.59
	LN 9	73.01	14.76	0.78	5.92	0.12	1.52	1.26	0.80	1.82
	Average	*66.05*	*17.64*	*0.85*	*6.46*	*0.11*	*2.25*	*2.81*	*0.89*	*2.94*
	st. dev.	*±4.51*	*±1.65*	*±0.04*	*±0.87*	*±0.03*	*±0.41*	*±1.45*	*±0.13*	*±0.72*
Group 2	LN 10	68.73	15.39	0.76	5.19	0.05	1.94	3.44	0.70	3.80
	LN 11	62.43	18.45	0.73	6.96	0.22	2.33	4.80	0.55	3.54
	LN 12	67.36	18.51	0.77	6.39	0.12	1.86	1.62	0.64	2.73
	LN 14	63.62	18.77	0.88	7.28	0.06	2.56	2.13	1.12	3.58
	LN 15	66.21	18.01	0.81	8.02	0.05	1.75	2.16	0.39	2.59
	LN 16	65.33	17.35	0.81	7.01	0.09	1.99	2.99	0.65	3.78
	LN 17	66.89	16.93	0.81	6.62	0.17	2.42	2.03	0.94	3.18
	LN 18	62.69	18.02	0.81	5.75	0.08	2.26	6.22	0.71	3.45
	LN 19	66.19	18.56	0.86	6.13	0.06	2.29	1.93	0.80	3.16
	LN 20	63.50	19.50	0.79	6.48	0.06	2.15	3.36	0.59	3.57
	LN 21	63.11	19.90	0.82	7.37	0.13	2.19	2.45	0.85	3.17
	Average	*65.10*	*18.13*	*0.80*	*6.66*	*0.10*	*2.16*	*3.01*	*0.72*	*3.32*
	st. dev.	*±2.14*	*±1.24*	*±0.04*	*±0.80*	*±0.06*	*±0.25*	*±1.40*	*±0.20*	*±0.40*
Clay	LC	62.40	20.63	0.99	6.40	0.08	2.97	1.92	1.48	3.13
	BC	66.10	16.61	0.62	4.47	0.09	1.93	7.06	0.75	2.38
	RC	66.52	23.13	1.24	7.36	0.06	0.23	0.51	0.14	0.80
	YC	83.89	11.93	0.66	2.70	0.05	0.06	0.30	0.15	0.26

As it regards the raw clay samples, it is evident that they are very different to each other. For example, silica and alumina contents of the samples LC, BC and RC are very similar to those of the pottery, while the sample YC exhibits a very high concentration over 80% of silica and a very low value of alumina (about 12%).

In order to compare the chemical data relative to the two groups of potsherds with those of local raw materials, variation diagrams between pairs of significant elements were used (Figure 3).
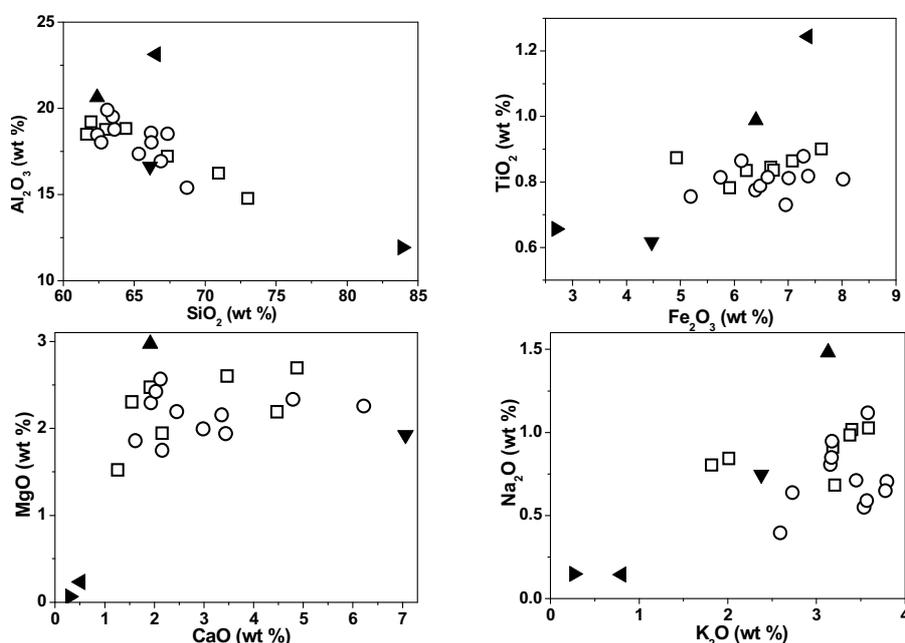
Figure 3. Chemical composition of the samples belonging to the two groups and of the raw clays represented in different binary diagrams: (□) Group 1; (○) Group 2; (▲) LC; (▼) BC; (◄) RC; (►) YC.

The results of the two ceramic groups show that the samples are chemically heterogeneous, and they do not evidence the two groups obtained by petrographic examination.

The differences in the chemical composition of the pottery samples allow rejecting the hypothesis of the use of a unique but very heterogeneous sediment for the pottery-making. The more reliable hypotheses are the following:

(i) two sources of raw clay materials, with and without microfossils respectively, were used with the addition of the same type of temper;

(ii) it was a unique source of raw clay material, not containing microfossils, which is modified adding temper with or without microfossils.

9

The comparison between pottery and clays does not show any overlap for RC and YC, while LC and BC should not be retained incompatible, especially if we take into account that the introduction of temper can modify the whole chemical composition in a significant way. But it is obvious that deeper investigations on the local clays composition are required in order to identify the correct hypothesis.

In a previous study [9] it has been established that the slip of the "Lumea Noua" pottery consists of carbonatic clay with a high content of illite, while iron-rich materials have been used for the painted decorations.

Mineralogical composition of the ceramic bodies

The mineral phases identified in the XRD patterns of representative pottery samples from each petrographic group are reported in Table 2.

Table 2.
Mineralogical composition of the "Lumea Noua" pottery samples and of the raw materials as determined from the XRD patterns

	Sample	Qtz	Ill	Chl	Cc	K	Pl	Kfs	Other phases	Temp (^{0}C)
Clay	LC	xxxx	xx	xx	xx	tr.	xx	tr.	Mo (tr.)	----
	BC	xxx	x	-	x	tr.	-	x	-	----
	RC	xxx	tr.	-	-	xx	-	-	Go (tr.)	----
	YC	xxxx	tr.	-	-	xx	-	-	-	----
Group 1	LN 1	xxxx	x	-	-	-	xx	x	Mo	700-800
	LN 6	xxxx	xx	-	-	-	xx	-	He	850-900
	LN 7	xxxx	x	tr.	-	tr.	xx	tr.	-	~600
	LN 8	xxxx	x	-	-	-	x	x	-	850-900
Group 2	LN 10	xxxx	xx	-	x	-	xx	x	Do (tr.)	600-700
	LN 11	xxxx	xx	-	x	-	x	-	Do	600-700
	LN 12	xxxx	x	-	-	-	x	x	-	850-900
	LN 18	xxxx	x	-	-	-	xx	-	-	850-900
	LN 21	xxxx	xx	-	-	-	xx	x	-	850-900

Gr. – group; Qtz – quartz; Ill – illite; Chl – chlorite; Cc – calcite; Pl – plagioclase; K – kaolinite; Kfs – K-feldspar; Mo – Montmorillonite Do – dolomite; He – hematite; Go – goethite; tr. – traces.

It is well known that during firing the clays decompose and chemical reactions occur which lead to the formation of new microcrystalline mineral phases, which depend mainly on the composition of clays, the kiln atmosphere and the firing temperature [10]. The firing temperatures can be estimated by the mineralogy of the potsherd bodies, assuming that the phase association present in the sample reflects the one formed during firing and that no important changes occurred during burial.

A temperature interval was assigned to each of the investigated potsherds on the basis of the minerals present in the assemblage identified by XRD and taking into consideration the thin-section observations.

As can be seen from Table 2, many investigated "Lumea Noua" samples were fired at 850-900^{0}C. In the case of LN 10 and LN 11, the absence of chlorite and the contemporaneous presence of dolomite and calcite indicate a low firing temperature between 600 and 700^{0}C.

Since kaolinite loses its stability rather abruptly at 550–600^{0}C, for sample LN 7 a lower firing temperature (around 600^{0}C) was hypothesized.

EXPERIMENTAL SECTION

Description of the pottery samples

A set of 21 pottery fragments belonging to the "Lumea Noua" culture, were selected as experimental samples. They were supplied from the collection of the "1 Decembrie 1918" University. Examples of "Lumea Noua" potsherds are presented in Figure 4.

| LN 1 | LN 10 | LN 18 | N 1 |

Figure 4. Examples of pottery samples belonging to "Lumea Noua" culture

Macroscopically, the potsherds consisting of rim or fragment of vessels are covered with a white or a white-yellowish slip and decorated with red, red-orange to purple or brown bands or geometrical models. In some cases, parallel black lines are also drawn on the slip.

In addition, four samples of different local clays, named "Limba Clay" (LC), "Brown Clay" (BC), "Red Clay" (RC) and "Yellow Clay" (YC), originating from natural deposits situated in the surroundings of the archaeological site have also been investigated.

Methods

All samples were analyzed from the petrographic, chemical and mineralogical points of view.

11

The microscopic examination by transmitted polarized light was carried out on pottery thin-sections using a Leitz Laborlux 11 POL optical microscope. The main goal was to discriminate among groups of pottery having similar "ceramic fabrics".

The chemical composition of the ceramic bodies (for major and minor elements) and of the raw clays was determined using a Philips PW 1480 XRF spectrometer. The test specimens were obtained by cutting small pieces from each ceramic fragment. After removing the slip and decoration layers by a lancet, the cut pieces were ground to powder in an agate mortar and a quantity of 0.5 grams of powder was used to prepare the tablets by pressing it on a boric acid support at approximately 2000 kg/cm^2. The chemical data were completed by determining the ignition loss (IL) of the dried sample after calcination at 1000^0C.

The mineral composition was estimated using a SIEMENS X-ray diffractometer with copper anticathode, scanning an angular range between $4°$ and $64° 2 \theta$ with a step of $2°/min$.

CONCLUSIONS

The results of the archaeometrical investigations on "Lumea Noua" artefacts allowed the individualization of two different types of ceramic body with and without microfossils respectively. In spite of this, all the artefacts could be probably retained of local provenance.

The samples are chemically heterogeneous, suggesting that different starting raw clay materials were used for their production.

Archaeometric data allowed "reconstructing" the stages used to produce the "Lumea Noua" artefacts; the proposed flow-manufacturing processes consists of: (i) preparation of the paste by mixing raw clays, (probably illitic clays) with temper (quartz - feldspatic sand) and water; (ii) shaping the clays by hands pressure; (iii) smoothening and partial drying; (iv) application of the slip, consisting very probably of a fine-grained carbonatic clay with high illite content; (v) polishing the surface; (vi) painting using iron-rich materials; (vii) final drying and (viii) firing at temperatures between 600 and 900^0C.

Further and more detailed investigations on different clays sources and on other "Lumea Noua" pottery collected from the archaeological sites from Transylvania will allow us to identify the raw materials used and to ascertain exactly their origin or to discriminate between sources.

ACKNOWLEDGEMENTS

REFERENCES

1. H. Mommsen, *Journal of Radioanalytical and Nuclear Chemistry,* **2001**, *247,* 657.

2. G. Lazarovici, L. Ghergari, C. Ionescu*, Angvstia,* **2002**, *7*, 7.

3. A. Goleanu, A. Marian, M. Gligor, C. Florescu, S. Varvara, *Revue Roumaine de Chimie,* **2005***, 11-12*, 939.

4. J. Lichardus, *Studijné Zvesti. Archeologickeho ústavu Slovenskej académie vied. Nitra,* **1969**, *17*, 219.

5. G. Goldman, J. G. Szénásky, *Nyíregyháza,* **1994**, *XXXVI,* 225.

6. M. Potushniak, *Nyíregyháza,* **1997**, *XXXIX,* 35.

7. Gh. Lazarovici, J. Németi, *Acta Musei Porolissensis*, **1983**, *VII,* 17.

8. B. Fabbri, G. Guarini, E. Arduino, M. Coghe, *Proceeding of 1st European workshop on archaeological ceramics, Roma, Italy,* **1994**, 183.

9. P. Ricciardi, S. Varvara, B. Fabbri, S. Gualtieri, M. Gligor, *Proceeding of 10a Giornata di Archeometria della Ceramica, Roma, Italy,* **2006** (in press).

10. C. Rathossi, P. T. Katagas, C. Katagas, *Journal of Applied Clay Science,* **2004**, *24*, 313.

In memoriam prof. dr. Liviu Oniciu

SYNTHESIS AND ELECTROCHEMICAL BEHAVIOUR OF *BIS*-(10-ETHYLPHENOTHIAZINYL)-PHENYLMETHANE

DELIA GLIGOR[a], LIANA MURESAN[a], IONEL CATALIN POPESCU[a], CASTELIA CRISTEA[a], GABRIELA CORMOS[b]

ABSTRACT. *Bis*-(10-ethylphenothiazinyl)-phenylmethane was obtained by the condensation of 10-ethyl-phenothiazine with benzaldehyde in the presence of acid catalysts. The electrochemical behavior of *bis*-(10-ethylphenothiazinyl)-phenylmethane adsorbed on spectrographic graphite has been investigated. Cyclic voltammetric measurements performed in aqueous buffer solutions at different potential scan rates pointed out to a quasi-reversible, surface-confined redox process, with a negative formal standard potential of -55 mV *vs.* SCE (10 mV s^{-1}). The voltammetric response involves the transfer of 1e$^-$, with a heterogeneous rate constant of 18.9 s^{-1} (pH 7). The modified electrodes showed a good electrochemical stability.

Keywords: *10-alkylphenothiazine, modified electrodes, cyclic voltammetry*

INTRODUCTION

The condensation reaction of phenothiazine with aromatic aldehydes (benzaldehyde, *o-, m-* and *p*-nitrobenzaldehyde) in acid media was already reported [1]. The mild electrophile generated by the aldehyde in the presence of methanesulfonic acid is responsible for the substitution of the phenothiazine ring and *bis-(*10*H*-phenothiazin-3-yl)-methane derivatives were obtained as major reaction products. 10*H*-Phenothiazine is characterized by enhanced reactivity towards electrophilic substitution, but the introduction of alkyl functional groups at different positions affects both orientation of subsequent substitution and the overall reactivity [2]. Thus, 10-alkylphenothiazine is a "slightly deactivated" substrate for electrophilic substitution. Theoretical explanations are based on both electronic and steric effects. Due to the *sp*^{3} hybridization state of the two heterocyclic heteroatoms (nitrogen and sulfur), phenothiazine molecular structure is folded about S-N axis with a dihedral angle of about 150^0 [3], influenced by the presence of substituents. According

---

[a] *"Babeş-Bolyai" University, Faculty of Chemistry and Chemical Engineering, 400028 Cluj-Napoca*
[b] *"L. Blaga" University, Faculty of Medicine, Sibiu*

to the spatial position of the substituent attached to nitrogen with respect to the dihedral angle, two distinct configurations may appear as it can be seen in figure 1.

10*H*-Phenothiazine is characterized by an "*intra*" orientation of the hydrogen atom (by pointing inside with respect to the dihedral angle, figure 1a), while 10-ethylphenothiazine preferentially adopts an "*extra*" orientation of the ethyl group due to steric reasons (figure 1b).
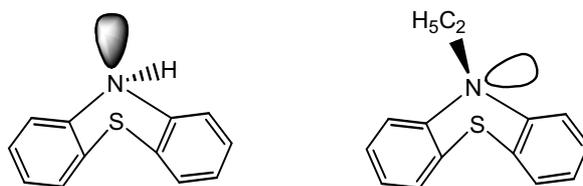
Figure 1. Configurations of phenothiazine derivatives
a) 10H-Phenothiazine, b) 10-Ethylphenothiazine

These two configurations are not electronically equivalent, according to the possibility of conjugation of the nitrogen lone pair of electrons with the adjacent benzene π system. In 10*H*-phenothiazine, the transmission of the electronic effects is very efficient and electrophilic substitution occurs easily. The reduced participation of the nitrogen lone pair to the extended π system in 10-ethylphenothiazine structure due to steric hindrance explains the decreased reactivity in electrophilic substitution.

In this paper, we describe the synthesis of *bis*-(10-ethylphenothiazin-3-yl)-phenylmethane (**1**)**,** a new product obtained by the condensation between 10-ethylphenothiazine and benzaldehyde. The electrochemical behavior and electrochemical stability of **1** adsorbed on spectrographic graphite were investigated by cyclic voltammetric (CV) measurements performed at different scan rates. The heterogeneous electron transfer rate constant (k_s) was estimated using Laviron treatment [4].

RESULTS AND DISCUSSIONS

Synthesis

The condensation of 10*H*-phenothiazine with benzaldehyde generated *bis-(*10*H*-phenothiazin-3-yl)-phenylmethane in good yields, when methane sulfonic acid was employed as catalyst and the reaction mixture was heated to reflux in ethanol solution [1]. These reaction conditions were modified in order to perform the condensation of less reactive 10-ethylphenothiazine with benzaldehyde. *Bis-(*10-ethylphenothiazin-3-yl)-phenylmethane (**1**) was obtained using acetic acid as a solvent (Scheme 1). After refluxing the reaction mixture several hours, the condensation product **1** precipitated from the reaction mixture and was easily separated by filtration.
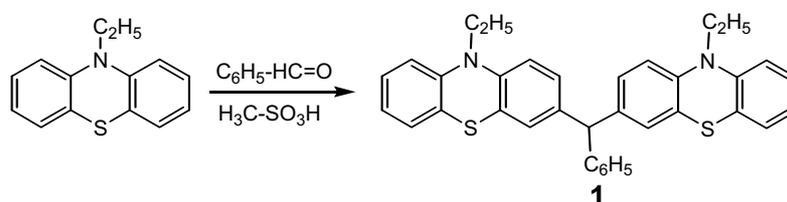
Scheme 1

The structure assignment of **1** is supported by NMR spectroscopic data. The presence of the ethyl substituent was revealed by the coupled signals situated at 1.2 ppm (t, 6H) and 3.1 ppm (q, 4H) and the proton in the methine bridge generated a singlet signal situated at 3.8 ppm.

Electrochemical behaviour of bis-(10-ethylphenothiazin-3-yl)-phenylmethane-modified graphite electrode

The electrochemical behavior of **1** adsorbed on spectrographic graphite (G/**1**) was investigated using CV measurements, at different potential scan rates. As it can be seen from figure 2A, the cyclic voltammogram recorded for G/**1** electrode presents a peak pair with the formal standard potential placed at -55 mV *vs.* SCE (pH 7). It is the most negative value recorded in a series of phenothiazine derivatives based on bis-(10*H*phenothiazin-3-yl)-methane and bis-(10*H*phenothiazin-3-yl)-phenylmethane [5]. This suggests that compound **1** participates easier to oxidation processes and is explained by the reduced participation of the nitrogen lone pair to the extended π system in the 10-ethylphenothiazine unit responsible for redox equilibria. The oxidation wave ($E_{pa}^{0/+1}$= -43 mV *vs.* SCE) can be assigned to the radical cation formation of one phenothiazine unit in the molecular structure. Scheme 2 shows the proposed reaction scheme for the electrochemical processes occurring during the voltammetric experiments.
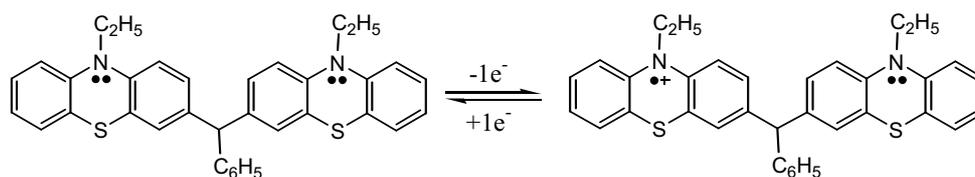
Scheme 2

The electrochemical parameter ΔE indicates a quasi-reversible redox process, taking into consideration its value of 24 mV, as criterion for the process reversibility. This value is smaller than those obtained for the related compounds mentioned above [5], suggesting a more reversible electron transfer.

17

The width at half peak height (E_{FWHM}) was different to the corresponding ideal case (E_{FWHM} = 90.6/n mV, where n is the number of electrons). The observed discrepancies (140 and 33 mV for anodic and cathodic process, respectively) prove the existence of repulsive interactions between the adsorbed redox species (radical cations generated in the anodic process) and attractive ones (neutral molecules or dimers formed during the cathodic process) [5,6].

As expected for surface confined redox active species [4], the cyclic voltammograms recorded for a wide range of potential scan rates (0.01 – 0.8 V s^{-1}) showed a linear dependence of the peak currents (I_p) on the electrode potential scan rate (v). The slope of log I_p vs. log v dependence was close to one (0.88 ± 0.03 and 0.98 ± 0.04 for anodic and cathodic process, respectively), confirming once again the existence of adsorbed species. The number of electrons involved in the redox process, estimated from I_p vs. v dependence [7] was found close to 1 (within ± 10%), in accordance with the predicted value for the cation formation.
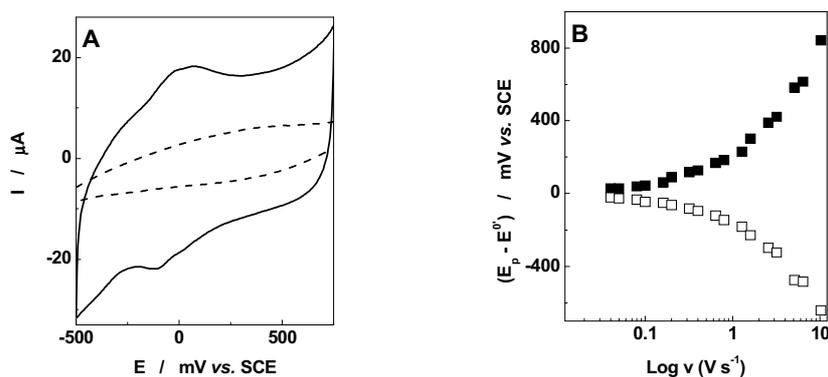
Figure 2. (A) Cyclic voltammograms of graphite electrode (---) and of compound **1** adsorbed on graphite (—) and (B) experimental dependence of (E_p - $E^{o'}$) on the scan rate, corresponding to **1** adsorbed on graphite electrodes. Experimental conditions: starting potential, -500 mV vs. SCE; potential scan rate, 100 mV s^{-1} (A); supporting electrolyte, 0.1 M phosphate buffer (pH 7).

The heterogeneous electron transfer rate constant (k_s, s^{-1}) was estimated at pH 7, using the treatment proposed by Laviron [4] (figure 2B) and it was found equal to 18.9 s^{-1}, while the transfer coefficient (α) was 0.52. The k_s value is higher than those determined for phenothiazine (1.7 s^{-1}) [8], which proves that compound **1** is more active electrochemically than phenothiazine.

The stability of modified electrodes was tested by measuring the variation of phenothiazine electrochemical signal in a defined time range. It is known that the immobilization stability of a compound on graphite electrode is decided by the number of conjugated aromatic rings from the molecule. Thus, the electrochemical stability tests of the G/**1** were performed in potentiodynamic conditions: the electrode potential was continuously cycled within the potential range covering the domain of the phenothiazine redox activity, in phosphate buffer solution, pH 7. From the recorded voltammograms a progressive decrease of the electrode surface coverage was observed, while the voltammogram shape remains invariant (results not shown). This behaviour proves the G/**1** good electrochemical stability and its relatively strong adsorption on the graphite surface.

The kinetic interpretation of the deactivation process showed that it obeys first-order kinetics. The slopes of kinetic plots were used to determine the values of the deactivation rate constants, as an average of the anodic and cathodic process and a value of $3.45 \cdot 10^{-13}$ mol cm^{-2} s^{-1} was obtained. The value of deactivation rate constant is smaller in comparison with other phenothiazine derivatives, octachloro-phenothiazinyl and heptachloro-hydroxy-phenothiazine (k_{deact} = $27.5 \cdot 10^{-10}$ mol cm^{-2} s^{-1} and $1.3 \cdot 10^{-8}$ mol cm^{-2} s^{-1}, respectively) [9]. This is due to the structure of **1**, which is favorable for increasing the electrochemical stability of modified graphite electrode.

CONCLUSIONS

The condensation of 10-ethylphenothiazine, a slightly deactivated phenothiazine substrate, with benzaldehyde in the presence of acid catalysts generated *bis-(*10-ethylphenothiazin-3-yl)-phenylmethane (**1**) in good yields. Modified electrodes were prepared by adsorption of **1** on graphite. Electrochemical data show that oxidation process occurs easier for **1** as compared to related *bis-(*10*H*-phenothiazin-3-yl)-methane derivatives [4], as well as other derivatives containing phenothiazine units which were previously studied under the same conditions [8,9]. The linear dependence between peak current (I_p) and the potential scan rate (v) proves the existence of a redox couple adsorbed on electrode surface involving 1e$^-$.

The graphite electrodes modified with **1** presented a good electrochemical stability.

EXPERIMENTAL SECTION

Reagents from Merck were used.
TLC was used to monitor the reaction progress (Merck silica gel F 254 plates).
NMR spectra were recorded using a 300 MHz Brucker NMR spectrometer.
FT-IR spectra were recorded using a Brucker Vector 22 FT-IR spectrometer.

Bis(10-ethylphenothiazin-3-yl)-phenylmethane (1)

10-Ethylphenothiazine 0,5 g (2,5 mmol) was solved in acetic acid (50 mL), methanesulfonic acid (0.5 mL) was added and then benzaldehyde (1.5 mmol) was added drop wise under vigorous stirring at room temperature. The reaction mixture was heated to reflux for 4 hours. The pink precipitate accumulated was filtered and washed several times with warm methanol; the precipitate was suspended in THF and then filtered. 0.4 g powder was obtained, yield 67%.

^{1}H-NMR (300MHz, DMSO-d_6)**:** δ=1.2 ppm (t, 6H), 3.1ppm (q, 4H), 3.8 ppm (s, 1H), 6.61-7.2 ppm (m, 19H).

IR (cm^{-1}): 3100, 1595, 1487, 1314, 794, 740.

Electrode preparation

A spectrographic graphite rod (Ringsdorff-Werke, GmbH, Bonn-Bad Godesberg, Germany), of ~ 3 mm diameter, was wet polished on fine (grit 400 and 600) emery paper (Buehler, Lake Bluff, Ill., USA). Then, a graphite piece of suitable length was carefully washed with deionized water, dried, and finally press-fitted into a PTFE holder in order to obtain a graphite electrode having, in contact with the solution, a flat circular surface of ~ 0.071 cm^2. The modified graphite electrode was obtained by spreading onto the electrode surface 2 μl of 1 mM derivative **1** solution in dimethylsulfoxide, and leaving them for one day at room temperature to evaporate the solvent. Before immersion in the test solution the modified electrodes were carefully washed with deionized water.

For each electrode, the surface coverage (Γ, mol cm^{-2}) was estimated from the under peak areas, recorded during the CV measurements at low scan rate (< 10 mV s^{-1}). The presented results are the average of 3 identically prepared electrodes.

Electrochemical measurements

CV measurements were carried out in a conventional three-electrode electrochemical cell. A saturated calomel electrode (SCE) and a coiled Pt wire served as reference and counter electrode, respectively. The cell was connected to a computer-controlled voltammetric analyzer (Autolab-PGSTAT10, Eco Chemie, Utrecht, Netherlands). The supporting electrolyte was a 0.1 M phosphate buffer, pH 7 prepared using $K_2HPO_4 \cdot 2H_2O$ and $KH_2PO_4 \cdot H_2O$ from Merck (Darmstadt, Germany).

REFERENCES

1. G. Cormoş, C. Cristea, I. Filip, I. A. Silberg, *Studia Universitatis Babes-Bolyai, Chemia*, **2006***, LI, 2*, 155.
2. C. Bodea, I. A. Silberg, „Advances in Heterocyclic Chemistry", Academic Press, **1968**, vol 9, pp. 430.
3. J.J. H. McDowell, *Acta Crystallographica, Section B: Structural Science*, **1976**, *32*, 5.
4. C. Cristea, G. Cormos, D. Gligor, I. Filip, L. Muresan, I. C. Popescu, *Journal of New Materials for Electrochemical Systems*, submitted, **2008**.
5. R. W. Murray, "Introduction to the Chemistry of Molecularly Designed Electrode Surfaces", in "Techniques of Chemistry", W.H. Saunders, Jr., (ed.), J. Wiley, **1992**, vol. XXII, pp. 9.
6. R. Laviron, *Journal of Electroanalytical Chemistry*, **1979***, 101*, 19.
7. R. W. Murray, "Chemically Modified Electrode", in "Electroanalytical Chemistry", A.J. Bard (ed.), M. Dekker, New York, **1984**, vol. 13, pp. 191.
8. D. Gligor, "Electrozi modificati pentru oxidarea electrocatalitica a NADH", PhD Thesis, Cluj-Napoca, **2002**.
9. D. Gligor, L. Muresan, I. C. Popescu, I. A. Silberg, *Revue Roumaine de Chimie*, **2003**, *48*, 463.

In memoriam prof. dr. Liviu Oniciu

MOTT-SCHOTTKY ANALYSIS OF ELECTRODEPOSITED ZnS THIN FILMS

ADRIAN NICOARA[*]

ABSTRACT. Some semiconductor properties, flat band potential and donor density, of electrodeposited ZnS thin films were evaluated by Mott-Schottky analysis. To this aim the depletion region capacitance of semiconductor/ solution interface was determined by analysis of impedance spectrums.

Keywords: *ZnS, thin film, semiconductor, impedance spectroscopy.*

INTRODUCTION

In recent years, extensive studies have been carried out on preparation and characterization of large band gap semiconductors, such as TiO_2, ZnS, ZnO, SnO_2, due to their application in photovoltaic-photoelectrochemical energy conversion and photoconductors [1-4]. Devices based on these materials require obtaining of thin films, usually by the means of vacuum deposition techniques (i.e., molecular beam epitaxy, vapour phase epitaxy or metal-organic chemical vapour deposition) or spray pyrolysis [5-7]. However, chemical and electrochemical depositions are attractive alternatives, mainly due to their lower cost and to advantages related to the use of ambient temperature and pressure. The electrodeposition is further advantaged by an easier control of the film growth, by using electric charge as process advance variable, and by higher yields, restricting the film formation on the electrode interface [8-10].

The properties of electrodeposited thin films can be obtained by examining electronic structures of the semiconductor/solution interface. Electrochemical and electrophotochemical techniques of investigation are well-suited for obtaining of some important properties of the semiconductor, namely donor density and flat-band potential, both factors influencing the efficiency of photoelectrical and photochemical application of semiconductors. There are a number of such techniques used for measuring these properties;

[*] *Universitatea Babeş-Bolyai, Facultatea de Chimie şi Inginerie Chimică, Str. Kogălniceanu Nr. 1, RO-400084 Cluj-Napoca, Romania, anicoara@chem.ubbcluj.ro*

the flat-band potential (E_{fb}) can be determined either by measuring the photopotential or the onset of the photocurrent as a function of radiation intensity, or by measuring the capacitance of the space charge region into semiconductor [1, 11, 12]. The latter technique, employed in this work, allows the determination avoiding the use of controlled level of electromagnetic radiation that would have requested a more sophisticated instrumental setup.

The selected determination method of a semiconductor/electrolyte interface flat-band potential was performed using a correlation between capacitance of the semiconductor depletion layer and applied voltage bias, correlation common known as Mott-Schottky analysis. Several methods of capacitance measurement are described in literature, among which a.c. voltammetry, capacitive reactance and impedance spectroscopy measurements are the most utilized [13].

The aim of present work is to perform a Mott-Schottky analysis on semiconductor ZnS thin film electrodes by means of impedance spectroscopy.

RESULTS AND DISCUSSION

A common approach in describing the response of a system to an a.c. perturbation is the recourse to an electrical equivalent circuit, composed by resistances, R, and capacitances, C.

The most complex equivalent circuit takes into account the behaviour of all the elementary steps that accompany the charge transfer across the semiconductor/solution interface. It uses elements for solution phase (R_s), depletion region (R_{dep} and C_{dep}), electric double-layer (C_{dl}), and for the charge transfer (R_{ct}) and mass transport (R_{dif} and C_{dif}). These electric elements describe the charge transport into solution and semiconductor phases, charge accumulation on semiconductor/solution interface and elementary steps of the faradaic process, respectively. Solely depletion region capacitance is of interest in present investigation.
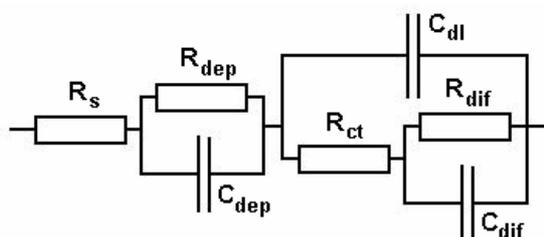

Figure 1. General equivalent circuit of a metal/semiconductor/solution system.

Depending on the experimental conditions employed, the contribution of some elementary steps can be neglected, as summarised in ref. [13]. In present study, by using a reasonable high concentration of electrolyte solution which increases C_{dl}, one can set aside not only the faradaic terms (R_{ct}, R_{dif} and C_{dif}) as the low reactance of C_{dl} acts as a shunt, but also the C_{dl} itself as it is connected in series with another capacitance of lower value. Accordingly, a simplified equivalent circuit that retains only R_s, R_{dep} and C_{dep} is further discussed and utilised.

It is now at hand to discuss about choosing the method of capacitance measurement. When using a.c. voltammetry or capacitive reactance (X_C) measurements of pulsation ω, the presence of R_s and R_{dep} resistance will cause an under-evaluation of measured capacitance (C_{meas}):

$$C_{meas} = \frac{1}{\omega X_C} = \frac{C_{dep} R_{dep} + 1/\omega}{R_{dep} + R_s + \omega C_{dep} R_{dep} R_s} \tag{1}$$

Eq. 1 evidences the conditions necessary for accurate capacitance determination, namely $\omega >> 1/C_{dep} R_{dep}$ and $R_s << R_{dep}/(1 + \omega C_{dep} R_{dep})$, which are often difficult to fulfil. Nevertheless, taking into account the advantages of measuring into a frequency domain, impedance spectroscopy measurements allow calculation of every element of equivalent circuit.

The impedance spectroscopy measurements were performed on aluminium electrode uncovered or covered by ZnS thin layers obtained by electrodeposition on potential controlled conditions at -1.25 or -1.45 V vs. SCE, see ref. [14]. Impedance spectrums are measured for dc bias values (E_{cc}) in the range of -0.5 to -1.7 V vs. SCE, avoiding, as possible, sulphide oxidation or zinc ion reduction, both reactions compromising the semiconductor properties.

Obtained spectrums of both electrodes exhibit only one depressed semi-circular loop as predicted by the simplified equivalent circuit. Fig. 2 presents measured spectrum, as Nyquist plots, for the film deposited at -1.25 V vs. SCE for selected d.c. biases presented in legend.

A critical part of any attempt to use impedance spectroscopy to measure capacitance is the numerical correlation between the measured data and a selected equivalent circuit. In present work, a complex non-linear least squares (CNLS) fitting procedure was selected, which involves minimizing of:

$$S(\theta) = \sum_{i=1}^{n} \left[\left(Z_{re,i} + jZ_{im,i} \right) \Big|_{measured} - Z_M(f_i, \theta) \right]^2 = \sum_{i=1}^{n} \left[\varepsilon_i \right]^2 \tag{2}$$

and uses the measured impedance and the model impedance:

25

$$Z_M(f_i, \theta) = Z_{M,re,i}(f_i, \theta) + jZ_{M,im,i}(f_i, \theta) \tag{3}$$

where f is the frequency, j is the complex operator, θ is here a 4-element real vector of (R_s; R_{dep}; C_{dep}; α), and ε_i is an identically distribution complex error term, with the real and imaginary components being independent on each other [15].

It is known that on polycrystalline electrodes the double-layer capacitance is often frequency dependent. Whatever of atomic scale (i.e., steps, kinks and dislocations) or larger (i.e., scratches, pits and grooves), surface irregularities cause this capacitance dispersion phenomenon. To characterize this phenomenon, the response of the capacitance can be approximated to a constant phase element; in other words $C(f) \propto (j\,2\pi f)^{1-\alpha}$, with exponent α value between 0.7 and 0.9 is common with solid electrodes [16]. On these bases, the components of the model impedance are:

$$Z_{M,re,i}(f_i, \theta) = R_s + \frac{R_{dep}\left[1 + 2\pi f_i R_{dep} C_{dep} \sin(\alpha)\right]}{1 + 4\pi f_i R_{dep} C_{dep} \sin(\alpha) + (2\pi f_i R_{dep} C_{dep})^2} \tag{4}$$

$$Z_{M,im,i}(f_i, \theta) = -\frac{2\pi f_i R_{dep}^2 C_{dep} \cos(\alpha)}{1 + 4\pi f_i R_{dep} C_{dep} \sin(\alpha) + (2\pi f_i R_{dep} C_{dep})^2} \tag{5}$$
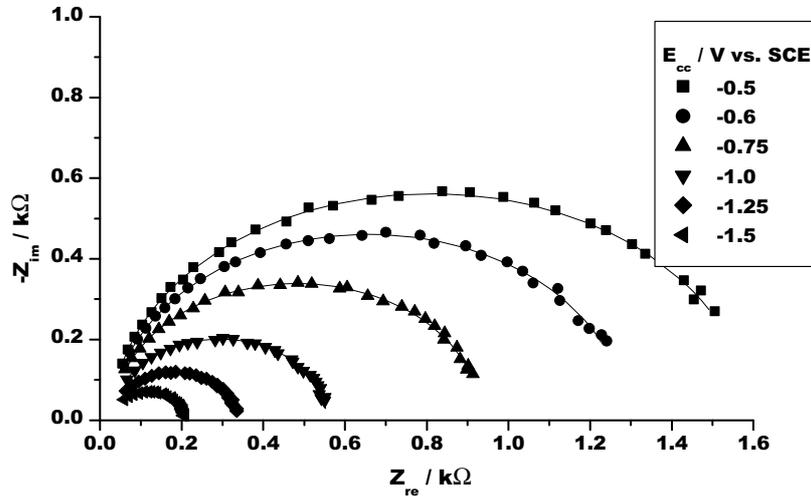

Figure 2. Influence of applied dc potential (for selected values presented in the legend) on Nyquist plot of measured impedance spectra for the ZnS film obtained at -1.25V vs. SCE. Continuous lines denote the fitted spectrums.

The fittings were performed in Microcal Origin 5.0 using the simplex algorithm. The results of the fitting procedure are the components of θ. To evaluate graphically the fitting goodness, corresponding fitted curves are also presented in fig. 2. From the components of fitted vector, analysis is restricted to depletion region capacitance C_{dep}. Fig. 3a depicts the influence of applied dc bias on the capacitance values of the three investigated electrodes. The significantly higher values are obtained for the uncovered electrode; in this case, due to absence of semiconductor film, the determined capacitance corresponds to the electric double-layer.

(a) **(b)**
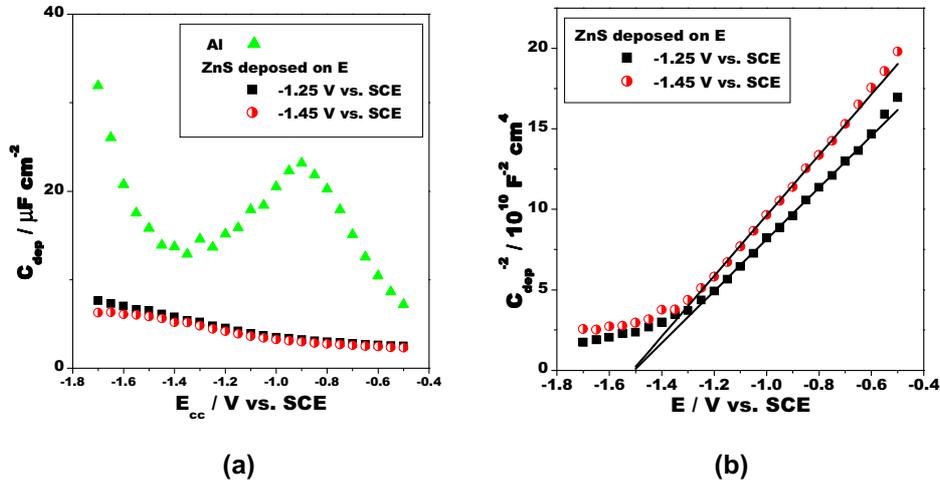
Figure 3. Influence of applied dc potential on calculated C_{dep} (fig. 2a) and Mott-Schottky linearization (fig. 2b). Presented data correspond to Al electrode uncovered and covered with a ZnS film electrodeposed as indicated in legend.

The flat-band potential of a semiconductor/solution junction can be calculated from the Mott-Schottky equation [17]:

$$1 / C_{dep}^2 = \frac{2}{e_o N_d \varepsilon A^2} (E - E_{fb}) \qquad (6)$$

where A is the interfacial area, e_o the elementary charge, N_d the donor density and ε the dielectric constant of the semiconductor. Accordingly, a plot of $1/C_{dep}^2$ vs. E should give a straight line with the flat-band potential as x-axis intercept and the slope allowing calculation of donor density.

It is clear from the data presented in fig. 3b that Mott-Schottky equation is valid within a wide potential range, of about 0.7V, which indicates a well-defined electronic surface state of deposited film. Wider linear potential range,

that exceeds 1V, can be obtained only for high organised solids, namely single crystals. Furthermore a positive slope is an indication of an n-type semiconductor.

At negative potentials (roughly for E< -1.2 V vs. SCE) a significant deviation from linearity is observed. This deviation is very likely related to the presence of surface states because an electronic structure change, as a result of elementary zinc formation by reduction, would have decreased the depletion region capacitance dramatically. Accordingly, at lowest investigated potentials the reduction process corresponds to sulphur or polysulphide reduction, since a 1:1.1 Zn:S molar ratio for the obtained film was previously establish [14].

When the data in fig. 3b are fitted using equation (6), a value for the flat-band potential of (-1.51 ± 0.02) V vs. SCE was calculated. This value is in good agreement with that found in the literature (-1.54 V vs. SCE) for a single crystal ZnS [18]. The donor density was estimated to be (7.4 10^{18} and 6.9 10^{18}) cm^{-3} for the films obtained by electrodeposition at -1.25 and -1.45 V vs. SCE, respectively. The donor density values should be regarded with caution because the surface area of the irregularly crystallites contained by the semiconductor thin film could only be estimated with a rather poor accuracy. But, assuming potential independence of surface area, on basis of increasing the slope of Mott-Schottky plot when electrodeposition takes place at a more negative potential, one can discuss about the nature of reaction causing the excess of sulphur in electrodeposited film. Because elementary sulphur has no implication into charge transport, reduction of thiosulphate takes place more likely to polysulphide than to elementary sulphur.

CONCLUSIONS

Impedance spectroscopy was employed in order to obtain information about the electric charge depletion in a semiconductor thin film of ZnS obtained from electrodeposition from acidified thiosulphate solution containing zinc ion. The investigation of two ZnS films, obtained by electrodeposition at -1.25 and -1.45 V vs. SCE, allowed calculation of the flat-band potential of (-1.51 ± 0.02) V vs. SCE and the donor density was estimated to be (7.4 10^{18} and 6.9 10^{18}) cm^{-3}, respectively.

In a previous paper electrodeposition of ZnS thin films was investigated by cyclic voltammetry and electrochemical quartz crystal microbalance allowed the estimation of an 1:1.1 Zn:S stoechiometric ratio. The present Mott-Schottky analysis suggested that the excess sulphur of ZnS films is caused by the presence of zinc polysulphide, excluding the presence of elementary sulphur, as the donor density of semiconductor is potential dependent.

EXPERIMENTAL SECTION

The impedance spectroscopy measurements were performed using a computer controlled potentiostat (Elektroflex EF-451, Hungary) by means of a customised Turbo Pascal^{TM} software application. A 10mV ac perturbation, with frequencies in range of 0.3 to 10 KHz, was superimposed to the imposed voltage bias.

A standard three-electrode electrochemical cell configuration was employed for the measurements. The reference electrode was a double-junction saturated calomel electrode (SCE) and the counter electrode was a spiralled Pt wire. The working electrode was obtained by electrodeposing a 1μm thin film of ZnS onto an Al (refined, 99.5% purity) disk electrode (A=0.032 cm^2). Electrodeposition details are presented elsewhere [14]. The electrolyte solution employed was Na_2SO_4 0.2 M (p.a. Riedel de Haen), being prepared using distillated water.

All measurements were performed with the cell introduced into a dark casket and kept at 20 $\pm$ 1 ^{o}C.

ACKNOWLEDGMENTS

REFERENCES

1. L. D. Partain, "Solar Cells and Their Applications", John Wiley and Sons, New York, **1995**, chapters 1,2.

2. J. McEvoy, M. Gratzel, *Solar Energy and Materials for Solar Cells*, **1994**, *32*, 221.

3. B. O' Regan, M. Gratzel, *Nature*, **1991**, *353*, 737.

4. A. M. Fernandez, P. J. Sebastian, *Journal of Physics. D: Applied Physics*, **1993**, *26*, 2001.

5. Ch. Bouchenaki, B. Ullrich, J. P. Zielinger, H. Nguyen Cong, P. Chartier, *Journal of Crystal Growth*, **1990**, *101*, 797.

6. C. Saravani, K. T. R. Reddy, P. J. Reddy, *Semiconductor Science Technology*, **1992**, *6*, 1036.

7. H. Nguyen Cong, P. Chartier, *Solar Energy and Materials for Solar Cells*, **1993**, *30*, 127.

8. S. A. Al Kuhaimi, Z. Tulbah, *Journal of Electrochemistry Society,* **2000**, *147*, 214.

9. M. Sasagawa, Y. Nosaka, *Electrochimica Acta*, **2003**, *48*, 483.

10. M. Innocenti, G. Pezzatini, F. Forni, M. L. Foresti, *Journal of Electrochemical Society*, **2001**, *148*, C357.
11. S. Burnside, J.-E. Moser, K. Brooks, M. Gratzel, D. Cahen, *Journal of Physical Chemistry B,* **1999***, 103,* 9328.
12. B. Yacobi, "Semiconductor Materials An Introduction to Basic Principles", Kluwer, New York, 2003, chapter 1.
13. V. Lehmann, "Electrochemistry of Silicon Instrumentation", Wiley-VCH, Weinheim, **2002**, chapter 5.
14. A. Nicoara, *Studia Universitatis Babes-Bolyai, Chemia,* **2004**, *XLIX*, 65.
15. J. R. Macdonald, "Impedance spectroscopy. Emphasizing solid materials and systems", John Wiley and Sons, New York, **1987**, chapter 6.
16. A. Sadkowski, *Journal of Electroanalytical Chemistry*, **2000**, *481*, 222.
17. *K. Rajeshwar, "Fundamentals of Semiconductor Electrochemistry and Photo-electrochemistry" in "Encyclopedia of Electrochemistry, Vol 6 Semiconductor Electrodes and Photoelectrochemistry" (A.J. Bard, ed.), Willey, Weinheim, **2002**,* chapter 1.
18. Y. Xu, M. A. A. Schoonen, *American Minerals*, **2000**, *85*, 543.
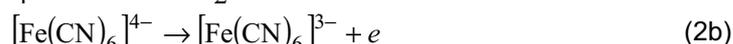
In memoriam prof. dr. Liviu Oniciu

ABOUT THE POSSIBILITY OF USING THE ELECTROCHEMICAL IMPEDANCE SPECTROSCOPY AS A METHOD OF CLASSIFYING THE DRUGS

N. BONCIOCAT[a]

ABSTRACT. The proposed EIS method uses the *reference redox dielectrode*:

$$\text{Pt} \left| \left[\text{Fe(CN)}_6\right]^{3-} / \left[\text{Fe(CN)}_6\right]^{4-}, \text{KCl} \right. \text{ (in excess), } O_2 \text{ physically dissolved (1)}$$

which, e.g., in weak acidic media, has the reactions:

$$\frac{1}{4}O_2 + H^+ + e \rightarrow \frac{1}{2}H_2O \tag{2a}$$

$$\left[\text{Fe(CN)}_6\right]^{4-} \rightarrow \left[\text{Fe(CN)}_6\right]^{3-} + e \tag{2b}$$

In the case of the *reference redox dielectrode* (1), the *pseudo-capacitance* $C_W(\omega)$, introduced by Warburg to explain the phase difference between the current and the tension, has led to expressions of the Nyquist plots, obtaned in the domain of very small radial frequencies ω, in good agreement with the experimetal data. Consider now the *multielectrode*:

$$\text{Pt} \left| \left[\text{Fe(CN)}_6\right]^{3-} / \left[\text{Fe(CN)}_6\right]^{4-}, \text{KCl} \right. \text{ (in excess), v ml (LD), } O_2 \text{ physically}$$

dissolved (3), where LD= liquid drug.

New additional reactions appear, and we don't know them. Therefore, it is necessary to give a criterion of classifying the drugs which doesn't imply the knowledge of the additional reactions. Consequently, we have considered that to explain the phase difference between the current and the tension, it is also correct to replace $C_W(\omega)$, either by a series arrangement $C^*_W(\omega)$, $L^*_W(\omega)$, or by a parallel one $C^{**}_W(\omega), L^{**}_W(\omega)$ of course, if one maintains the value of the impedance of $C_W(\omega)$. The quantities $C^*_W(\omega)$, $L^*_W(\omega)$, as well as $C^{**}_W(\omega), L^{**}_W(\omega)$ are *theoretical quantities* (i.e., not *real quantities*), but they permit to determine what values must have the quotients $L^*_W(\omega)/ C^*_W(\omega)$, or $L^{**}_W(\omega)/ C^{**}_W(\omega)$, for both, the *charge transfer*, and the *diffusion*, resistances of the multielectrode [3] regain the values corresponding to the dielectrode (1). In this way, *a criterion of classifying the medicaments, based on the values of above-mentioned quotients, has resulted*.

Keywords: electrochemical impedance spectroscopy, drug analysis

[a] *Babes-Bolyai University, Faculty of Chemistry and Chemical Engineering, Department of Physical Chemistry, 11 Arany Janos, Cluj-Napoca, Romania*

INTRODUCTION

In a series of papers, Bonciocat at al., have shown that the faradaic current density of an electrode redox reaction occuring with combined limitations of charge transfer and nonstationary, linear, semiinfinite diffusion, is the solution of an integral equation of Volterra type [1-7]. By solving this integral equation, new methods of direct and cyclic voltammetry, applicable in aqueous electrolytic solution, or in molten salts, have been developed [8-20]. Similarly, the above mentioned integral equation has led to a new approach to the Electrochemical Impedance Spectroscopy when only the charge transfer and diffusion limitations are present[21-23]. Very recently has been shown that the (E I S) method may have important applications in drug research [24,25].

Some results already obtained are needed to understand the development given in this paper. We briefly remind them, and for details, see [22,24]. They refer to *redox multielectrodes* and give the *parametric equation* of their Nyquist plots in the domain of very small frequencies (round $\nu = \dfrac{\omega}{2\pi}$ = 0.2Hz). The equation which we are interested in, is:

$$Re = R_{sol} + \left(\gamma R_{ct}\right) + \frac{J_1\left[\omega\left(t - \tau\right)\right]}{\sqrt{2\pi}}\left(\gamma\sigma\right)\omega^{-1/2} \tag{4}$$

Re represents the real part of the impedance of the measuring cell, ω the radial frequency of the alternating current, R_{sol} the solution resistance, τ the moment of the time when the *alternating overtension* is superposed over the *constant overtension* η, applied at t=0, and t is the time when the Nyquist plot recording ends. C_d represents the double layer capacity, and $J_1[\omega(t - \tau)]$ the Fresnel integral:

$$J_1\left[\omega\left(t - \tau\right)\right] = \int\limits_0^{\omega\left(t - \tau\right)} \frac{\cos x}{x^{1/2}}\,dx \tag{4'}$$

whose value tends to $\sqrt{\pi/2} \cong 1.253$ for sufficiently great values of the product $\omega(t - \tau)$.

$(\gamma\, R_{ct})$ and $(\gamma\, \sigma)$ express the *charge transfer*, respective *diffusion*, limitations, and they have the meanings:

$$\frac{1}{\left(\gamma R_{ct}\right)} = \frac{1}{\gamma_1 R_{ct1}} + \frac{1}{\gamma_2 R_{ct2}} + \dots \tag{5}$$

$$\frac{1}{\left(\gamma\sigma\right)} = \frac{1}{2}\left(\frac{1}{\gamma_1\sigma_1} + \frac{1}{\gamma_2\sigma_2}\dots\dots\right) \tag{5'}$$

where the terms in the right-hand sides of eqs.(5,5') refer to the individual electrode reactions occuring simultaneously at the interface. For the aim of this paper, it is not important to give their expressions.

The last term in eq.(4), represents the *Warburg diffusion resistance* $R_W(\omega)$ of the interface. It is an ohmical term that *doesn't introduce* a phase difference between the current and the tension. To explain the phase difference between the current and the tension, Warburg has introduced a *pseudo-capacitance* $C_W(\omega)$ in the series circuit by which represents the Faraday impedance of the interface:

$$Z_F \quad = \quad R_{ct} \quad R_W(\omega) \quad C_W(\omega) \tag{6}$$

$C_W(\omega)$ introduces a Warburg capacitive reactance $X_{C_W}(\omega)$ situated along the imaginary axes of the complex plane, and having the expression:

$$X_{C_W}(\omega) = -\frac{J_2[\omega(t-\tau)]}{\sqrt{2\pi}}(\gamma\sigma)\omega^{-1/2}j \tag{7}$$

where:

$$J_2[\omega(t-\tau)] = \int_0^{\omega(t-\tau)} \frac{\sin x}{x^{1/2}}dx \tag{7'}$$

Like the Fresnel integral (4'), also this Fresnel integral tends to $\sqrt{\pi/2}$, for sufficiently great values of $\omega(t-\tau)$.

From eq.(7) it fallows:

$$C_W(\omega) = \frac{1}{\omega|X_{C_W}(\omega)|} = \frac{\sqrt{2\pi}}{J_2[\omega(t-\tau)]} \cdot \frac{1}{(\gamma\sigma)\omega^{-1/2}} \cdot \frac{1}{\omega} \tag{8}$$

From the expressions of $R_W(\omega)$ (i.e., the last term in eq.(4)) and $C_W(\omega)$ one gets:

$$R_W(\omega)C_W(\omega) \cong \frac{J_1[\omega(t-\tau)]}{J_2[\omega(t-\tau)]} \cdot \frac{1}{\omega} \cong \frac{1}{\omega} \tag{9}$$

for times of recording sufficiently large

Concerning the electric scheme of the measuring cell needed to obtain the Nyquist plots, it refers only to the electrode under study, because the impedance of the reference electrode is practically equal to zero. Consequently,

in the scheme one must enter excepting the Faraday impedance Z_F (see (6)), the double layer capacity C_d and the resistance of the solution. Of course, this is an oversimplifyed scheme, but as we shall see, for the aim of this paper it is adequate.

Thus:

(I)
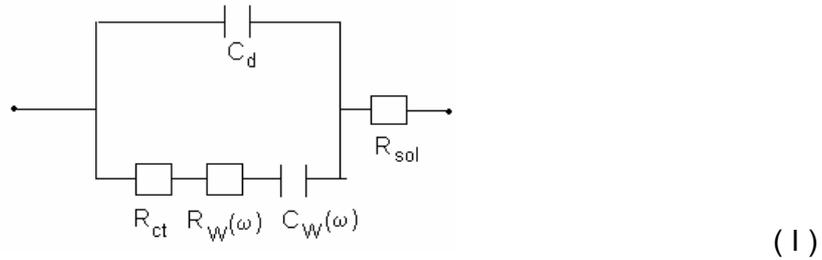
This scheme is considered to be adequate for the *reference redox dielectrode*; because the expressions of the Nyquist plots in the domain of very small values ω, obtained on its basis, have proved to be in good agreement with the experimental data.

To propose a criterion of classifying the drugs, we have considered other two schemes. In one, the pseudo-capacitance $C_W(\omega)$ is replaced by a series arrangement, $C^*_W(\omega),\ L^*_W(\omega)$, in the other, by a parallel arrangement $C^{**}_W(\omega), L^{**}_W(\omega)$, but maintaining the impedance of the Warburg pseudo-capacitance, i.e.,

$$Z_{C_W} = Z^*_{series} = Z^{**}_{parallel} \tag{10}$$

of course, the *charge transfer* resistance R_{ct}, and the *Warburg diffusion* resistance, $R_W(\omega)$ will change, becoming $R^*_{ct},\ R^*_W(\omega)$, respective R^{**}_{ct}, $C^{**}_W(\omega)$. Therefore, these two schemes are:

(I*)

respective

(I**)

34
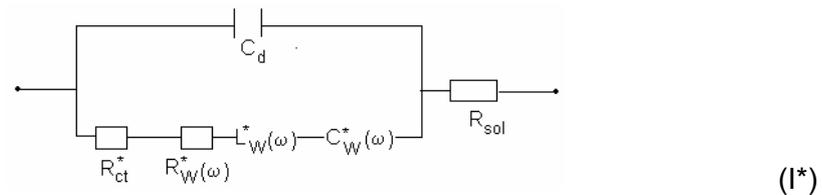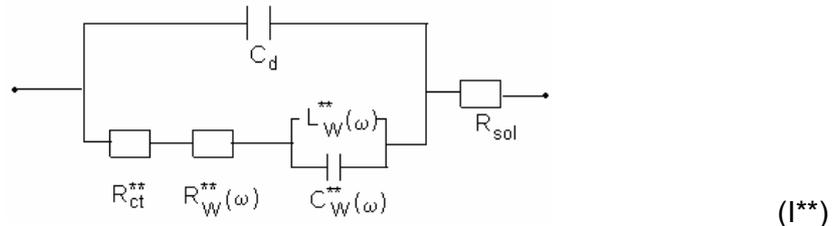
In addition, we shall consider that also the *total ohmical resistance* $R_{ct} + R_W(\omega)$ preserves its value, i.e.,

$$R_{ct} + +R_W(\omega) = R_{ct}^* + R_W^*(\omega) = R_{ct}^{**} + R_W^{**}(\omega) \tag{11}$$

THEORETICAL SECTION

The theoretical development given in this paper is based on the following idea: to explain the phase difference between the current and the tension, we shall use instead of *one theoretical quantity* (as the *pseudo-capacitance* $C_W(\omega)$ introduced by Warburg, *two theoretical quantities*, namely, a *pseudo-capacitance*, and a *pseudo-inductance*.

Because the phase differences introduced by these physical quantities are different, and depend on their arrangement, i.e., in series or in parallel, we shall analyse separately these two possibilities.

1. Characteristic quantities of the scheme (I^*) for very small ω

As one knowns, in the complex plane, the impedance of an inductance L is $\omega L j$, and of a capacitance C is $-\dfrac{1}{\omega C} j$. Then from the equality $Z_{C_W}(\omega) = Z_{series}(\omega)$ (see eqs.(10), one gets:

$$\left(\omega L_W^*(\omega) - \frac{1}{\omega C_W^*(\omega)} \right) j = -\frac{1}{\omega C_W(\omega)} j \tag{12}$$

i.e.,

$$\omega L_W^*(\omega) = \frac{1}{\omega C_W^*(\omega)} - \frac{1}{\omega C_W(\omega)} \tag{12'}$$

Because $\omega L_W^*(\omega)$ is a positive quantity, it follows:

$$\boxed{C_W^*(\omega) = \alpha^* C_W(\omega); \; \alpha^* < 1, \;\; \text{and} \;\; \omega L_W^*(\omega) = \frac{1 - \alpha^*}{\alpha^*} \cdot \frac{1}{\omega C_W(\omega)}} \tag{13}$$

Further, the product $R_W(\omega) C_W(\omega)$ depending only on ω (see eq. (9)), it is normal to consider that eq.(9) remains valid for the scheme (I^*) too. Then:

$$R_W^*(\omega) C_W^*(\omega) = R_W(\omega) C_W(\omega) \tag{14}$$

and therefore:

35

$$R_W^*(\omega) = \frac{1}{\alpha^*} R_W(\omega) \tag{15}$$

Coming back to eqs.(11) and using eq.(15), it results:

$$R_{ct}^* = \left(1 - \frac{1}{\alpha^*}\right) R_W(\omega) + R_{ct} \tag{16}$$

Let's write eq.(16) for multielectrodes and for $\omega_1 = 1.256 s^{-1}$. In addition, using the approximation:

$$J_1[\omega_1(t-\tau)] \cong \sqrt{\frac{\pi}{2}} \text{ , one gets:}$$

$$(\gamma R_{ct})^* = -\left(\frac{1-\alpha^*}{\alpha^*}\right) \frac{(\gamma\sigma)}{2\omega_1^{1/2}} + (\gamma R_{ct}) \tag{16'}$$

or:

$$R_{sol} + (\gamma R_{ct})^* = -\left(\frac{1-\alpha^*}{\alpha^*}\right)[0.446(\gamma\sigma)] + R_{sol} + (\gamma R_{ct}) \tag{17}$$

if one introduces the solution resistance too.

2. Characteristic quantities of the scheme (I^{**}), for very small ω

From the same eqs.(10) it follows $1/Z_{C_W} = 1/Z_{parallel}$, and thus:

$$\frac{1}{\omega L_W^{**}(\omega)j} + \omega C_W^{**}(\omega)j = \omega C_W(\omega)j \tag{18}$$

i.e.,

$$\frac{1}{\omega L_W^{**}(\omega)} = \omega C_W^{**}(\omega) - \omega C_W(\omega) \tag{18'}$$

$1/\omega L_W^{**}(\omega)$ being a positive quantity:

$$C_W^{**}(\omega) = \frac{1}{\alpha^{**}} C_W(\omega); \quad \alpha^{**} < 1, \text{ and}$$

$$\omega L_W^{**}(\omega) = \frac{\alpha^{**}}{1-\alpha^{**}} \cdot \frac{1}{\omega C_W(\omega)} \tag{19}$$

Further, eq.(9) remains valid for the scheme (I^{**}) too, and gives:

$$R_W^{**}(\omega)C_W^{**}(\omega) = R_W(\omega)C_W(\omega) \tag{20}$$

i.e.,

$$R_W^{**}(\omega) = \alpha^{**}R_W(\omega) \tag{20'}$$

Using eq.(20') to express the term $R_W^{**}(\omega)$, eq.(11) leads to:

$$R_{ct}^{**} = \left(1-\alpha^{**}\right)R_W(\omega)+R_{ct} \tag{21}$$

For $\omega_1 = 1.256 s^{-1}$ and $J_1\left[\omega_1(t-\tau)\right] \cong \sqrt{\pi/2}$, eq.(21), written for multielectrodes, takes the final form:

$$\boxed{R_{sol} + \left(\gamma R_{ct}\right)^{**} = \left(1-\alpha^{**}\right)\left[0.446\left(\gamma\sigma\right)\right]+R_{sol}+\left(\gamma R_{ct}\right)} \tag{22}$$

3. Estimation of $R_{sol} + (\gamma R_{ct})$ and $(\gamma\sigma)$

Suppose that the Nyquist plots are recorded using 10 points per decade, starting with $\nu_1 = 0.2 Hz$ and ending at 10^5 Hz. Then, the first point P_1 corresponds to $\omega_1 = 2\pi\nu_1 = 1.256 s^{-1}$, and the second point P_2 to $\omega_2 = \omega_1 10^{0.1} = 1.582 s^{-1}$.

Let's suppose that the intervals of time $(t - \tau)$ required to record the Nyquist plots are sufficiently great to be permitted the approximation $J_1\left[\omega_1(t-\tau)\right] \cong J_2\left[\omega_1(t-\tau)\right] \cong 1.253$. Then, writing eq.(4) for the two points P_1 and P_2, one gets:

$$\frac{Re(P_1)-X}{Re(P_2)-X} = \left(\frac{\omega_1}{\omega_2}\right)^{-1/2} ; \qquad X = R_{sol}+\left(\gamma R_{ct}\right) \tag{23}$$

and consequently:

$$\boxed{R_{sol}+\left(\gamma R_{ct}\right) \cong \left[Re(P_2)-\frac{Re(P_1)-Re(P_2)}{0.122}\right]} \tag{24}$$

where: $0.122 = (\omega_1/\omega_2)^{-1/2} - 1$.

Coming back to eq.(4), and using the expression(24) of $R_{sol}+(\gamma R_{ct})$, one gets:

$$(\gamma\sigma) \cong \frac{\sqrt{2\pi}\,\omega_1^{1/2}}{J_1[\omega_1(t-\tau)]}\left[Re(P_1)-Re(P_2)+\frac{Re(P_1)-Re(P_2)}{0.122}\right] \tag{26}$$

i.e.,

$$\left|(\gamma\,\sigma) \cong 20.6\,\left|Re(P_1) - Re(P_2)\right|\right| \qquad\qquad (26')$$

EXPERIMENTAL SECTION

Two liquid drugs have been tested: the Swedish Bitter (Original Schweden Tropfen, BANO) and the Energotonic complex (ENERGOTONIC-multivitamin complex, Plant Extract). The *reference redox dielectrode*(RRD) and the *multieletrodes* (i.e., RRD containing the respective liquid drug: Bitter or Energotonic) had the compositions given above (see (1 and 3)) we only mention that in all three cases the total volume has been V=300ml and v_{Bitter} = 50ml, respective $v_{Energotonic}$ = 20ml. In Table 1-3 are reproduced from the papers[24, 25] the horizontal coordinates of the points $P_1(\omega_1)$, $P_2(\omega_2)$ corresponding to the 12 Nyquist plots obtained experimentally (three values for the constant overtension η, and for each value of η four values for τ). Of course, these coordinates represent the real parts $Re(P_1)$, $Re(P_2)$, of the corresponding Niquist plots: -Im vs Re, and permit to get the values of $R_{sol} + (\gamma\,R_{ct})$, respective of $(\gamma\,\sigma)$, by using the formulae (24 and 26'). As one sees, there is a good compatibility betwen the values corresponding to a given value of η , but appear differences when one passes to an other value of η. However, in this paper we are not interested in explaining the origin of these differences. We are interested only in comparing the effect that the too drugs investigated have in changing the values $R_{sol} + (\gamma\,R_{ct})$ and $(\gamma\,\sigma)$ of the *reference redox dielectrode*. For this reason, and because the thee values of η are close values, we shall compare the mean values resulted by using all Nyquist plots.

Table 1.

Reference Redox Dielectrode R R D

η	τ	$Re(\omega_1)$	$Re(\omega_2)$	$R_{sol} + (\gamma R_{ct})_{RRD}$	$(\gamma\,\sigma)_{RRD}$
(V)	(s)	(Ω)	(Ω)	(Ω)	$(\Omega\,s^{-1/2})$
0	0	1368	1274	504	1938
0	10	1343	1242	414	2082
0	100	1324	1230	460	1938
0	1000	1299	1211	490	1814
-0.05	0	1838	1712	679	2597
-0.05	10	1838	1685	431	3154
-0.05	100	1820	1676	496	2968
-0.05	1000	1784	1646	515	2845
0.05	0	2703	2486	707	4473
0.05	10	2703	2486	707	4473
0.05	100	2703	2486	707	4473
0.05	1000	2689	2473	703	4453

Mean= 572   Mean= 3101

38

Table 2.

R R D Containing Swedish Bitter (B)

η (V)	τ (s)	$Re(\omega_1)$ (Ω)	$Re(\omega_2)$ (Ω)	$R_{sol} + (\gamma R_{ct})_B$ (Ω)	$(\gamma \sigma)_B$ ($\Omega\ s^{-1/2}$)
0	0	4236	3791	143	9173
0	10	4297	3851	195	9194
0	100	4419	3932	- 60	10039
0	1000	4595	4054	- 380	11152
-0.05	0	6495	5676	- 1037	16883
-0.05	10	6559	5707	- 1277	17563
-0.05	100	6559	5739	- 982	16903
-0.05	1000	6527	5739	- 720	16244
0.05	0	5676	4973	- 789	14492
0.05	10	5946	5243	- 519	14492
0.05	100	5946	5243	- 519	14492
0.05	1000	5838	5135	- 627	14492

Mean= - 548   Mean= 13760

Table 3.

R R D Containing Energotonic Complex (E)

η (V)	τ (s)	$Re(\omega_1)$ (Ω)	$Re(\omega_2)$ (Ω)	$R_{sol} + (\gamma R_{ct})_E$ (Ω)	$(\gamma \sigma)_E$ ($\Omega\ s^{-1/2}$)
0	0	1358	1273	576	1752
0	10	1325	1240	543	1752
0	100	1287	1197	459	1855
0	1000	1263	1178	481	1752
-0.05	0	2525	2323	667	4164
-0.05	10	2525	2313	575	4370
-0.05	100	2535	2333	677	4164
-0.05	1000	2535	2354	870	3731
0.05	0	1912	1771	615	2907
0.05	10	1926	1785	629	2907
0.05	100	1933	1798	691	2783
0.05	1000	1946	1805	649	2907

Mean= 619   Mean= 2920

1. Estimation of drugs effects

As one sees from the Tables1-3, the effects of the investigated drugs consist in changing the values of $R_{sol} + (\gamma R_{ct})_{RRD}$ and $(\gamma \sigma)_{RRD}$.

Because the RRD containing the drug investigated corresponds, either to a scheme of type (I^*), or to one of type (I^{**}), we shall estimate the effects of drugs by the values of the quotients $L_W^*(\omega_1)/C_W^*(\omega_1)$, or $L_W^{**}(\omega_1)/C_W^{**}(\omega_1)$ for which these schemes become equivalent to the scheme (I) corresponding to the RRD electrode.

Let's start with the Swedish Bitter. From table2, one sees that the mean value of $R_{sol} + (\gamma R_{ct})_B$, i.e., -548Ω, is less than the mean value of $R_{sol} + (\gamma R_{ct})_{RRD}$, equal to 572$\Omega$ (se Table 1). Consequently, it must *increase* to 572Ω, and equation (22) shows that this increase implies *a parallel arrangement* (i.e., a *scheme* I**) and a value α_B^{**} given by:

$$1 - \alpha_B^* = \frac{[R_{sol} + (\gamma R_{ct})_{RRD}] - [R_{sol} + (\gamma R_{ct})_B]}{0.446 (\gamma \sigma)_{RRD}} =$$

$$\frac{572 + 548}{0.446 \cdot 3101} = 0.810 \tag{27}$$

In the case of Energotonic complex, Table 2 shows that the mean value $R_{sol} + (\gamma R_{ct})_E$ =619Ω must *decrease* to 572Ω, and equation (17) shows that this decrease implies *a series arrangement* (i.e., a *scheme* I**), and a value α_E^* given by:

$$1 - \frac{1}{\alpha_E^*} = \frac{[R_{sol} + (\gamma R_{ct})_{RRD}] - [R_{sol} + (\gamma R_{ct})_E]}{0.446 \cdot (\gamma \sigma)_{RRD}} =$$

$$\frac{572 - 619}{0.446 \cdot 3101} = -0.034 \tag{28}$$

Therefore, eqs.(27 and 28) give: $\alpha_B^{**} = 0.190$ and $\alpha_E^* = 0.967$

2. The proposed criterion of classifying the drugs

From eqs.(13) written for $\alpha^* = \alpha_E^*$, $\omega = \omega_1$ and $J_1[\omega_1(t - \tau)] \cong \sqrt{\pi/2}$ one gets:

$$\lambda_E^*(\omega_1) = \frac{L_W^*(\omega_1)}{C_W^*(\omega_1)} = \frac{1 - \alpha_E^*}{(\alpha_E^*)^2} \cdot \left[\frac{1}{\omega_1 C_W^*(\omega_1)}\right]^2 =$$

$$\frac{1 - \alpha_E^*}{(\alpha_E^*)^2} \cdot [0.446 (\gamma \sigma)_{RRD}]^2 \tag{29}$$

and similarly, from eqs.(19), results:

$$\lambda_B^{**}(\omega_1) = \frac{L_W^{**}(\omega_1)}{C_W^{**}(\omega_1)} = \frac{(\alpha_B^{**})^2}{1 - \alpha_B^{**}} \cdot [0.446 (\gamma \sigma)_{RRD}]^2 \tag{30}$$

Introducing the values of α_E^* and α_B^{**}, the proposed criterion takes for two drugs investigated the values:

$$\lambda_E^*(\omega_1) = 67505\,\Omega^2; \qquad \lambda_B^{**}(\omega_1) = 85259\,\Omega^2 \qquad (31)$$

CONCLUDING REMARKS

1. $L_W^*(\omega_1)$ $C_W^*(\omega_1)$ and $L_W^{**}(\omega_1)$, $C_W^{**}(\omega_1)$ play the role of *theoretical quantities* that have permitted to develop *an advantageous physico-mathematical deduction* of the proposed *criterion of classifying the drugs*.
2. The proposed criterion is a *qualitative* one, because it divides the drugs into two classes, (I^*) or (I^{**}) depending on what type of arrangement is necessary to estimate their action, i.e., a *series* or a *parallel* arrangement; it is also a quantitative criterion, because it estimates numerically these actions by the values $\lambda^*(\omega_1)$ or $\lambda^{**}(\omega_1)$.
3. For a drug that *has no effect*, α^* and α^{**} are equal to unity. Consequently, for such a drug, $\lambda^*(\omega_1) = 0$, and $\lambda^{**}(\omega_1) = \infty$. It fallows that for a drug belonging to the class (I^*), the *greater* the value of $\lambda^*(\omega_1)$, the *greater* is its effect, and for a drug belongingto the class (I^{**}), the *smaller* the value of $\lambda^{**}(\omega_1)$, the *greater* is its effect.

The values resulted for the two drugs investigated, i.e., $\alpha_E^* = 0.957$, respective $\alpha_B^{**} = 0.190$, show that the Energotonic complex has a *much smaller effect than the Swedish Bitter*, because α_E^* is very close to unity, while α_B^{**} is more close to zero than to unity. The values resulted for $\lambda_E^*(\omega_1)$ and $\lambda_B^{**}(\omega_1)$ lead to the same conclusion, because $\lambda_E^*(\omega_1)$ is more close to zero than $\lambda_B^{**}(\omega_1)$ to infinity.

REFERENCES

1. N. Bonciocat, S. Borca, St. Moldovan*, Bulgarian Academy Scientific Communication*, **1990**, *23*, 289.
2. A. Cotarta, Ph.D Thesis, Chemical Research Institute, Bucharest, **1992**.
3. N. Bonciocat, *Electrokhimiya*, **1993**, *29*, 92.
4. N. Bonciocat, ''Electrochimie si Aplicatii'', Dacia Europa - Nova, Timisoara, **1996**, chapter 5.

5. N. Bonciocat, A. Cotarta, *Revue Roumaine de Chimie*, **1998**, *43*, 925.

6. N. Bonciocat, A. Cotarta, *Revue Roumaine de Chimie*, **1998**, *43*, 1027.

7. N. Bonciocat, "Alternativa Fredholm in Electrochimie", Editura MEDIAMIRA, Cluj-Napoca, **2005**, chapter 2.

8. N. Bonciocat, "Electrochimie si Aplicatii", Dacia Europa-Nova, Timisoara, **1996**, cap.6, 268.

9. N. Bonciocat, "Electrochimie si Aplicatii", Dacia Europa-Nova, Timisoara, **1996**, chapter 6.

10. A. Radu (Cotarta), Ph.D. These, Institut National Polytechnique de Grenoble, **1997**.

11. N. Bonciocat, A. Cotarta, "A new approach based on the theory of variational calculus in studying the electrodeposition process of chromium in the system $Cr^0/CrCl_2$, LiCl-KCl", *Contract Copernicus 1177-2* "Utilisation de sels fondus en metallurgie", Final Report of European Community, July 1998.

12. I. O. Marian, E. Papadopol, S. Borca, N. Bonciocat, *Studia Universitatis Babes-Bolyai, Cluj Napoca, Seria Chemia*, **1998**, *43*, 91.

13. N. Bonciocat, *Scientific Bulletin Chemistry Series Politechnica University Timisoara*, **1998**, *43*(57), 5.

14. N. Bonciocat, "*Alternativa Fredholm in Electrochimie*", Editura MEDIAMIRA, Cluj-Napoca, **2005**, chapter 5.

15. N. Bonciocat, E. Papadopol, S. Borca, I. O. Marian, *Revue Roumaine de Chimie*, **2000**, *45*, 981.

16. N. Bonciocat, E. Papadopol, S. Borca, I. O. Marian *Revue Roumaine de Chimie*, **2000**, *45*, 1057.

17. I. O. Marian, R. Sandulescu, N. Bonciocat, *Journal of Pharmaceutical and Biomedical Analysis*, **2000**, *23*, 227.

18. I. O. Marian, N. Bonciocat, R. Sandulescu, C. Filip, *Journal of Pharmaceutical and Biomedical Analysis*, **2001**, *24*, 1175.

19. N. Bonciocat, A. Cotarta, J. Bouteillon, J. C. Poignet, *Journal of High Temperature Material Processes*, **2002**, *6*, 283.

20. N. Bonciocat, I. O. Marian, R. Sandulescu, C. Filip, S. Lotrean *Journal of Pharmaceutical and Biomedical Analysis*, **2003**, *32*, 1093.

21. N. Bonciocat, "Alternativa Fredholm in Electrochimie", Editura MEDIAMIRA, Cluj-Napoca, **2006**, chapter 2.

22. N. Bonciocat, A. Cotarta, "*Spectroscopia de Impedanta Electrochimica in cazul limitarilor de transfer de sarcina si difuziune*", Editura Printech, Bucuresti, **2005**, chapter 9.

23. N. Bonciocat, I. O. Marian, "*Metoda Impedantei Faraday si variantele sale*", Presa Universitara Clujeana, **2006**, chapter 5.

24. N. Bonciocat, A. Cotarta, *Annals of West University of Timisoara, Series Chemistry,* **2006**, *15*(2), 137.

25. N. Bonciocat, A. Cotarta, *Revista de Chimie*, **2008**, *in press*.

In memoriam prof. dr. Liviu Oniciu

PHOTOCONDUCTIVE PROPERTIES OF CdS ELECTRODEPOSITED THIN FILMS

CARMEN ROBA[a], LIVIU DOREL BOBOS[b], ANDREEA OLTEAN[b], IULIU-OVIDIU MARIAN[b], BARBU-RADU-HORATIU MISCA[b], DORIN MANCIULA[a]

ABSTRACT. CdS films electrodeposited on ITO substrate were investigated from optical and electrical point of view. Spectra present a maximum in red domain at 734.5 nm and 732.5 nm respectively. The electro deposited films are photo sensible. Static characteristics are linear in normal conditions of temperature and the non-radiative recombination plays a small role within the photoconduction processes.

Keywords: *CdS electrodeposited films, photoconduction*

INTRODUCTION

Thin films of metallic chalcogenides represent a new field of investigation for functional devices technologies at large scale. The importance of these layers in the construction of photo resistors, laser diode and some integrated structures are crucial. Photoconductive CdS films were usually deposited on metallic or insulated substrates by sputtering, using mixtures of Ar-H_2S as sputtering gas in a diode system on suitable cleaned substrate [1]. Non-vacuum methods are susceptible to contamination. The electrochemical deposition was reported in literature [2-4]. The major advantage is the low cost of this procedure.

In this paper were analyzed some spectral and electrical properties of thin electrodeposited films. All electrochemical parameters such as deposition potential, cathodic current and the rate of deposition were recently reported [5]. The deposited CdS film has shown a good adherence to ITO substrate due to its texture and preliminary electrochemical procedures to obtain the optimum storage. Optical and microscopically inspection confirm the uniformity of electro deposition.

---

[a] *Babeş-Bolyai University, Faculty of Environmental Sciences; Romania, Cluj-Napoca, No. 4 Stefan cel Mare Street*

[b] *Babeş-Bolyai University, Faculty of Chemistry and Chemical Engineering, Romania, Cluj-Napoca, No. 11 Arany-Janos, e-mail: iomar@chem.ubbcluj.ro*

RESULT AND DISCUSSIONS

The absorption of radiation, which generates the non-equilibrium carriers, leads to the appearance of additional conductivity usually call photoconductivity.

Two samples with rectangular geometries, P_1 (1/2 cm) and P_2 (5/6 mm) were investigated in order to determinate the ohmic resistance of CdS film in light and dark conditions. The ohmic contacts were made by using Ag Degussa conductive pasta and two Cu terminals in order to observe the longitudinal photoconduction.
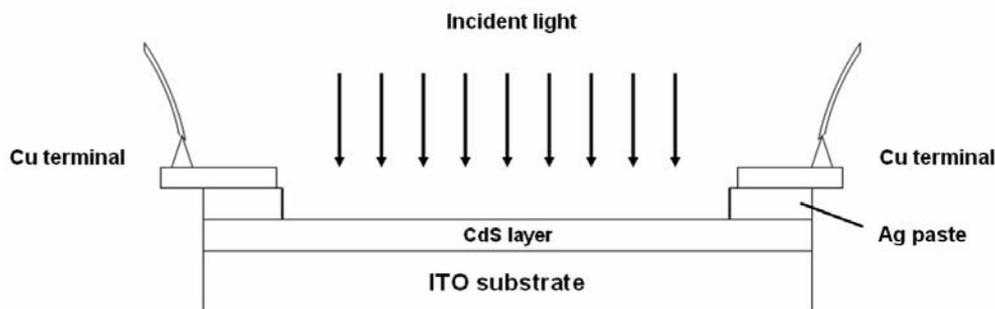
Figure 1. The electrodeposited sample (cross section view)

Determinations carried out on two samples in dark and light conditions in absence of polarization, were obtained at small interval of time (5-10 s) and at small incident flux (power density 0.6 W/cm^2). In these conditions, it had not been observed a notable ohmic resistance variation due to the free way of photo-generated carriers or because of intercrystallite barriers if these exist. However, the small ohmic resistance values of the electrodeposited (P_1 and P_2) film are uncommon when these are compared with commercial one (20 M Ω). This situation is generated probably by some structural defects or under the influence of the material composition. Some properties (bulk resistance), can be masked by the contamination of the outermost film layer. The structural defects perhaps act like a trap for the charge carriers.

It has been noticed that the illumination time (5 - 10 s) did not influence the photo sensible layer ohmic resistance (102 Ω for (P_1) and 69 Ω for (P_2)). The differences between values are due to different geometry of films.

A homemade lineament device with 5 mm diameter diaphragm was attached to the spectrophotometer. The spectrum was realized by comparing the CdS film deposited onto ITO substrate to ITO substrate free of CdS films. A large band in red domain and NIR was thus observed (Fig.2). The different

absorbance data comes from different thickness of investigated films P_1(Abs = 0.1681 at 734.5 nm) and P_2(Abs = 0.1407 at 732.5 nm). A small drift appears in spectrum at P_1 toward NIR (842 nm) as compaired to P_2 (832 nm). This observation confirms different geometry but also different superficial aggregation.
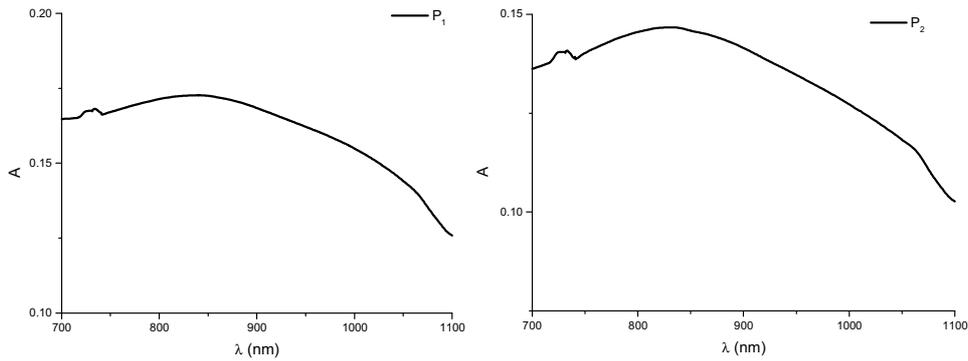

Figure 2. The spectral characteristics of the investigated CdS films

The assertive convention of polarization was selected due to symmetry of static characteristic in connection with coordinate axis. The current - voltage dependence is linear in both conditions (absence or presence of illumination) in normal temperature conditions:

$$I = I_0 + I_L = (C_0 + C_f \Phi)\, U.$$

The flux modification induces only different slope in static characteristics, where I_L, I_0 is the current in light and dark conditions, C_0, C_f constants that are determined by physical properties and constructive characteristics of the photo-sensible film and U the polarization tension. Also in this relation, the incident flux Φ plays an important role. By using the small polarization voltage and IR filter, we were able to avoid the intense field or the excessive heating of the photo sensible film.

A photo response was recorded for 30 s illumination time at each value of polarization voltage (Fig.3). The non-radiative contribution at photoconduction phenomenon due to carrier recombination led to a difference of only 0.01 degree for three selected wavelengths in red domain (700 nm, 730 nm, 760 nm).

To verify the film stability, static characteristic and the ohmic resistance of sample have been measured again after a month period. Deviations from traced spectrum have not been observed. This observation had demonstrated that aging phenomenon during this period does not appear. Because the films

were kept in special enclosures, the danger of contamination was eliminated. The areas where the Ag diffusion it is possible, refers to the specific regions of the ohmic contacts. Is also possible the indium diffusion from ITO substrate to CdS layer. To observe this phenomenon, supplementary analytical investigations are necessary to be made in the specific zone.
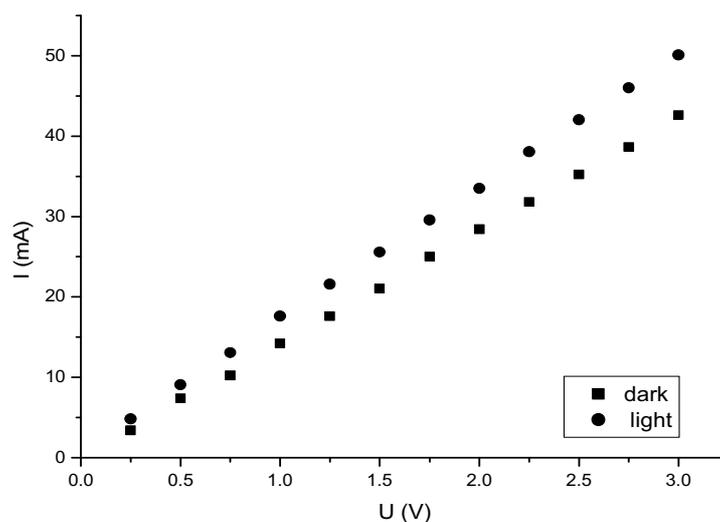

Figure 3. The static characteristic of P_1 film in light and dark conditions.

CONCLUSIONS

Two CdS films electrodeposited on ITO substrate, with different rectangular geometries (2 cm^2 and 0.30 cm^2) were investigated from optical and electrical point of view. Spectra present a maximum in red domain. The electro deposited films are photo sensible. Static characteristics are linear in normal conditions of temperature and the non-radiative recombination plays a small role within the photoconduction processes.

EXPERIMENTAL SECTION

The deposition process was achieved in solutions containing $CdSO_4$ and $Na_2S_2O_3$ ($Cd_2^+/S_2 O_3^{2-}$ ratios of 2/1 and 200/1), at pH 3, on ITO glass previously cleaned by ultrasonnation for 15 minutes, in a 1:1 acetone-ethanol mixture.

The ohmic resistance of electrochemical deposited film was measured with a digital ohmmeter in both dark and light conditions (the incident light flux for illumination conditions was supplied by 30 W Hg source). Using the Able-Jasco V-530 spectrometer attained the spectral characteristics of the examined thin films. The static characteristics I = f (U) and the contribution of non-radiative recombination was obtained by using a digital device [6]. Changing of temperature was observed without polarization, in monochromatic conditions. The red domain for the recombination contribution was selected with a Specol monochromator.

REFERENCES

1. D. B. Frazer, H. Melchior, *Journal of Applied Physics*, **1972**, *43*, 3120.

2. S. Denisson, *Journal of Material Chemistry*, **1994**, *4*, 41.

3. V. I. Birss, L. E. Kee, *Journal of Electrochemical Society*, **1986**, *133*, 2097.

4. J. Nishino, S. Chatani, Y. Uotami, Y. Nosaka, *Journal of Electrochemical Society,* **1999**, *473*, 217.

5. D. Gligor, L. Muresan, L. D. Bobos, I. C. Popescu, *Studia Universitatis Babes-Bolyai, Chemia*, **2004**, *49*, 137.

6. M. Barau, M. Crisan, M. Gartner, A. Jitianu, M. Zaharescu, A. Ghita, V. Cosoveanu, V. Danciu, O. I. Marian*, Journal of Sol-Gel Science and Technology*, **2006**, *37*, 175.

In memoriam prof. dr. Liviu Oniciu

NANO- AND MICROPARTICLE DISTRIBUTION ON SOLID AND FLEXIBLE SUBSTRATES – PART I

DORIN MANCIULA[a,b], IULIU-OVIDIU MARIAN[b], BARBU-RADU-HORATIU MIŞCA[b]

ABSTRACT. By using the self-assembling process, it is possible to generate a large number of various structural organizations in which individual elements get together into regular patterns under suitable conditions. Two-dimensional self-assembled networks placed on solid and flexible substrates were obtained from solutions containing nano- and micro sized polymer spheres by evaporating the solvent in proper environmental conditions. The entire procedure is uncomplicated and it has been demonstrated as readily reproducible. The parameters used for the duration of the process are as well very easy to control.

Key words: nanotechnology, self-assembly, nano/microparticles

INTRODUCTION

Nanotechnology represents a large scientific domain and moreover a multidisciplinary field which combines varied concepts from different areas, such as supramolecular chemistry, applied physics, functional devices, materials and colloidal science [1]. Moreover, this area is mainly centered on the study, synthesis, design, and characterization of nanoscale materials, which are close related to many modern technologies in use today. Developments in the field of nanotechnology also serve as useful tools in other research fields such as biology, chemistry and physics [2-6]. Many materials properties change radically at small length scales. The phenomena, which occur at the nanoscale level, can lead to creation of materials that may display new properties in comparison to the properties they exhibit on a macro scale level. Many research fields are able today to study and develop different

[a] *Babeş-Bolyai University, Faculty of Environmental Sciences; Romania, Cluj-Napoca, No. 4, Stefan cel Mare Street, Postal code 400192, Tel: +40 264-405 300, Fax: +40 264-599 444; e-mail: dimro21@googlemail.com*

[b] *Babeş-Bolyai University, Faculty of Chemistry and Chemical Engineering, Romania, Cluj-Napoca, No. 11 Arany-Janos, Postal code 400028, Tel: +40 264-593833, Fax: +40 264-590 818*

categories of materials that demonstrate distinctive properties due to their small dimensions. Carbon nanotubes [7], nanoparticles [8], nanorods [9], and various nanoscale materials [10] that can be successfully used for bulk and for medical applications, especially in nanomedicine [11] and microelectronics [12] give some common examples of such materials. In addition, a large interest now is focused on the colloid science, which has given the opportunity to enlarge the number of materials with practical relevance in the field of nanotechnology and numerous examples of nanotechnology in modern use can be mentioned today. Some of the most common nanotechnological applications of different types of nano- and micro scaled materials, consists of particle insertion in cosmetics, food products, paints and different category of plastic materials which can be used for instance in food packaging, cloth making or for coating various surfaces and furthermore for producing various types of surfaces, fuel catalysts and also disinfectants. [13,14]. In this paper are presented several methods, which were used to obtain two-dimensional self-assembled networks placed on solid substrates from solutions containing nano- and micro sized polymer spheres.

RESULTS AND DISCUSSION

Self-assembling during solvent evaporation is a simple and low cost technique, frequently used for 2D and 3D assembly of colloidal crystals. It is possible to grow millimeter-sized arrays and to control the thickness of the array by varying the initial concentration of the suspension for each method used. The particle distribution results for each method used are presented next. The outcome generated by using the spin casting of the liquid suspension is depicted in figure 1. Good results were obtained for spheres of smaller sizes (200-500 nm) using this technique.
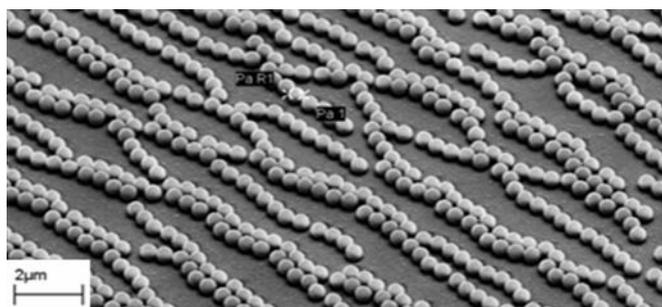

Figure 1. Polymer bead layer prepared by spin coating
on glass substrate.

50

For the fabrication of a two-dimensional monolayer, the solvent was evaporated in two modes, either by using a heating oven (65°C for 8h), or at room temperature (24h) by tilting the substrates at a small angle (2-20°) between the normal surface and gravity, to induce particle arrangement. Substrates free of impurity were used immediately after they were cleaned. For the situation of particle self-assembling by means of suspension evaporation within the heating oven, the structure of the self-assembled aggregate depends on the rate of solvent evaporation. A slow evaporation of the solvent leads to ordered colloidal crystals (figure 2).
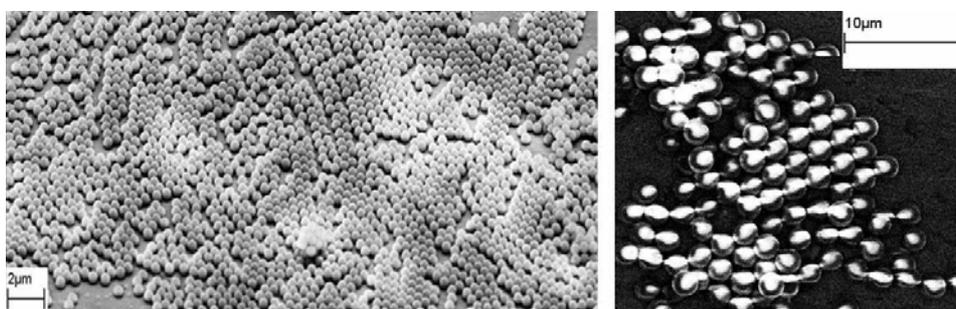
Figure 2. Monolayer formation following the suspension evaporation on glass (left) and polystyrene (right).

By tilting the substrates, the gravity acts as an additional force affecting the template and influencing the arrangement of the particles (figure 3).
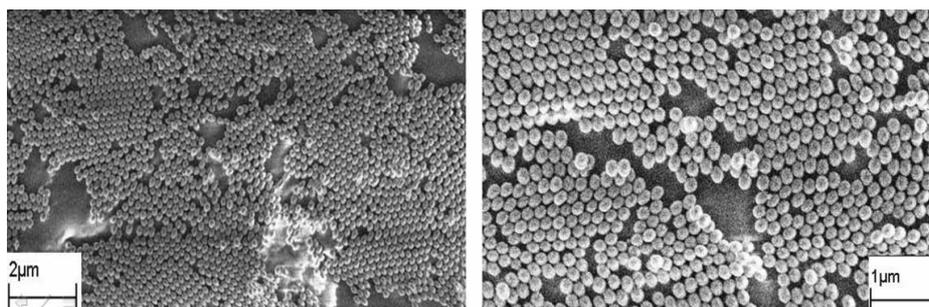
Figure 3. Monolayer formation following the suspension evaporation on tilted glass (left) and polystyrene (right).

The spacing and the distribution of the micro spheres are influenced by the sizes and deposition times of the micro beads. Longer deposition times lead to a close agglomeration of the beads, especially for spheres of

51

smaller sizes (200-500nm), without generating a monolayer of highly ordered hexagonal closely-packed micro-beads, while for spheres with wider diameters (3-5µ) an "island" agglomeration is generated. A shorter deposition time is responsible for increased space between the spheres on the substrate. The higher the tilting angle is, the more defects seen during the distribution, along with the multilayer formation. A high concentration of the suspension may also lead to defects in multilayer formation. Therefore, a small value (max. 2% solid content in the aqueous solution/suspension) has been chosen for substrate deposition via solvent evaporation.

By using the dipping technique, a well-distributed monolayer of highly ordered, hexagonal, closely packed micro beads can be generated (figure 4). To achieve a good distribution, particles must be monodispersed and must be absorbed onto the substrate. Several other conditions must also be met, such as a good suspension quality, a stable atmosphere around the cell and a good substrate quality. The dipping speed has a strong influence over the monolayer formation. A high dipping speed may lead to a multilayer deposition over the substrate, while a lower dipping speed might not be adequate enough for generating a close-packed monolayer.
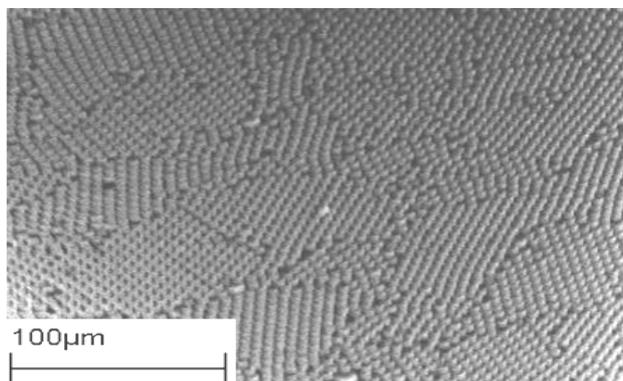

Figure 4. Particle monolayer produced on glass
by means of dip-coating process

The interactions of the particles that were deposited onto the surface can be attributed to electrostatic and lateral capillary forces that are able to influence adjacent particles and cause them to be attracted to each other, forming two-dimensional arrays of dense hexagonal packing. To form fine particle monolayer on large-sized areas, the quality of the suspension has to be also considered. After forming and drying, the micro-sized monolayer particle arrays display a radiant iridescent coloring when illuminated in white light.

52

CONCLUSIONS

Two-dimensional self-assembled networks and configurations made of nano- and micro-sized polymer spheres may be simply obtained from a solution containing the polymer spheres. Ordered configurations are obtained by means of solvent evaporation under proper experimental conditions. The driving force of the process is the capillary interaction, but the basic condition for having a superior self-assembled structure into an ordered pattern is the simultaneous presence of long-range repulsive and short-range attractive forces. The self-assembly procedure can be easily influenced by external parameters and therefore the sensitivity to environmental perturbations may lead to visible changes in the final structure or even compromise it. The solvent evaporation rate must not unfold too rapidly, to avoid generating instabilities and defects that may arise within the array. Particle concentrations and solvent composition may also play an important role in determining particle deposit morphologies. The substrate immersion within the colloidal solution was considered to be the best methods for preparing a high quality and well ordered monolayer.

EXPERIMENTAL SECTION

As solid substrates during the experiments, microscope glass slides and polystyrene Petri dishes were used. For preparing the substrates, which holds the micro bead monolayer, several consecutive steps were followed. A substrate clean up has been completed in the beginning of the experiment. All glass substrates were cleaned with a solution consisting of 3:1 mixture of sulfuric acid and 30% hydrogen peroxide, for 3h and then rinsed with de-ionized water and dried. The Petri dishes were made from clear polystyrene and were clean and sterilized. Several procedures were afterward tested to the successful distribution of the micro beads onto the substrates.

A two-dimensional monolayer of polymer beads (1µm) was prepared first by spin casting the liquid suspension onto the glass substrate at 1700 rpm for 20 seconds. The next effort for the fabrication of a two-dimensional monolayer array consists of accumulating the nano/micro spheres into a closely packed arrangement, onto both a cleaned glass surface and a dirt free polystyrene substrate (Petri dish) by evaporating the suspension into a heating oven at 65°C for 8 hours. The suspension evaporation was also completed by tilting a glass substrate at room temperature at a small angle between the normal surface and gravity. Nano- and micro particle monolayer can also be obtained by using the particle self-assemble procedure on vertical substrates, by means of solvent evaporation as the driving force behind the fabrication process.

During the experiments, the following equipments and materials were used: inverted Axio Observer microscope (Zeiss), scanning electron microscope (SEM) Gemini 1530 (Zeiss), microscope slides (76x26mm), cover-

slips (24x50mm); polyMMA micro beads (BASF): particle size 200nm and solid content of 24.5%; polystyrene-co-MMA (BASF): particle size 200nm, 80% MMA, 20% styrene and 24.6% solid content; polystyrene (BASF): particle size 1μm, solid content: 9.4%; polystyrene micro spheres (Polysciences, Inc.). The concentrations of the polystyrene micro sphere solutions used for the duration of experiments are presented in table 1.

Table 1.

Polystyrene nano/micro spheres used during experiments

Diameter (μ)	Concentration (%)		
0.202	2.56	2.61	2.67
0.465	2.62	2.65	
0.477	2.69		
0.495	2.66		
0.987	2.54		
0.989	2.60	2.69	
1.091	2.76		
1.826	2.70		
5.658	2.65		

REFERENCES

1. Q.Yan, F.Liu, L.Wang, J.Y. Leea, X.S. Zhao, *Journal of Material Chemi*stry, **2006**, *16*, 2132.

2. F. Wang, A. Lakhtakia, ''Selected papers on nanotechnology: Theory and modeling'', SPIE Press, **2006**, pp. 182.

3. M.B. David, ''Nano-hype: The truth behind the nanotechnology'', Prometheus Books, **2006**, pp.185.

4. J.D. Shanefield,'' Organic additives and ceramic processing'', Kluwer Academic Publishers, **1996**, pp. 115.

5. H. Geoffrey, M. Michael,'' Nanotechnology: Risk ethics and law'', Earthscan Publications, **2006**, pp. 3.

6. A. Lakhtakia, ''The handbook of nanotechnology, Nanometer Structures, Theory, modeling, and simulation'', SPIE Press, **2004**, pp.26.

7. D. Srivastava, C. Wei, K. Cho, *Applied Mechanics Reviews*, **2003**, *56*, 215.

8. V.J Mohanraj, Y. Chen, *Tropical Journal of Pharmaceutical Research*, **2006,** *5*, 561.

9. P.I. Wang, Y.P. Zhao, G.C. Wang, T.M. Lu, *Nanotechnology*, **2004,***15*, 218.

10. B. Baretzky, M.D. Baró, G.P. Grabovetskaya, J. Gubicza, M.B. Ivanov, *Revue of Advanced Materials Science*, **2005**, *9*, 45.

11. F.A. Robert, Jr., *Journal of Computational and Theoretical Nanoscience*, **2005**, *2*, 1.

12. A.S. Dimitrov, K. Nagayama, *Langmuir,* **1996**, *12*, 1303.

13. H.M. Peter, B.H. Irene, V.S. Oleg, *Journal of Nanobiotechnology*, **2004**, *2*,12.

14. F. Buentello, D. Persad, B. Erin, M. Douglas, S. Abdallah, P. Singer, *PLoS Medicine*, **2005**, *2*, 300.

In memoriam prof. dr. Liviu Oniciu

AMPEROMETRIC BIOSENSOR FOR ETHANOL BASED ON A PHENOTHIAZINE DERIVATIVE MODIFIED CARBON PASTE ELECTRODE

DELIA GLIGOR[a,*], ELISABETH CSOREGI[b], IONEL CATALIN POPESCU[a]

ABSTRACT. A new amperometric biosensor for ethanol, based on carbon paste electrode modified with alcohol dehydrogenase (ADH), polyethylenimine (PEI) and using a phenothiazine derivative (DDDP; 16H,18H-dibenzo[c,1]-7,9-dithia-16,18-diazapentacene) as redox mediator for NADH recycling, was developed. The biosensor response is the result of mediated oxidation of NADH, generated in the enzymatic reaction between ADH and ethanol (in the presence of NAD$^+$). The biosensor sensitivity (calculated as the ratio I_{max}/K_M^{app}) was 0.035 mA M^{-1} and the detection limit was 0.26 mM, while the linear response range was from 0.1 to 20 mM ethanol.

Keywords: *amperometric biosensors, alcohol dehydrogenase, ethanol, nicotinamide adenine dinucleotide, phenothiazine derivative, polyethyleneimine, modified carbon paste electrodes.*

INTRODUCTION

Nicotinamide adenine dinucleotide (NAD$^+$/NADH) dependent dehydro-genases catalyze the oxidation of compounds of great interest in analysis, such as carbohydrates, alcohols and aldehydes. Selective, sensitive and simple devices for the monitoring of ethanol are required from different fields such as biotechnology, food and clinical analysis [1] and, consequently, a lot of biosensors for ethanol detection were proposed [1-15].

Because the direct electro-oxidation of NADH, required for its recycling in biosensor functioning, involves high overpotentials on conventional electrodes [16-18], many efforts were directed towards discovering and characterizing new efficient electrocatalysts [19,20]. Among the most frequently investigated mediating schemes are those based on the direct adsorption of electron mediators onto electrode surface to obtain modified electrodes with electrocatalytic activity for NADH oxidation [21].

[a,*] *Department of Physical Chemistry, Babes-Bolyai University, 400028 Cluj-Napoca, ROMANIA; e-mail address: ddicu@chem.ubbcluj.ro*
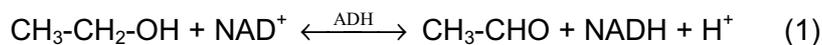[b] *Department of Analytical Chemistry, Lund University, P.O. Box 124, SE-22100 Lund, Sweden*

Taking advantage of their remarkable strong adsorption on graphite surface associated with high electrocatalytic efficiency, organic dyes, i.e. phenazines, phenoxazines and phenothiazines derivatives were extensively used as electrocatalysts for NADH oxidation [22-24]. Continuing our preoccupation in this domain [13,25] and taking advantage of a new phenothiazine derivative, 16H,18H-dibenzo[c,1]-7,9-dithia-16,18-diazapentacene (DDDP), which was successfully used to design efficient electrocatalytic schemes for NADH recycling [26-28], the possibility to develop a simple and inexpensive biosensor for ethanol determination, by immobilization of alcohol dehydrogenase and polyethylenimine (PEI) on carbon paste modified with DDDP, was investigated.

RESULTS AND DISCUSSIONS

1. Bioelectrocatalysis at DDDP modified carbon paste electrodes

In alcohol dehydrogenase (ADH) based biosensor, the enzyme catalyzes the oxidation of ethanol to acetaldehyde, in the presence of nicotinamide adenine dinucleotide (NAD$^+$) and the reduced NADH can be detected amperometrically, according to the following reactions:

$$CH_3\text{-}CH_2\text{-}OH + NAD^+ \xleftarrow{\quad ADH \quad} CH_3\text{-}CHO + NADH + H^+ \quad (1)$$

$$NADH + M_{ox} \longrightarrow NAD^+ + M_{red} + H^+ \quad (2)$$

$$M_{red} \longrightarrow M_{ox} + 2e^- + H^+ \quad (3)$$

This approach has some important characteristics for ethanol monitoring in real samples, because it is not oxygen dependent and is more selective for ethanol [11].

In the present case, ADH and the oxidized form of DDDP (as electrocatalyst) are both present in the carbon paste, whereas NAD$^+$ is dissolved into the electrolyte solution. When ethanol is added to the stirred solution contacting the biosensor, the enzymatic reaction 1 occurs and NADH diffuses to the DDDP-modified carbon paste electrode, where it is catalytically oxidized back to NAD$^+$ (reaction 2). The electrochemical re-oxidation of the mediator (reaction 3) yields an analytical signal proportional to the rate of ethanol oxidation, which itself is proportional to the ethanol concentration if the concentrations of the other reactants are kept constant and ADH is unsaturated. A steady state current will be achieved if the enzyme and mediator are efficiently retained in the carbon paste electrode and the reaction rates of reactions 2-3 are high enough, allowing a continuous and fast recycling of NAD$^+$.

Electrical communication of the redox-active center of enzymes with an electrode surface is a fundamental element for the development of amperometric biosensor devices [30]. For this reason carbon paste was chosen as electrode material for ADH immobilization. In a previous work [28] it

was demonstrated that the DDDP-modified carbon paste electrode (DDDP-CPEs) can efficiently catalyze the oxidation of NADH. The present results show that the DDDP-CPEs can also catalyze the oxidation of enzymatically generated NADH from the reaction of NAD^+ and ethanol catalyzed by ADH (reactions 1-3).

Since NAD^+ and mediator concentrations are constant, the increase in the electrocatalytic current depends only on the ethanol concentration (NADH formation), and this characteristic was used as the basis of the development of a biosensor for ethanol determination.

The cyclic voltammograms recorded for DDDP-modified carbon paste electrode, incorporating ADH, in the presence of NAD^+ and ethanol (results not shown) proved that the electrode is able to sustain the catalytic cycle described by reactions 1-3. After addition of 10 mM NAD^+ and 50 mM ethanol, a good electrocatalytic effect of DDDP for the enzymatically produced NADH was clearly observed (the anodic current is enhanced and the cathodic one is diminished). Obviously, no catalytic current can be observed in the absence of NAD^+ and/or ethanol (results not shown).

2. Influence of NAD^+ concentration

The NAD^+ coenzyme also plays a major role in the biosensor mechanism (see reactions 1-3). Thus, the effect on the biosensor response was evaluated for 50 mM ethanol, at different NAD^+ concentrations in the electrolyte solution (results not shown). It was observed that the response increases with increasing NAD^+. Based on these results, 10 mM of NAD^+ was employed in the development of further biosensors.

3. Response to ethanol of ADH-PEI-DDDP-CPE

Fig. 1A presents the ADH-PEI-DDDP-CPE amperometric response to successive injections of ethanol, and gives qualitative information on the response rate, as well as on the signal stability. In order to diminish the mass transport effect on the biosensor response the ADH-PEI-DDDP-CPE was rotated with 500 rpm.

The biosensor response time was very short, reaching of its $t_{95\%}$ in 1 minute, as observed in fig. 1A. This response time is good considering that it is a carbon paste electrode.

Fig. 1B shows a calibration curve obtained from 1 to 100 mM of ethanol, in 0.1 M phosphate buffer at pH 7. The values of the kinetic parameters (I_{max} and K_M^{app}) were calculated by fitting the experimental data to the Michaelis-Menten equation (fig. 1B). A linear response is observed up to 20 mM ethanol.

The sensitivity for ethanol (estimated as the I_{max}/K_M^{app} ratio) of ADH-PEI modified carbon paste based biosensor was 0.035 mA/M.
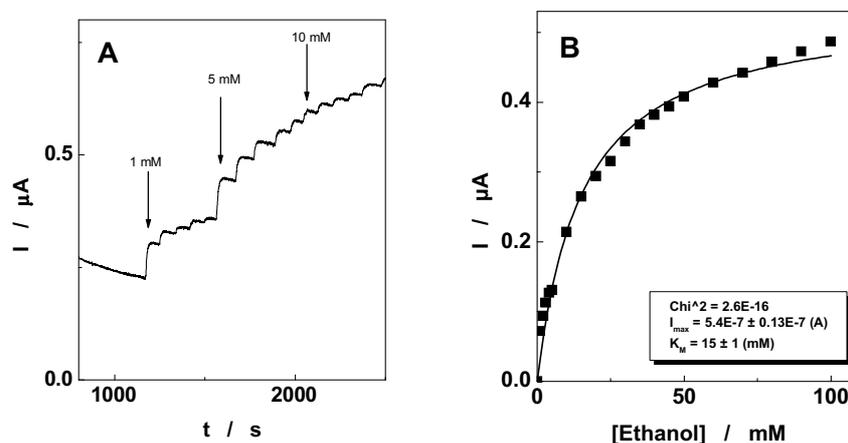
Figure 1. (A) Amperometric response to successive additions of ethanol and (B) calibration plots for ADH-PEI-DDDP-CPE. Experimental conditions: applied potential, +430 mV *vs.* Ag|AgCl/KCl$_{sat}$; supporting electrolyte, 0.1 M phosphate buffer pH 7 containing 10 mM NAD$^+$; rotation speed, 500 rpm.

Kinetic parameters were also estimated using the Lineweaver–Burk, Hanes–Woolf and Eadie–Hoffstee linearizations of Michaelis-Menten equation (table 1). The values obtained for K_M^{app}, I_{max} and sensitivity are in good accordance with those obtained by Michaelis-Menten fitting (fig. 1B). This behavior was attributed to the good reproducibility of the ADH-PEI-DDDP-CPE response, reflected by small fluctuations of the experimental data involved in the calibration curve (fig. 1B).

The value of K_M^{app} is higher than those observed for the free enzyme in solution (3.2 mM for dissolved ADH; Pt rotated disk electrode; using hexacyanoferrate(III) as mediator; at pH 8.8 [31]) and for immobilized enzyme in carbon paste electrode (10 mM for ADH immobilized using glutaraldehyde/bovine serum albumin cross-linking procedure, in Meldola Blue adsorbed on silica gel modified niobium oxide [11]). As expected, the ADH immobilization lead to an increase of K_M^{app} value in comparison with the corresponding values obtained when ADH was dissolved in solution. Additionally, a small increase (of 1.5) was observed between the values of K_M^{app} for the present study and that obtained in the above example [11]. These results showed that the immobilization procedure did not promote a significant change in the enzyme selectivity/activity [11].

Detection limits around 0.26 mM ethanol could be estimated considering a signal/noise ratio of 3.

58

Table 1.

Kinetic parameters of DDDP-ADH-PEI-CPE biosensors.
Experimental conditions: as in figure 2.

K_M^{app} (mM)	I_{max} (µA)	Sensitivity (µA M^{-1})	R / no. of exp. points
Lineweaver – Burk linearization			
17.1 ± 1.8	0.55 ± 0.02	32.2 ± 2.3	0.9942 / 13
Hanes- Woolf linearization			
17.8 ± 1.7	0.56 ± 0.01	30.9 ± 2.4	0.9990 / 15
Eadie – Hoffstee linearization			
18.2 ± 1.8	0.57 ± 0.02	31.3 ± 4.2	0.9886 / 13

The biosensor showed a good operational stability, as verified by data from repetitive analyses recorded over 6 h periods of continuously operating.

Also, the proposed biosensor presented good storage stability, which allowed measurements with the same response, for 1-2 days, when the biosensor was stored in a refrigerator, at 4^0C. Decreasing of response towards ethanol with 88 %, after three days of storing is due to enzyme deactivation, because DDDP-CPE presents a good stability for NADH oxidation and DDDP remains immobilized in carbon paste more than a month [28].

CONCLUSIONS

The phenothiazine derivative, 16*H*,18*H*-dibenzo[c,1]-7,9-dithia-16,18-diazapentacene, adsorbed on carbon paste electrode was very useful for a simple and effective way to develop biosensors for ethanol determination.

The analytical signal is due to the electrocatalytic oxidation of enzymatically generated NADH at ADH-PEI-DDDP-carbon paste electrodes. The proposed ADH-PEI-DDDP-CPE biosensor exhibited a good sensitivity (0.035 mA/M), a fast response ($t_{95\%}$ < 1 min.) and a linear domain of concentration up to 20 mM, as well as a good operational and storage stability.

EXPERIMENTAL SECTION

Materials

Alcohol dehydrogenase (ADH), EC 1.1.1.1. from yeast, was obtained from Sigma (St. Louis, MO, USA). The phenothiazine derivative, 16*H*,18*H*-dibenzo[c,1]-7,9-dithia-16,18-diazapentacene (DDDP) was synthesized according to a previously published procedure [29]. The supporting electrolyte used in the electrochemical cell was a solution of 0.1 M sodium phosphate, pH 7.0 (Merck, Darmstadt, Germany).

Potassium chloride was purchased from Merck (Darmstadt, Germany) and absolute ethanol (99.7 %) from Kemetyl (Stockholm, Sweden). Polyethylenimine (PEI) and NAD^+ were purchased from Sigma (St. Louis, MO, USA).

Preparation of the DDDP-modified carbon paste electrodes

100 µl of a 0.001% (w/v) DDDP solution prepared in tetrahydrofuran (Labscan Limited, Dublin, Ireland) were added to 100 mg of carbon powder and adsorption of the mediator was allowed to proceed in vacuum until total evaporation of the solvent. DDDP-modified carbon paste electrodes (DDDP-CPEs) were obtained by thoroughly mixing the obtained DDDP-modified carbon paste with 25 µl of paraffin oil.

Preparation of the ADH-PEI-modified carbon paste electrodes

To 10 mg of DDDP-modified carbon paste, 200 µl solution formed by 5 mg ADH (400 U / mg) and 1 ml of 0.2 % (w/v) PEI was added, and adsorption of the enzyme was allowed to proceed in vacuum until a dried carbon powder was obtained.

The modified carbon paste was put into a cavity of an in-house made Teflon holder using pyrolytic graphite in the bottom for electric contact and then screwed onto a rotating disk electrode device (RDE; EG&G Model 636, Princeton, Applied Research, Princeton, NJ, USA). The final geometrical area of the modified carbon paste electrodes was equal to 0.071 cm^2.

Electrochemical measurements

Cyclic voltammetry and rotating disk electrode experiments were carried out using a conventional three-electrode electrochemical cell. The modified carbon paste was used as working electrode, a platinum ring as counter electrode and an Ag|AgCl/KCl$_{sat}$ as reference electrode. An electro-chemical analyzer (BAS 100W, Bioanalytical Systems, West Lafayette, IN, USA) was connected to a PC microcomputer for potential control and data acquisition. For rotating disk electrode experiments an EG&G rotator (Princeton Applied Research, Princeton, NJ, USA) was used.

ACKNOWLEDGEMENTS

REFERENCES

1. E. Domínguez, H. L. Lan, Y. Okamoto, P. D. Hale, T. A. Skotheim, L. Gorton, *Biosensors & Bioelectronics*, **1993**, *8*, 167.

2. W. J. Blaedel, R. C. Engstrom, *Analytical Chemistry*, **1980**, *52*, 1691.

3. F. Y. Bernadette, R. L. Christopher, *Analytical Chemistry*, **1987**, *59*, 2111.

4. M. Somasundrum, J. V. Bannister, *Journal of Chemical Society, Chemical Communications*, **1993**, 1629.

5. A. Karyakin, O. A. Bobrova, E. A. Karyakina, *Journal of Electroanalytical Chemistry*, **1995**, *399*, 179.

6. C.-X. Cai, K.-H. Xue, Y-. M. Zhou, H. Yang, *Talanta*, **1997**, *44*, 339.

7. M. J. Lobo Castanon, A. J. Miranda Ordieres, P. Tunon Blanco, *Biosensors & Bioelectronics*, **1997**, *12*, 511.

8. J. Razumiene, R. Meskys, V. Gureviciene, V. Laurinavicius, M. D. Reshetova, A. D. Ryabov, *Electrochemistry Communications*, **2000**, *2*, 307.

9. J. Razumiene, V. Gureviciene, V. Laurinavicius, J. V. Grazulevicius, *Sensors and Actuators B: Chemical*, **2001**, *78*, 243.

10. J. Razumiene, A. Vilkanauskyte, V. Gureviciene, V. Laurinavicius, N.V. Roznyatovskaya, Y. V. Ageeva, M. D. Reshetova, A. D. Ryabov, *Journal of Organometallic Chemistry*, **2003**, *668***, 83.

11. A. S., Santos, R. S. Freire, L. T. Kubota, *Journal of Electroanalytical Chemistry*, **2003**, *547*, 135.

12. M. Niculescu, R. Mieliauskiene, V. Laurinavicius, E. Csoregi, *Food Chemistry*, **2003**, *82*, 481.

13. D. M.Gligor, G. L. Turdean, L. M. Muresan, I. C. Popescu, *Studia Universitatis Babes-Bolyai, Chemia***, 2004**, *XLIX*, 93.

14. K. Svensson, L. Bulow, D. Kriz, M. Krook, *Biosensors & Bioelectronics,* **2005**, *21***, 705.

15. J. Razumiene, J. Barkauskas, V. Kubilius, R. Meskys, V. Laurinavicius, *Talanta*, **2005**, *67*, 783.

16. H. Jaegfeldt, *Journal of Electroanalytical Chemistry*, **1980**, *110,* 295.

17. J. Moiroux, P. J. Elving, *Analytical Chemistry*, **1978**, *50*, 1056.

18. Z. Samec, P. J. Elving, *Journal of Electroanalytical Chemistry*, **1983**, *144*, 217.

19. L. Gorton, E. Dominguez, *Reviews in Molecular Biotechnology*, **2002**, *82*, 371.

20. L. Gorton, E. Dominguez, "Electrochemistry of NAD(P)+/NAD(P)H in Encyclopedia of Electrochemistry", Wiley, New York, **2002**.

21. I. C. Popescu, E. Dominguez, A. Narvaez, V. Pavlov, I. Katakis, *Journal of Electroanalytical Chemistry*, **1999**, *464*, 208.

22. L. Gorton, A. Torstensson, H. Jaegfeldt, G. Johansson, *Journal of Electroanalytical Chemistry*, **1984**, *161*, 103.

23. J. Kulys, G. Gleixner, W. Schuhmann, H.-L. Schmidt, *Electroanalysis*, **1993**, *5*, 201.

24. L. T. Kubota, L. Gorton, Electroanalysis, **1999**, *11*, 719.

25. F. D., Munteanu, D. Gligor, I. C. Popescu, L. Gorton, *Revue Roumaine de Chimie*, **2005**, *51*, 25.

26. D. Dicu, L. Muresan, I. C. Popescu, C. Cristea, I. A. Silberg, P. Brouant, *Electrochimica Acta*, **2000**, *45*, 3951.

27. V. Rosca, L. Muresan, C. Cristea, I. A. Silberg, I. C. Popescu, *Electrochemistry Communications*, **2001**, *3*, 439.

28. F. D. Munteanu, D. Dicu, I. C. Popescu, L. Gorton, *Electronalysis*, **2003**, *15*, 383.

29. I. A. Silberg, C. Cristea, *Heterocyclic Communications*, **1995**, *2*, 117.

30. E. Katz, V. Heleg-Shabtai, B. Willner, I. Willner, A. F. Buckmann, *Bioelectrochemistry & Bioenergetics*, **1997**, *42*, 95.

31. M. K. Ciolkosz, J. Jordan, *Analytical Chemistry*, **1993**, *65*, 164.

In memoriam prof. dr. Liviu Oniciu

CARACTÉRISATION OPÉRATIONNELLE D'UN BIOCAPTEUR AMPÉROMÉTRIQUE POUR LA DÉTECTION DE L'ANION NITRATE

ANA-MARIA TODEA, LIANA MARIA MUREŞAN, IONEL CATALIN POPESCU[*]

RÉSUMÉE. L'étude a été centré sur le développement d'un biocapteur ampérométrique pour la détection de l'anion nitrate et a envisagé l'amélioration de la stabilité du biocapteur par l'utilisation d'une matrice enzymatique composite. Ainsi, sur une première couche polymérique, obtenue par l'électropolymérisation "*in situ*" d'un dérivé pyrrolique amphiphilique du viologène, a été déposée l'enzyme (nitrate réductase) immobilisée par adsorption sur une argile hydrophilique (laponite). Finalement, une dernière couche polymérique a été deposée par l'électropolymerization d'un dérivé pyrrolique-viologène soluble dans l'eau. La limite de détection du biocapteur est 0,5 µM, tandis que sa sensibilité, calculée de la pente de la région linéaire, est de 37,7 mA $M^{-1}cm^2$. La valeur assez petite de K_M^{app} (0.29 mM), déterminée par modélisation de la dépendance Michaelis-Menten, indique que l'argile utilisée offre un milieu biocompatible avec l'enzyme.

Mots clef: biocapteur ampérométrique, anion nitrate

INTRODUCTION

Au cours des dernières années, la détection électrochimique des espèces chimiques d'intérêt dans la protection de l'environnement a retenu l'attention de nombreux chercheurs, due à ses caractéristiques très attrayantes au niveau du rapport performances (sensibilité, limite de détection, sélectivité, temps de réponse, robustesse etc.) / efforts de réalisation (simplicité, coût réduit, versatilité etc.). De plus, le couplage des transducteurs électrochimiques (potentiométriques et surtout ampérométriques), réalisés à base d'électrodes modifiées, avec des éléments de reconnaissance biologique (de nature métabolique ou immunospécifique) a donné lieu à l'apparition d'un outil très performant, le biocapteur électrochimique (voir, par ex. [1]).

[*] *Département de Chimie Physique, Université Babeş-Bolyai, 11 Rue Arany Janos, 400028 Cluj-Napoca, Roumanie; cpopescu@chem.ubbcluj.ro*

Des biocapteurs pour l'anion nitrate ont été fabriqués par l'incorporation de la nitrate réductase (NR) dans des différentes matrices polymériques [2, 3]. Malgré les caractéristiques analytiques très intéressantes de ces dispositifs, leur utilisation est fortement diminuée en raison de leur instabilité fonctionnelle, essentiellement déterminée par la fragilité du récepteur biologique [4].

Notre étude, centré sur le développement d'un biocapteur pour la détection de l'anion nitrate par l'immobilisation de la nitrate réductase dans une matrice composite, a envisagé l'amélioration de la stabilité du biocapteur par l'utilisation combinée de l'électropolymérisation "*in situ*" de deux dérivés pyrroliques (Schème 1) et d'une argile (laponite). Laponite est un matériel avec une grande stabilité thermique, mécanique et chimique, ayant des propriétés remarquables d'échangeurs d'ions et qui, suite à sa structure particulière, permet l'obtention de vitesses élevées de diffusion du substrat, lors qu'il est présent dans l'architecture d'une matrice enzymatique [5].

Le laponite a été employée avec succès dans la construction des biocapteurs ampérométriques pour la détection de glucose [6], de l'anion NO_3^- [7] et pour la construction des biocapteurs conductimétriques [8]. D'autre part, les dérives polypyrroliques-viologène assurent simultanément l'immobilisation de l'enzyme, le contact électrique avec le matériel électrodique [7, 9 -11] et la création d'un microenvironnement favorable pour augmenter la durée de vie du récepteur biologique.

RESULTATS ET DISCUSSION

Le biocapteur a été caractérisé par voltammétrie hydrodynamique cyclique en tampon TRIS 0,1 M (pH 7,5), dans le domaine de potentiel -0,7 - -0,3 V *vs.* Ag/AgCl. Les voltammogrammes typiques obtenues pour le biocapteur **poly 1 / NR-laponite / poly 2**, en absence et en présence de l'anion nitrate pour différentes concentrations, sont présentées dans la figure 2.

Comme on peut voir dans la figure 2, en absence des nitrates on obtient une onde à caractère quasi-réversible, correspondant au couple MV^{2+}/MV^+ ($\varepsilon^{0'}= 0,55$ V / Ag/AgCl/KCl_{3M}). Par contre, en présence de différentes concentrations de l'anion nitrate une augmentation prononcée du courrant cathodique a été mise en évidence, en parallèle avec la diminution progressive du courrant anodique. Ce comportement est la preuve directe de l'activité bioélectrocatalytique de l'électrode **poly 1 / NR-laponite / poly 2** pour la réduction de l'anion nitrate.

Le comportement électrocatalytique du biocapteur met en évidence un très bon contact électrique entre le centre redox de la NR et la surface de l'électrode de travail, par l'intermédiaire des groupes viologène de la matrice polymérique. À la fois, celui-ci prouve l'efficacité de la communication
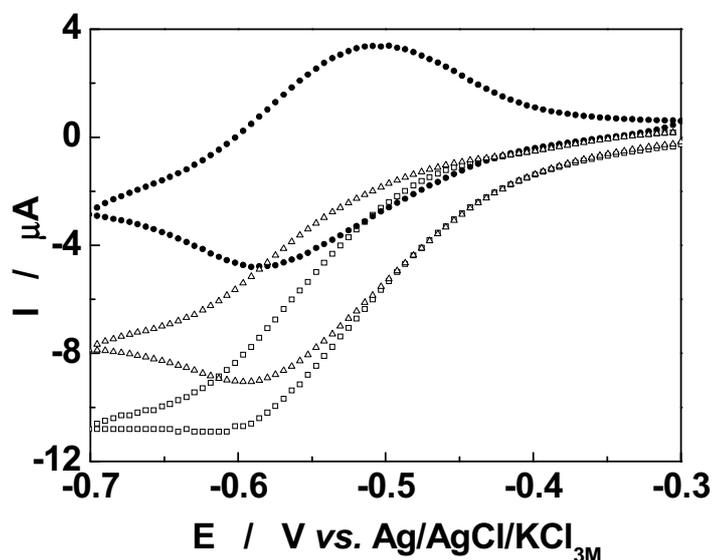
Figure 2. Réponse voltammétrique du biocapteur **poly 1 / NR-laponite / poly 2** en absence (•) et en présence de NO_3^-: (Δ) 0,25 mM; (□) 5 mM. Conditions expérimentales: tampon TRIS 0,1 M (pH 7,5); vitesse de balayage, 5 mV/s; 1000 rpm; 30 ^{0}C.

électrique entre le film de **poly 1**, en contact avec la surface de l'électrode et le polymère **poly 2**, qui est incorporé dans l'argile. Par conséquent, le schéma de la détection bioampèrométrique de l'anion nitrate sur l'électrode **poly 1 / NR-laponite / poly 2** est la suivante:

$$2V^{+\bullet} + NO_3^- + H_2O \xrightarrow{NR} 2V^{2+} + NO_2^- + 2OH^-$$

$$2V^{2+} + 2e^- \xrightarrow{electrode} 2V^+$$
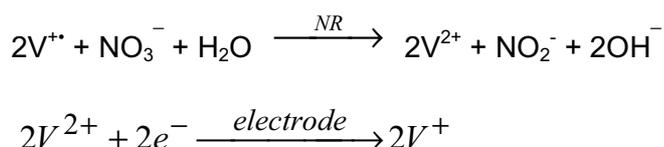
L'augmentation du courant cathodique, due á la réduction du nitrates à nitrite, a permis le traçage d'une courbe de calibration, basée sur des mesures voltammétriques (figure 3). On peut constater facilement l'allure typique correspondant à une cinétique Michaelis-Menten. Les paramètres cinétiques caractéristiques (I_{max} et K_M) ont été estimés à l'aide du logiciel Origin (figure 3).
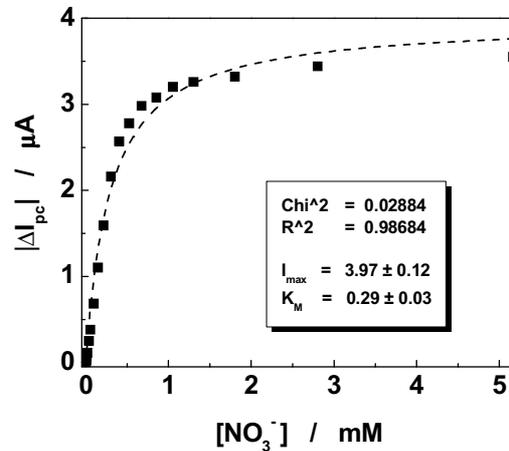
Figure 3. Courbe de calibration pour le dosage de NO_3^- par voltammétrie hydro-dynamique cyclique en utilisant le biocapteur **poly 1 / NR-laponite / poly 2**. Conditions expérimentales: domaine de potentiel, -0,7 - -0,3 V *vs.* Ag/AgCl; tampon, TRIS 0,1 M (pH 7,5); 30 ^{0}C; vitesse de balayage, 5 mV/s; 1000 rpm.

Comme on peut observer dans la figure 4 la réponse du biocapteur est linéaire jusqu'à la concentration de 0.15 mM NO_3^-. Les paramètres correspondant à la dépendance linéaire entre ΔI_{pc} et $[NO_3^-]$ sont marqués dans la figure 4. La limite de détection est 0,5 µM, tandis que sa sensibilité, calculée de la pente de la région linéaire, est de 37,7 mA $M^{-1}cm^2$.
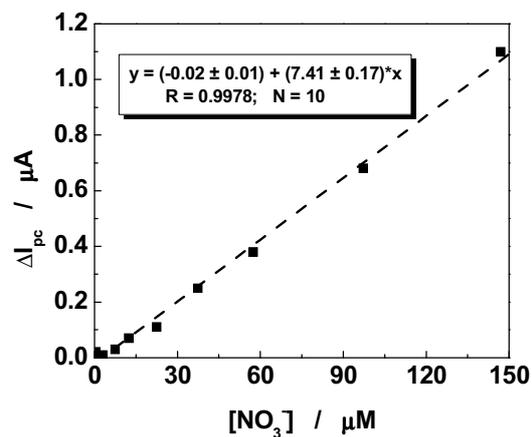
Figure 4. Domaine linéaire de la courbe de calibration pour le dosage de NO_3^- avec le biocapteur **poly 1 / NR-laponite / poly 2**. Conditions expérimentales: comme en figure 3.

La valeur assez petite de K_M^{app}, déterminée par modélisation de la dépendance Michaelis-Menten de la pente de la représentation linéaire $1/\Delta I_p = f(1/c)$ indique le fait que l'argile offre un milieu biocompatible avec NR. Le caractère hydrophile du laponite et l'absence des réactions chimiques pendant l'immobilisation de l'enzyme préviennent la dénaturation de la NR.

Une étude préliminaire de la stabilité du biocapteur indique une maintenance de 100% de la réponse pendant 48 heures. L'efficacité du biocapteur diminue jusqu'à 80,2 % après 72 heures et jusqu'à 68 % après 96 heures. La diminution du signal est due à la perte de viologène et à la dénaturation de l'enzyme.

CONCLUSIONS

Les recherches ont conduit à l'obtention d'un biocapteur, **poly 1/NR-laponite/poly 2,** pour l'anion NO_3^-, basé sur une matrice enzymatique composite.

Le comportement électrocatalytique du biocapteur **poly 1/NR-laponite/ poly 2** met en évidence un bon contact électrique entre le centre redox de l'enzyme immobilisée et la surface de l'électrode en carbone vitreux. L'efficacité de la communication électrique entre le film du polymère 1, en contact avec la surface de l'électrode et le polymère 2, qui se trouve incorporé dans l'argile, se reflète dans les valeurs des paramètres bioélectroanalytiques qui se situent parmi les meilleurs dans le domaine.

SECTION EXPERIMENTALE

Le dispositif experimental

Les études électrochimiques ont utilisé un potentiostat (AUTOLAB 100, ECOchemie, Utrecht, Pays Bas) et une cellule électrochimique thermostatée, á trois électrodes: l'électrode de travail en carbone vitreux (Φ = 5mm); l'électrode auxiliaire en fil d'Ag; l'électrode de référence, Ag/AgCl/KCl$_{3M}$.

Préparation de l'électrode modifiée

La méthode d'immobilisation comporte deux étapes: (i) l'immobilisation de l'enzyme (nitrate réductase, **NR**) dans une argile hydrophilique (laponite), déposée sur une couche polymèrique du médiateur redox, obtenue par l'électropolymerisation d'un dérivé pyrrolique-viologène amphiphilique (**monomère 1**; n = 12); (ii) la déposition sur la couche précédente d'une couche polymèrique, préparée par l'électropolymerisation d'un dérivé pyrrolique- viologène soluble dans l'eau (**monomère 2**) (Schema 1).

L'électrode en carbone vitreux a été polie avec de la pâte de diamant et nettoyée par ultrasonnage pendant 20 minutes plongée dans l'eau distillée. Par suite, sur la surface de l'électrode on a déposé 20 µl de solution 5mM du **monomère 1**, dispersé dans l'eau distillée par ultrasonnage; puis, le solvant a été évaporé sous vide. L'électrode ainsi modifiée a été transférée dans une

67

cellule contenant une solution aqueuse 0,1 M de LiClO$_4$ et l'electropolymérisation du **monomère 1** a été réalisé par électrolyse potentiostatique (0,8 V *vs.* Ag/AgCl/KCl$_{3M}$) pendant 15 minutes, sous argon.

$$\text{(structure chimique)} \qquad (1)$$

$$\text{(structure chimique)} \qquad (2)$$
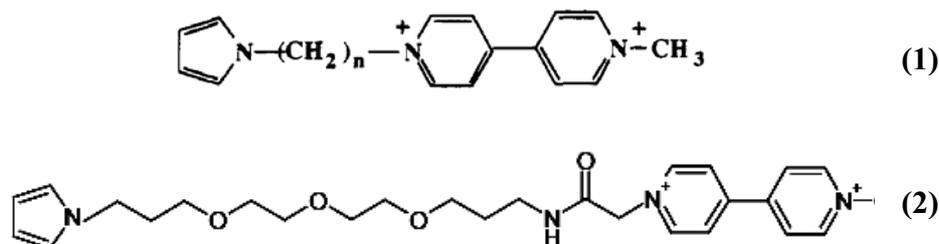
Schema 1

Séparément, on a préparé une suspension colloïdale de laponite en eau bidistillée et 33 µl de ce mélange (contenant 22 µg laponite et 22 µg NR) ont été déposés sur la couche polymérique 1 (**poly 1**). Après l'évaporation sous vide de l'eau et la formation d'un film adhèrent de NR-laponite sur la première couche polymérique, par l'électropolymérisation oxydative potentiostatique (0,8 V *vs.* Ag/AgCl/KCl$_{3M}$) d'un dérivé pyrrolique-viologène soluble dans l'eau (**monomère 2**), à partir d'une solution 5 mM, contenant 0.1 M LiCl$_4$, une dernière couche polymérique (**poly 2**) a été déposée sur l'électrode modifiée. La structure finale de l'électrode modifiée est représentée schématiquement dans la figure 1.
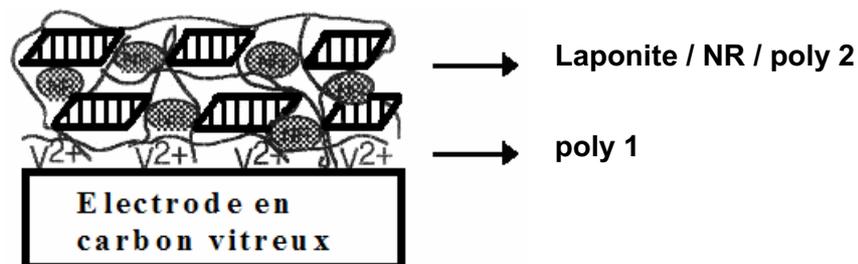
Laponite / NR / poly 2

poly 1

Electrode en carbon vitreux

Figure 1. Représentation schématique de l'électrode modifiée
(V^{2+}, viologène; ⬤, nitrate réductase; ▱, polymère).

REMERCIEMENTS

BIBLIOGRAPHIE

1. F. W. Scheller, F. Schubert, J. Fedrowitz (eds.), "Frontiers in Biosensorics I", Birkhauser Verlag, Basel, **1997**, chapitre 4, pp. 49.
2. L. M. Moretto, P. Ugo, M. Zanata, P. Guerriero, C. R. Martin, *Analytical Chemistry*, **1998**, *70*, 2163.
3. S. Cosnier, C. Innocent, Y. Jouanneau, *Analytical Chemistry*, **1994**, *66*, 3198.
4. G. L. Turdean, S. E. Stanca, I. C. Popescu, "Biosenzori amperometrici", Presa Universitara Clujeana, **2005**, chapitre 2, pp. 15.
5. S. Cosnier, K. Le Lous, *Journal of Electroanalytical Chemistry*, **1996**, *406*, 243.
6. S. Poyard, C. Martelet, N. Jaffrezic-Renault, S. Cosnier, P. Labbe, *Sensors and Actuators B*, **1999**, *58*, 380.
7. S. Da Silva, D. Shan, S. Cosnier, *Sensors and Actuators B*, **2004**, *103*, 397.
8. A. Senillou, N. Jaffrezic, C. Martelet, S. Cosnier, *Analytica Chimica Acta*, **1999**, *401*, 117.
9. S. Cosnier, B. Galland, C. Innocent, *Journal of Electroanalytical Chemistry*, **1997**, *433*, 113.
10. S. Cosnier, C. Gondran, A. Senillou, *Synthetic Metals*, **1999**, *102*, 1366.
11. G. Ramsay, S. M. Wolpert, *Analytical Chemistry*, **1999**, *71*, 504.

In memoriam prof. dr. Liviu Oniciu

AMPEROMETRIC BIOSENSORS FOR GLUCOSE AND ETHANOL DETERMINATION IN WINE USING FLOW INJECTION ANALYSIS

LAURA MUREŞAN[a, b, *]**, KINGA JUDITH ZOR**[b]**, MIHAELA NISTOR**[b]**, ELISABETH CSÖREGI**[b]**, IONEL CĂTĂLIN POPESCU**[a]

ABSTRACT. Reagentless amperometric biosensors for glucose and ethanol were developed and successfully applied for monitoring glucose and ethanol concentrations in wine during the fermentation process. The glucose biosensor was based on commercially available glucose oxidase and horseradish peroxidase co-immobilized on solid graphite using Os(II)-redox hydrogel (RH) [1]. In the case of ethanol biosensor, the quinohemoprotein dependent alcohol dehydrogenase was immobilized on the graphite electrode surface using the same RH [2]. Both biosensors were operated at low applied potentials (-50 mV *vs.* Ag/AgCl, KCl $_{0.1 M}$ for glucose biosensor, and +250 mV *vs.* Ag/AgCl, KCl $_{0.1 M}$ for ethanol biosensor), where biases from interferences are minimal. The bioelectroanalytical parameters, estimated from flow injection analysis measurements, were found as follows: sensitivity, 0.73 ± 0.01 µA mM^{-1} for glucose and 0.45 ± 0.01 µA mM^{-1} for ethanol; linear range up to 1 mM in both cases; detection limit, 7.0 µM for glucose and 8.9 µM for ethanol. The results for real samples were found in good agreement with those reported by Barsan et al. [3].

Keywords: *amperometric biosensors; ethanol; flow injection analysis; glucose; wine.*

INTRODUCTION

The measurement of ethanol and glucose plays an important role in the control of wine fermentation process and for assesing the quality of the final product. Methods commonly used for their determination like chromatography [4], spectrophotometry [5] or enzymatic test-kits [6] require long analysis times, complex instrumentation, high costs or tedious sample treatment. These drawbacks can be avoided using amperometric biosensors due to their characteristics as high selectivity, low cost, relative simple preparation and good stability [7].

---

[a] *Department of Physical Chemistry, Babes-Bolyai University, 400028 Cluj-Napoca, Romania*
* *e-mail address: lamur@chem.ubbcluj.ro*
[b] *Department of Analytical Chemistry, Lund University, 22100 Lund, Sweden*

PQQ-dependent dehydrogenases are attractive due to their oxygen independence and to the fact that display a direct electron transfer between their active center and certain electrodes [8, 9]. Quinohemoprotein dependent alcohol dehydrogenase (PQQ-ADH)-based biosensors were previously reported for the detection of ethanol in alcoholic beverages [2, 10].

Oxidases are usually more stable than dehydrogenases and their use imply the monitoring of hydrogen peroxide produced by the enzymatic reaction at applied potential higher than 500 mV *vs.* Ag/AgCl, KCl $_{0.1 M}$. The use of redox mediators immobilized on the electrode surface [11] is beneficial in order to overcome the use of such high applied potentials.

The properties of osmium redox polymers allow besides co-immobilization with the enzyme on the electrode surface, the use of low applied potentials for biosensor operation [12]. Thus, such biosensors are reagentless and less prone to interferences.

The aim of this work was to develop simple and low cost reagentless enzyme biosensors based on PQQ-ADH and glucose oxidase (GOx), respectively, for monitoring of key analytes in wine during the fermentation process. Os(II)-redox hydrogel was used for "wiring" the enzymes and the electrode and the whole mixture was cross-linked with poly(ethylene glycol) diglycidyl ether (PEGDGE) [13]. The biosensors present good reproducibility and their use has the advantage of requiring minimum sample treatment (dilution).

This work represents a part of a training session taking place at Fattoria dei Barbi, Montalcino, Italy, where several analytes of interest such as glucose and ethanol were analyzed by alternative techniques.

RESULTS AND DISCUSSIONS

I. Electrochemical behavior of the modified electrodes

The detection principle of glucose and ethanol biosensors is presented in figure 1.

The bienzyme system, presented in figure 1A, on one hand ensures a high selectivity of the measurements because at the low applied potential (-50 mV *vs.* Ag/AgCl, KCl $_{0.1 M}$) biases from interferences are minimal, and on the other hand, offers an increased sensitivity due to the presence of RH which mediates the electron transfer between HRP and the graphite electrode.

The monoenzyme system used for ethanol detection (figure 1B) is based on the electrical connection of PQQ-ADH to graphite electrode, via RH. The bioelectrocatalytic cycle is closed by electrochemical oxidation of Os(II) to Os(III) at a low applied positive potential (+250 mV *vs.* Ag/AgCl, KCl $_{0.1 M}$).
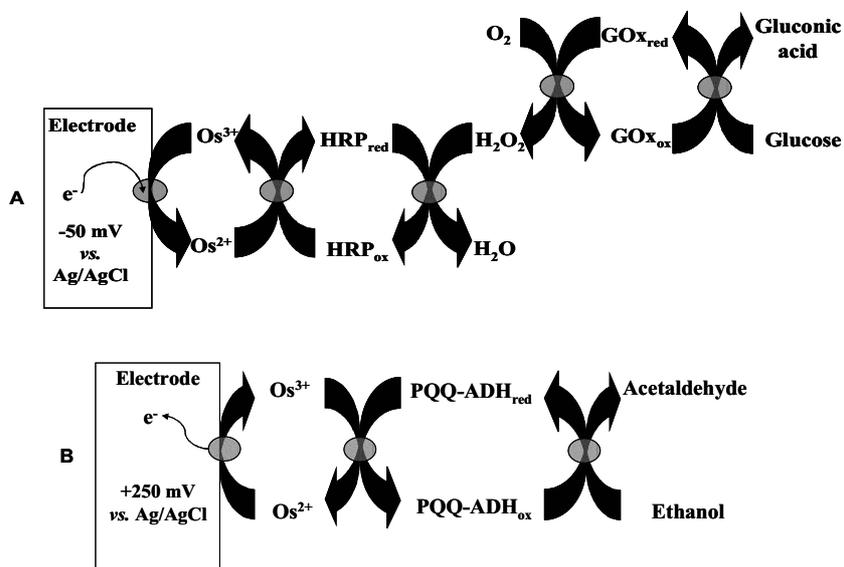
Figure 1. Detection principle for **(A)** glucose and **(B)** ethanol biosensors.
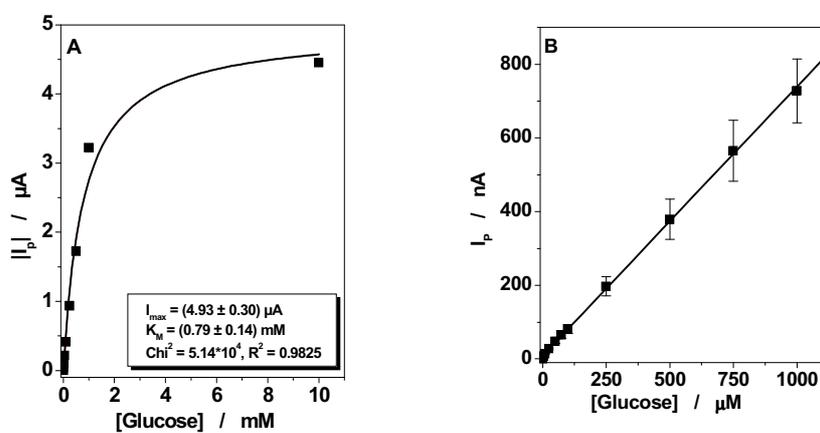

Figure 2. (A) Calibration curve and **(B)** linear range for glucose biosensor. *Experimental conditions*: flow rate, 0.5 ml min^{-1}; supporting electrolyte, 0.1 M phosphate buffer containing 0.1 M KCl, pH 7.2; applied potential, –50 mV *vs.* Ag/AgCl, KCl $_{0.1 M}$.

73

In order to investigate their electrochemical behavior, the prepared biosensors were integrated in a FIA system. Amperometric measurements were performed by injecting constant volumes of increasing substrate concentrations and recording the corresponding peak currents. As expected, both enzymes presented the Michaelis-Menten behavior. A calibration curve for glucose is presented in figure 2A. The kinetic parameters were found as: $I_{max} = (4.93 \pm 0.30)$ µA and $K_M = (0.79 \pm 0.14)$ mM. The linear range of the calibration curve is presented in figure 2B. The error bars stand for standard deviation, estimated for 6 enzyme electrodes.

The corresponding bioelectroanalytical parameters are synthesized in table 1.

The same procedure was followed for the ethanol biosensors and the calibration curve is presented in figure 3. The kinetic parameters estimated from the calibration curve were: $I_{max} = (2.25 \pm 0.01)$ µA and $K_M = (4.05 \pm 0.05)$ mM. As can be seen from figure 3B, small error bars indicate a quite good reproducibility of the results (standard deviation calculated as the mean of three independent measurements). The ethanol biosensor characteristics are summarized in table 1.
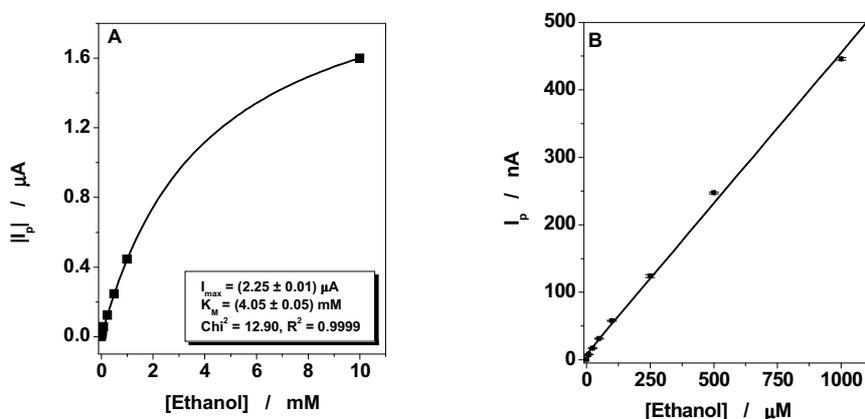

Figure 3. (A) Calibration curve and **(B)** linear range for ethanol biosensor.
Experimental conditions: flow rate, 0.5 ml min⁻¹; supporting electrolyte, 0.1 M acetate buffer containing 1 mM $CaCl_2$, pH 6.2; applied potential, +250 mV *vs.* Ag/AgCl, KCl $_{0.1 M}$.

The results are within the limits reported in the literature for different kind of glucose and ethanol biosensors. Good reproducibility, large linear range and relatively low detection limits make the developed biosensors suitable for applications in real samples.

Table 1.

Bioelectroanalytical parameters for glucose and ethanol biosensors.
Experimental conditions: see figures 2 and 3.

Biosensor	Sensitivity** (μA mM^{-1})	Linear range (μM)	Detection limit*** (μM)	R / N
Glucose	0.73 ± 0.01*	up to 1000	7.0	0.9997 / 11
Ethanol	0.45 ± 0.01*	up to 1000	8.9	0.9986 / 8

*standard deviation for 6 (glucose) or 3 (ethanol) measurements.
**calculated as the slope of the linear range.
***estimated for signal / noise ratio equal to 3.

II. Real samples measurements

After the biosensors were calibrated, measurements were performed in wine samples, collected at different fermentation times from a winery. Thus, the real samples were diluted (1:10000 for glucose and 1:400 for ethanol determination) in the corresponding buffers in order to get the response in the linear range of the calibration curves, and injected in the flow line. The results were expressed in g l^{-1} and represented as function of time elapsed from the beginning of sampling. As observed in figure 4, in 27 h from the beginning of the sampling (51 h from the beginning of the fermentation process), the glucose concentration decreased with 32.9 %, while ethanol concentration increased with 4.5 %.
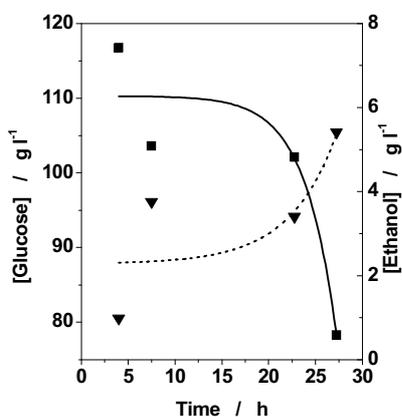

Figure 4. Variation in the glucose and ethanol concentrations during the alcoholic fermentation. Symbols: ■ glucose; ▼ ethanol. *Experimental conditions*: see figures 2 and 3. Obs: The first sample was collected after 24 h from the beginning of the fermentation process.

The results were similar to those obtained with a biosensor based on GOx-poly(neutral) red-BSA-GA adsorbed on carbon-film electrode as well as with those found by HPLC on analysis of the same samples [3]. The

observed differences are not significant and can be due to the different conservation conditions of the samples before being analyzed.

CONCLUSIONS

Bi- and *mono*enzyme biosensors for glucose and ethanol detection, based on GOx-HRP and PQQ-ADH, respectively, were developed and used in an off-line FIA system for wine fermentation monitoring.

The analytical parameters for both types of sensors were estimated from amperometric calibrations in flow injection mode. The biosensors presented good reproducibility and were successfully applied for analysis of glucose and ethanol during fermentation of wine.

EXPERIMENTAL SECTION

Reagents and solutions

Glucose oxidase from *Aspergillus niger* (EC 1.1.3.4.), PQQ dependent alcohol dehydrogenase from *Gluconobacter sp. 3.3* and horseradish peroxidase (HRP) (EC 1.11.1.7) were purchased from Sigma-Aldrich (Poole, UK), while poly(ethylene glycol) diglycidyl ether was supplied from Polysciences (Warrington, PA, USA).

Poly(1-vinylimidazole) complexed with Os (4,4'-dimethylbipyridine)$_2$Cl (PVI$_{10}$dmeOs) (figure 5) was prepared accordingly to a previously published procedure [12].

D(+) glucose anhydrous from Sigma-Aldrich (Poole, UK) and absolute ethanol 99.7% from Solveco Chemicals AB (Sweden) were used to prepare the standard solutions necessary for the sensor calibrations.

Acetic acid glacial 99% from Sigma-Aldrich (Poole, UK), sodium acetate dehydrate and calcium chloride dehydrate from Merck (Darmstadt, Germany) were used to prepare 0.1 M acetate buffer containing 1 mM CaCl$_2$ (pH 6.2). Disodium hydrogen phosphate dehydrate, sodium dihydrogen phosphate and potassium chloride purchased from Merck (Darmstadt, Germany), were utilized to prepare the 0.1 M phosphate buffer containing 0.1 M KCl (pH 7.2). All reagents were of analytical grade and used as received. If not otherwise indicated, the solutions were prepared in purified water obtained from a Milli-Q system (Millipore, Bedford, MA, USA).

Biosensors preparation

Considering the good properties reported for the redox hydrogel-based biosensors, amperometric biosensors for the detection of glucose and ethanol were developed accordingly to a previously described method [2, 10].
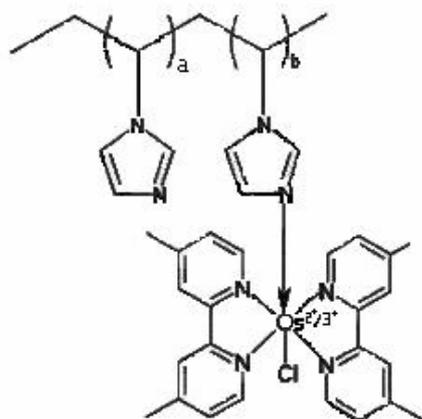
Figure 5. Structure of the Os(II)-redox hydrogel.

Prior to the modification, rods of spectroscopic graphite (Ringsdorff-Werke GmbH, Bonn-Bad, Germany, type RW001, 3.05 mm diameter) were mechanically polished on a wet fine emery paper (Tufback, Durite P1200, Allar, Sterling Heights, MI). The electrodes were rinsed with distilled water before coating them with 5 μL of enzyme mixtures, prepared as described below.

A mixture containing 2.9 mg ml^{-1} GOx, 0.7 mg ml^{-1} HRP, 1.15 mg ml^{-1} PVI$_{10}$–dmeOs, and 0.3 mg ml^{-1} PEGDGE (freshly prepared aqueous solution and used within 15 min) was used to prepare the glucose biosensors.

PQQ-ADH from *Gluconobacter* was previously reported as bioselective receptor for ethanol biosensor [9]. A mixture containing 1.7 mg ml^{-1} PQQ-ADH, 2.2 mg ml^{-1} PVI$_{10}$–dmeOs, and 0.55 mg ml^{-1} PEGDGE (freshly prepared aqueous solution and used within 15 min) was used for the preparation of ethanol biosensors. The composition of the modified electrodes is given in table 2.

Table 2.

The composition of enzyme matrix.

Type of biosensor	Composition	(%)
Glucose	GOx-HRP-PVI$_{10}$dmeOs-PEGDGE	57 : 14.2 : 22.8 : 6
Ethanol	PQQ-ADH-PVI$_{10}$dmeOs-PEGDGE	37.5 : 50 : 12.5

The electrodes were left to dry at room temperature and kept at + 4 ^{0}C until tested.

If not otherwise indicated, the presented results are average values of three equally prepared electrodes.

Real samples preparation

Must during fermentation (Fattoria dei Barbi, Montalcino, Italy, 2005) was monitored during a period of 27 hours, by analyzing the glucose and

ethanol concentrations with the developed biosensors in an off-line flow injection analysis (FIA) system. Taking into account that the concentration of the measured compounds is outside the working range of the sensors, dilution of the samples was necessary before injecting them into the FIA system. The samples were diluted 1:10000 (v/v) for glucose determination and 1:400 (v/v) for ethanol determination with the corresponding buffer solutions.

Electrochemical measurements

A mono-line FIA set-up consisting of a manual injection valve (Valco Instruments Co. Inc., Houston, TX, USA) with an injection loop of 100 µL, a peristaltic pump (Alitea AB, Stockholm, Sweden), a wall-jet electrochemical cell, a potentiostat (Zäta-Elektronik, Höör, Sweden) and a single channel recorder (Model BD 111, Kipp & Zonen, Delft, The Netherlands) was employed to operate the amperometric biosensors. The working electrodes were the enzyme-modified graphite electrodes, the reference electrode a Ag/AgCl, KCl $_{0.1 M}$ and the counter electrode a Pt wire. The system was operated at a constant potential of -50 mV *vs.* Ag/AgCl, KCl $_{0.1 M}$ in the case of glucose biosensor and +250 mV *vs.* Ag/AgCl, KCl $_{0.1 M}$ in the case of ethanol biosensor.

ACKNOWLEDGMENTS

REFERENCES

1. L. Gorton, G. Bremle, E. Csöregi, G. Jönsson-Pettersson, B. Persson, *Analytica Chimica Acta*, **1991**, *249*, 43.

2. M. Niculescu, R. Mieliauskiene, V. Laurinavicius, E. Csöregi, *Food Chemistry*, **2003**, *82*, 481.

3. M. M. Bârsan, J. Klincar, M. Batic, C. M. A. Brett, *Talanta*, **2007**, *71*, 1893.

4. R. Vonach, B. Lendl, R. Kellner, *Journal of Chromatography A*, **1998**, *824*, 159.

5. N. Choengchan, T. Mantima, P. Wilairat, P. K. Dasgupta, S. Motomizu, D. Nacapricha, *Analytica Chimica Acta*, **2006**, *579*, 33.

6. A. K. Sarker, H. Ukeda, D. Kawana, M. Sawamura, *Food Research International*, **2001**, *34*, 393.

7. M. I. Prodromidis, M. I. Karayannis, *Electroanalysis*, **2002**, *14*, 241.

8. A. Ramanavicius, K. Habermuller, E. Csöregi, V. Laurinavicius, W. Schuhmann, *Analytical Chemistry*, **1999**, *71*, 3581.

9. J. Razumiene, M. Niculescu, A. Ramanavicius, V. Laurinavicius, E. Csöregi, *Electroanalysis*, **2002**, *14*, 43.

10. M. Niculescu, T. Erichsen, V. Sukharev, Z. Kerenyi, E. Csöregi, W. Schuhmann, *Analytica Chimica Acta*, **2002**, *463*, 39.

11. L. Gorton, E. Dominguez, *Reviews in Molecular Biotechnology*, **2002**, *82*, 371.

12. T. J. Ohara, R. Rajagopalan, A. Heller, *Analytical Chemistry*, **1994**, *66*, 2451.

13. R. Antiochia, L. Gorton, *Biosensors & Bioelectronics*, **2007**, *22*, 2611.

In memoriam prof. dr. Liviu Oniciu

PASTED NICKEL ELECTRODES FOR ALKALINE BATTERIES

ELEONORA MARIA RUS[a], DELIA MARIA CONSTANTIN[a], GEORGETA ŢARĂLUNGĂ[b]

ABSTRACT. Pasted nickel electrodes for alkaline batteries were prepared by deposition of the electrodic mixture slurry (active material, conductive additives and binder) on nickel foam substrate and on nickelated iron grid, respectively.The electrochemical behaviour of these electrodes in 6N KOH electrolyte has been investigated by cyclic voltammetry and performance curves. From cyclic voltammograms were determined the electrochemical processes that occur on the electrodes in normal conditions, at overcharge and overdischarge.The coulombic efficiencies, calculated from charge-discharge curves in galvanostatic regime, demonstrated the better performance of pasted electrodes on nickel foam substrate.

Key words: *Pasted nickel electrodes, coulombic efficiencies, charge-discharge curves, Cyclic Voltammetry.*

INTRODUCTION

The structural and electrochemical characteristics of a given cathode material have a great influence on the performance of electrochemical power sources. Nickel hydroxide is a successful cathode material used in Ni-Cd, Ni-Zn, Ni-Fe, Ni-H$_2$ and in the more environmentally friendly Ni-MH systems [1-3].

Nickel based alkaline batteries are attractive since the nickel electrode can be fabricated with very large surface areas which lead to high capacities and high current densities. The electrolyte does not enter into the electrode reaction so that conductivity stays at a high level throughout the usable capacity of the battery. In addition, the nickel active material is insoluble in KOH electrolyte which leads to longer life and better abuse tolerance. Only a proton is involved in the charge/discharge reaction leading to very small density changes and improved mechanical stability of the electrode during cycling. Also, the gravimetric and volumetric energy densities are very good for the nickel electrode [4, 5].

---

[a] *Babeş-Bolyai University, Faculty of Chemistry and Chemical Engineering, 11 Arany Janos St. Cluj-Napoca 400024, Romania, norus@chem.ubbcluj.ro*

[b] *University of Agricultural Sciences and Veterinary Medicine, 3-5 Manastur St. 400509 Cluj-Napoca, Romania*

The processes that take place during charge-discharge of the nickel electrode are represented by the equation:

$$NiOOH + H_2O + e^- \Leftrightarrow Ni(OH)_2 + HO^- \; ; \; \varepsilon^0 = 0.490 \text{ V/NHE} \quad (1)$$
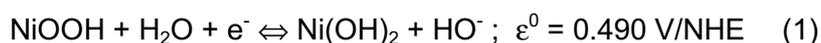
The active material of the nickel electrode consists of Ni(II) hydroxide in discharged state and Ni(III) oxihydroxide in charged state.

There are two primary commercial technologies for manufacturing nickel electrodes (which have been in existence for some 100 years): sintering and pasting.

A sintered electrode consists of a substrate, a porous Ni plaque sintered on the substrate, and an active mass of nickel hydroxide filled in the pores of the plaque. Sintered electrodes are characterized by high rate capability, good longevity, long-term storage, and low self-discharge. The electrode is widely used in portable NiCd and NiMH batteries and is highly preferred for high drain-rate applications.

Pasted electrodes, however, are gaining in popularity due to a reduced complexity in mass production, higher specific capacity, and lower environmental concerns. The performance of NiMH batteries using pasted nickel electrodes has advanced quickly and even the power density is approaching and outperforming those with sintered electrodes. A pasted electrode is made by pasting a slurry of active mass that contains nickel hydroxide, additives and binder materials into a porous substrate followed by drying and calendaring to finish the electrode [6, 7].

In our paper, the electrochemical behaviour of pasted nickel electrodes prepared by us on nickel foam substrate and on nickelated iron grid, respectively, is presented.

RESULTS AND DISCUSSION

Cyclic Voltammetry

The voltammograms recorded on a nickel plate in 6N KOH at different potential sweep rates are shown in Fig. 1.

The potential was scanned between the values at which oxygen evolution reaction (OER) and hydrogen evolution reaction (HER) occurred. Previously, the surface of the electrode was electrochemically treated by cathodic polarization at -1.1V for 5 minutes. The stabilized form of voltammograms was obtained, at v = 20 mV/s, only after 8 oxidation-reduction cycles.

This stabilized profile of voltammograms corresponds to obtaining of some reproductible discharge capacities of electrodes in batteries.

In the anodic sweep at ε = - 0.550 V, the formation of Ni(OH)$_2$ (peak A) takes place which at potentials between 0.530 - 0.630 V is oxidized to NiOOH (peak B). OER begins at 0.700 - 0.750 V, depending of sweep rates.

In the cathodic sweep, the reduction of NiOOH to Ni(OH)$_2$ (peak C) occurs at potentials between 0.300 - 0.400 V, while the reduction of Ni(OH)$_2$ to Ni is not observable because of HER.

The average potential, $\varepsilon' = \dfrac{\varepsilon_{a,p} + \varepsilon_{c,p}}{2}$, and the difference of peak positions, $\Delta\varepsilon_p = \varepsilon_{a,p} - \varepsilon_{c,p}$ of NiOOH / Ni(OH)$_2$ couple, was calculated from anodic and cathodic peak potential values , for all the sweep rates.
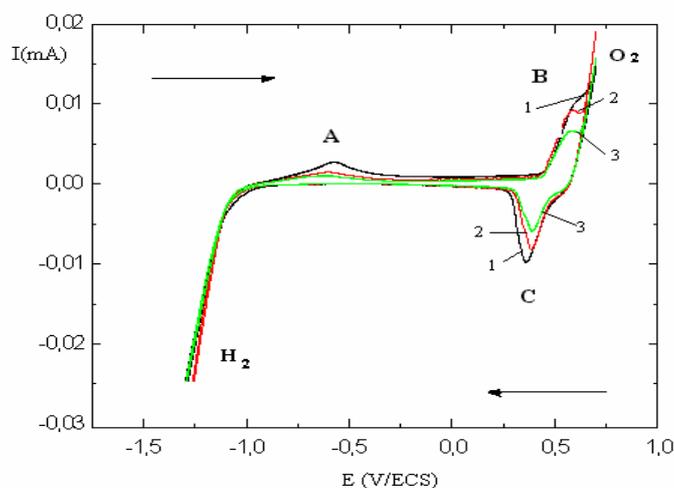

Figure 1. Cyclic voltammograms of nickel plate electrode in 6N KOH at v = 50 mV/s (1), v = 30 mV/s (2) and v = 20 mV/s (3)

The efficiency of processes was estimated from the anodic and cathodic peak currents ratio values ($I_{c,p} / I_{a,p}$) (table 1).

It was observed that the reversibility of oxidation-reduction processes estimated from $\Delta\varepsilon_p$ values is better as the sweep rates are smaller. The anodic and cathodic peak currents ($I_{a,p}$ and $I_{c,p}$) are higher as sweep rates increase. The $I_{c,p} / I_{a,p}$ ratio increases when sweep rate decreases.

The stabilized form of voltammograms for pasted nickel electrodes on nickelated iron grid and on nickel foam substrate, obtained after 5 oxidation-reduction cycles, for three sweep rates, are presented in figure 2 and figure 3.

Figure 2 shows that in the anodic sweep the peak B, corresponding to the charge process, is not observable because of OER (overcharge process) which take place at more negative potentials. But, the peak C recorded in the cathodic sweep is associated with the reduction of NiOOH formed in anodic sweep concomitantly with O$_2$ evolution.
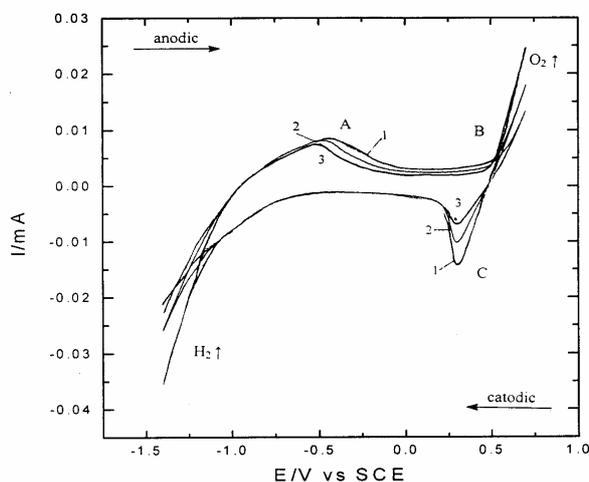
Figure 2. Cyclic voltammograms of pasted nickel electrode on nickelated iron grid in 6N KOH at v = 50 mV/s (1), v = 30 mV/s (2) and v = 20 mV/s (3)
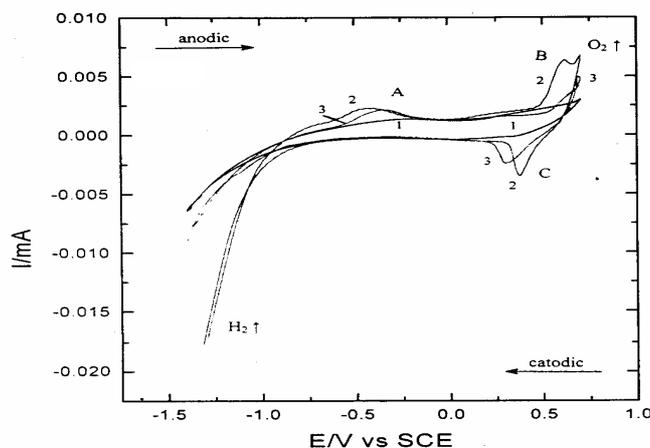

Figure 3. Cyclic voltammograms of pasted nickel electrode on nickel foam substrate in 6N KOH at v = 50 mV/s (1), v = 30 mV/s (2) and v = 20 mV/s (3)

For an efficient charge of the pasted nickel electrode on grid support, the oxygen evolution must be minimized.

The voltammograms presented in figure 3 show that OER occurs at more positive potential so that the charge process of electrode is better.

Thus, using nickel foam as support, the performance of pasted nickel electrodes in alkaline batteries is enhanced by minimizing of the parasitic O_2 evolution reaction and by improving the charge process, compared to electrodes on grid support.

The results of cyclic voltammetry measurements of tested electrodes related to the peak B and C are tabulated in Table 1.

Cyclic voltammetry measurements of tested electrodes in 6N KOH at 20 mV/s

Electrode	$\varepsilon_{a,p}(B)$ (V)	$\varepsilon_{c,p}(C)$ (V)	$\Delta\varepsilon_p$ (V)	ε' (V)	$I_{a,p}(B)$ (μA)	$I_{c,p}(C)$ (μA)	$I_{c,p}$ / $I_{a,p}$
Ni plate	0.529	0.408	0.121	0.468	6.6	5.8	0.97
Grid support	-	0. 308	-	-	-	6	-
Foam support	0.700	0.307	0.393	0.503	2.7	2.2	0.81

For pasted nickel electrode on foam support, the $I_{c,p}$ / $I_{a,p}$ ratio value demonstrates that the charge recovered on the cathodic sweep was very close with that of the previous anodic sweep, suggesting the high efficiency of processes.

Galvanostatic Charge-Discharge Curves
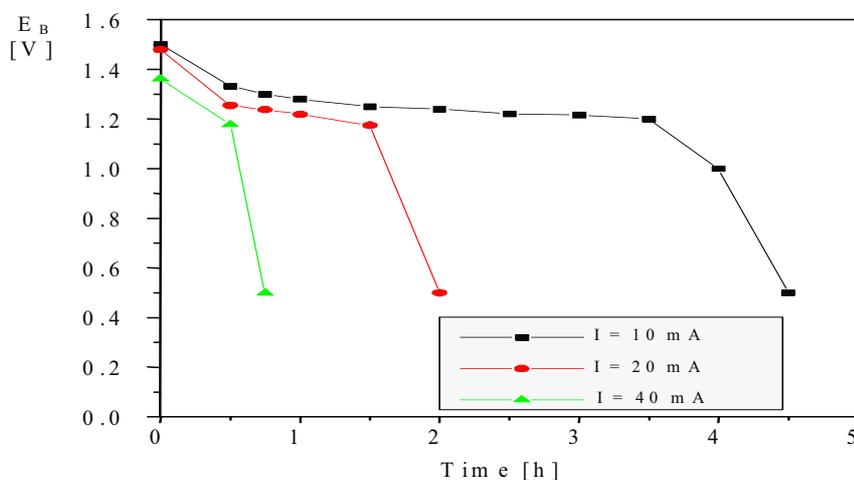The discharge curves of tested electrodes are shown in Fig. 4 and Fig. 5.

Figure 4. Discharge curves for pasted nickel electrode on nickelated iron grid at three discharge rates.

The charge capacities, C_{charge}, correspond to charging for 4h at I = 15 mA and the discharge capacities were determined from the plateaus of the discharge curves. The coulombic efficiencies r_F, calculated from the charge-discharge characteristics, are presented in table 2.
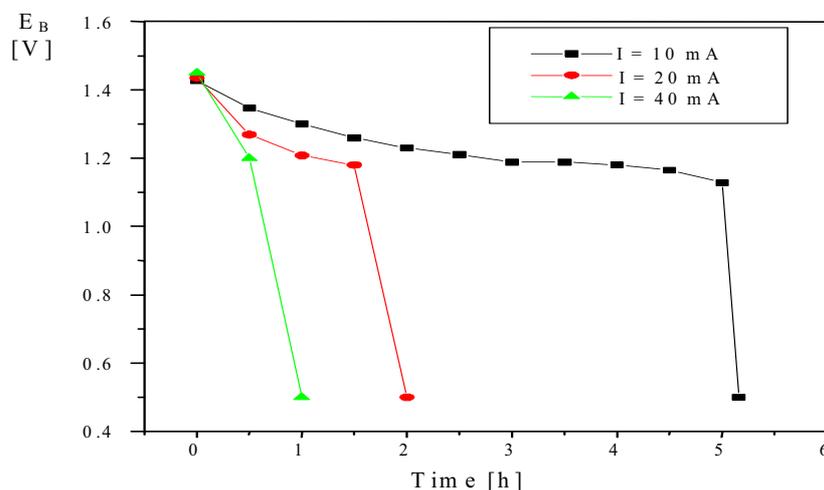
Figure 5. Discharge curves for pasted nickel electrode on nickel foam support at three discharge rates.

Table 2.

Coulombic efficiencies of tested electrodes

Electrode	C_{charge} (mAh)	$I_{discharge}$ (mA)	$t_{discharge}$ (h)	$C_{discharge}$ (mAh)	r_F (%)
Grid support	60	10	4.08	40.8	68.00
	60	20	1.66	33.2	55.33
	60	40	0.70	28.0	46.66
Foam support	60	10	5.16	51.6	86.00
	60	20	2.15	43.0	71.66
	60	40	0.92	36.8	61.33

It is obvious that the discharge capacities and coulombic efficiencies of the pasted nickel electrodes on nickel foam support are substantially increased compared to the electrodes on nickelated iron grid.

The pasted nickel electrodes on nickel foam support can be recomended for successful utilization as cathodes in alkaline batteries due to their electrochemical characteristics.

CONCLUSIONS

Two types of pasted nickel electrodes were realized by deposition of the electrodic mixture slurry consisting of NiOOH as active material, nickel powder and graphite as conductive additives and polyvinyl alcohol as binder on nickel foam substrate and on nickelated iron grid, respectively.

The electrochemical behaviour of these electrodes in 6N KOH electrolyte has been investigated by cyclic voltammetry and charge-discharge curves in galvanostatic regime, at room temperature.

It was established that both electrodes require five charge-discharge cycles to achieve a stabilized capacity, corresponding to formation process.

The charge process of nickel electrodes occurs in competition with OER and for an efficient charge of pasted nickel electrodes the oxygen evolution must be minimized.

Using nickel foam as support, the performance of pasted nickel electrodes in alkaline batteries is enhanced by minimizing of the parasitic O_2 evolution reaction and by improving the charge process, compared to electrodes on grid support.

The pasted nickel electrodes on nickel foam support can be recommended for successful utilization as cathodes in alkaline batteries due to their electrochemical characteristics.

EXPERIMENTAL SECTION

Pasted nickel electrodes for alkaline batteries were prepared by the following important steps:

♦ preparation of active material;
♦ preparation of electrodic mixture;
♦ realization of electrodes.

Active material was prepared in the charged form by chemical precipitation of $Ni(OH)_2$ from a $NiSO_4.7H_2O$ solution with a KOH solution followed by a chemical oxidation of $Ni(OH)_2$ to $NiOOH$ [8].

The prepared electrodic mixture consists of $NiOOH$ as active material, nickel powder and graphite as conductive additives and polyvinyl alcohol as binder. Two types of electrodes were realized by depositon of the electrodic mixture slurry on nickel foam substrate and on nickelated iron grid, respectively.

The electrochemical behaviour of these electrodes in 6N KOH electrolyte has been investigated by cyclic voltammetry and charge-discharge curves in galvanostatic regime, at room temperature.

The cyclic voltammetry experiments were performed by means of an Wenking HP 72 potentiostat, a PV2 programmer Meinsberg type, a MV 87 Pracitronic digital milivoltmeter and a NE 230 X-Y recorder. A platinum wire as counter electrode and a saturated calomel electrode (SCE) as reference were used.

The charge-discharge curves were performed in a half-cell consisting of pasted nickel electrode as working electrode, a nickel plate as counter electrode and a SCE as reference electrode. All the potentials given in this paper are referred to SCE.

REFERENCES

1. L. Oniciu, Eleonora Maria Rus, *Surse electrochimice de putere,* Ed. Dacia, Cluj-Napoca, **1987**, chapter 7.
2. B. Paxton, J. Newman, *Journal of Electrochemical Society*, **1997**, *144*, 3818.
3. J. Desilvestro, O. Haas, *Journal of Electrochemical Society,* **1990**, *137*, 5c.
4. A. Forrest, *Modern Battery Technology*, Center for Professional Advancement, Trumbore ed., **1995**, chapter 2.
5. D. Noreus, *Substitution of Rechargeable Ni-Cd Batteries,* Stockholm University, **2000**, 1.
6. J. J. C. Kopera, *Inside the Nickel Metal Hydride Battery,* Cobasys, 25 June **2004**, www.cobasys.com.
7. V. Srinivasan, B. C. Cornilsen, J. W. Weidner, *Journal of Solid State Electrochemistry,* **2005**, *9*, 61.
8. Delia Maria Constantin, Eleonora Maria Rus, Silvia Feşnic, *Producerea, transportul şi utilizarea energiei,* **2000**, *XIX*, 70.

In memoriam prof. dr. Liviu Oniciu

STRUCTURE, MORPHOLOGY AND ELECTROCHEMICAL PROPERTIES OF HIGH SURFACE AREA COPPER ELECTRODES OBTAINED BY THERMAL SPRAYING TECHNIQUES

ANDREA KELLENBERGER[a], N. VASZILCSIN[a], N. DUȚEANU[a], M.L. DAN[a], WALTRAUT BRANDL[b]

ABSTRACT. Three types of high surface area copper electrodes were prepared by thermal spraying techniques. CuAl electrodes were obtained by thermal arc spraying of two different wires (Cu and Al) followed by the alkaline dissolution of aluminum. Cu wire and Cu powder electrodes were obtained by combustion spraying of copper wires and powders, respectively. Several methods have been used to characterize the electrodes, including scanning electron microscopy, energy dispersive X-ray analysis and X-ray diffraction. The electrocatalytic activity of the electrodes was evaluated based on the steady-state polarization curves and electrochemical impedance data. It has been found that the structure of the prepared electrodes depends to a great extent on the deposition method, i.e. combustion spraying gives deposits with higher surface roughness and porosity. Decreasing the particles size leads to the increase of the porosity and surface roughness and also to the increase of the copper oxide content.

Keywords: high surface area electrodes, thermal spraying, electrocatalysis, electrochemical impedance spectroscopy

INTRODUCTION

Electrochemistry has been often seen as a potential route for the development of environmentally friendly and sustainable methods for energy generation and organic synthesis [1]. However, an important issue is the increase of the rate of electrochemical reactions, which is equivalent to the reduction of the overpotential. There are two important methods which may be applied independently or combined to attain this purpose: the increase of the electrode real surface area and the increase of the electrode intrinsic activity. The real surface area may be enlarged by appropriate preparation

[a] *"Politehnica" University of Timişoara, Faculty of Industrial Chemistry and Environmental Engineering, 300006 – Timisoara, P-ta Victoriei 2, Romania*
[b] *University of Applied Sciences Gelsenkirchen, Material Science Department, Neidenburger Str. 10, 45877 – Gelsenkirchen, Germany*

methods such as composite coating [2-4], powder pressing [5-7] or thermal spray [8-11], whereas the electrocatalytic activity is increased by doping [12] or surface modification.

High surface area electrodes have found numerous applications in electrocatalysis, especially for the gas evolution / consumption reactions such as: hydrogen evolution reaction (HER), hydrogen oxidation reaction (HOR) and oxygen reduction reaction (ORR), in some organic reduction reactions, in batteries and fuel cells [13].

Considerable research has been done in the past years on performant hydrogen cathodes with low hydrogen overpotential. The major application for such cathodes is the alkaline water electrolysis and alkaline chloride electrolysis. The activity for the hydrogen evolution reaction can be substantially improved by increasing the surface area of the electrode [14].

The aim of this work is to study the influence of the structure and morphology on the electrochemical activity of high surface area copper electrodes. The method used in this study to prepare the electrodes is the thermal spray deposition of an electroactive coating based on copper on a conducting carbon-stel support.

RESULTS AND DISCUSSION
SEM and EDX studies

The SEM micrographs taken for the surface of the electrodes and the OM micrographs taken for the cross-section of the electrodes are shown in Figures 1-3.
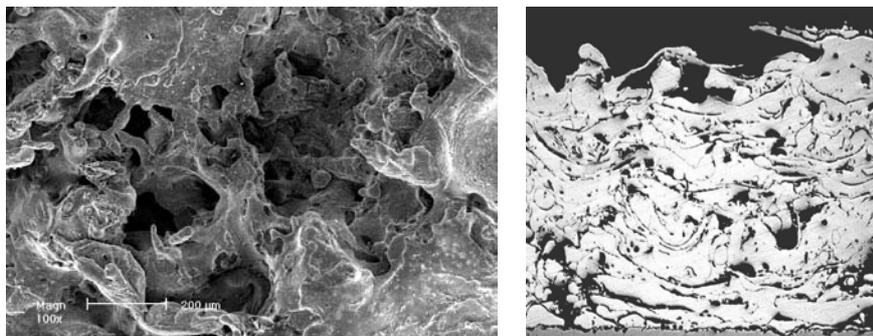

Figure 1. CuAl electrode after leaching;
(a) surface, magnitude 100×; (b) cross-section, magnitude 50 ×

The CuAl electrode shows a high irregular and rough structure, characterized by the formation of wide pores in the structure after the dissolution of aluminum. The cross section image reveals a complex layered structure with interlamelar porosity and inclusion of voids and oxide particles. The dimension of pores varies in a large range between 70 – 200 µm.
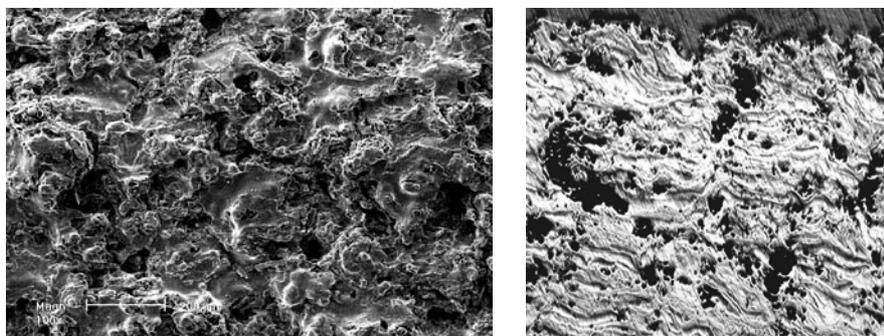
90

Figure 2. Copper wire electrode;
(a) surface, magnitude 100×; (b) cross-section, magnitude 50 ×

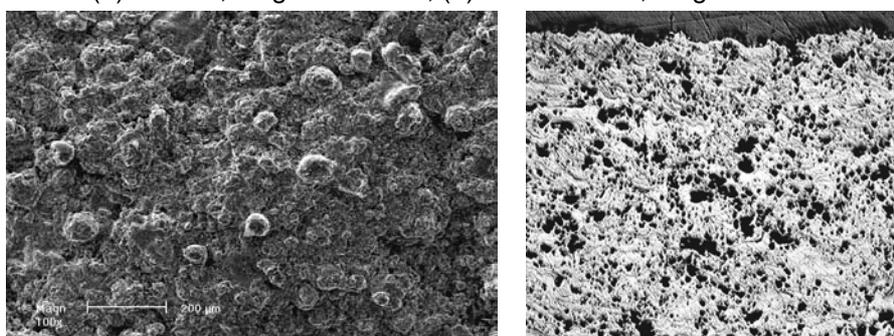**Figure 3**. Copper powder electrode;
(a) surface, magnitude 100×; (b) cross-section, magnitude 50 ×

The Cu wire and Cu powder electrodes show a much more regular structure and a uniform distribution of the pore sizes. The surface of the Cu wire electrode is characterized by the presence of molten droplets flattened during the impact with the substrate. The diameter of pores varies between 50 – 70 μm. In the case of Cu powder electrodes spherical shaped particles are present on the surface and the pore diameter is 10 – 30 μm.

The Energy Dispersive X-Ray analysis allows a semi-quantitative determination of the element composition of the coatings. The composition of the copper electrodes is given in Table 1.

Table 1.

Results of the EDX analysis of the copper electrodes.

Electrode	CuAl			Cu wire		Cu powder	
Composition	Cu wt%	Al wt%	O wt%	Cu wt%	Al wt%	Cu wt%	Al wt%
As sprayed	67.5	19.2	13.3	82.9	17.1	88.8	11.2
Leached	88.7	1.6	9.7				

Before leaching, the CuAl electrode has a relatively high content of aluminum which decreases more than tenfold after leaching. In all cases oxygen was also detected, indicating a certain degree of oxidation of the copper electrodes. Comparing the oxygen content of the electrodes the oxidation degree can be determined. Based on this values it has been calculated that the oxidation degree of Cu powder electrodes is 1.53 times higher than that of Cu wire electrodes.

X-Ray Diffraction was used to determine the phases obtained during the deposition process. The diffraction patterns of the CuAl coating (here not shown) before leaching shows the presence of the aluminum. After the dissolution of the aluminum only the peaks corresponding to copper appear.

The diffraction patterns of the Cu wire and Cu powder electrodes reveal the presence of the copper oxide, formed during the thermal spray process. As a representative example the X-ray spectra for the Cu powder electrode are given in Figure 4.
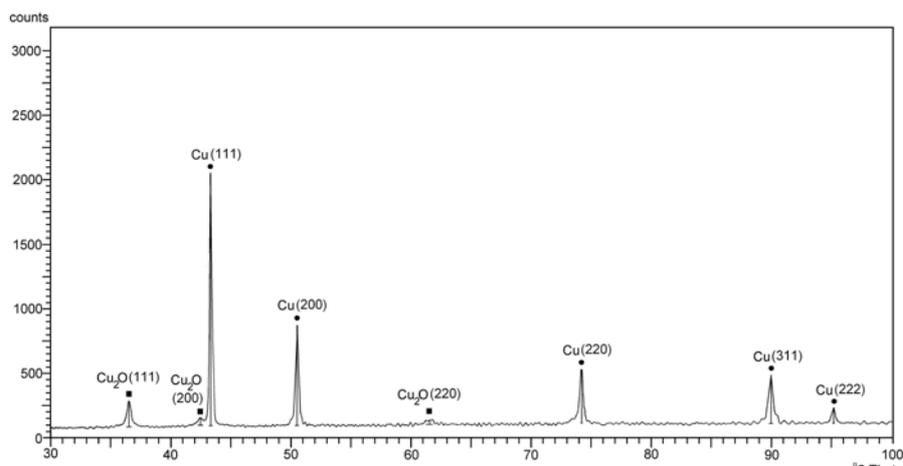

Figure 4. Diffraction patterns of the Cu powder electrode.

In both cases the RX spectra shows the characteristic peaks of Cu_2O at diffraction angles equal to $2\theta = 36.52$; 42.49; 61.45 for Cu wire and $2\theta = 36.51$; 42.46; 61.47 for Cu powder respectively. The height of the first peak may offer quantitative information about the oxidation degree of the electrodes. Thus, it has been obtained a 1.66 higher oxidation degree of the Cu powder electrode as compared with the Cu wire electrode. This value is in good agreement with that calculated from EDX data.

Electrochemical measurements

The electrochemical activity of the prepared electrodes was compared with that of a smooth copper electrode. The steady state polarization curves recorded in NaOH solution are given in Figure 5. At low current density a

depolarization of approximately 200 mV was found for the Cu powder electrode compared with the smooth copper electrode. However, at higher current densities the depolarization reduces to 100 mV, probably due to the occlusion of pores by hydrogen bubbles due to the intensification of the HER at more negative overpotential.
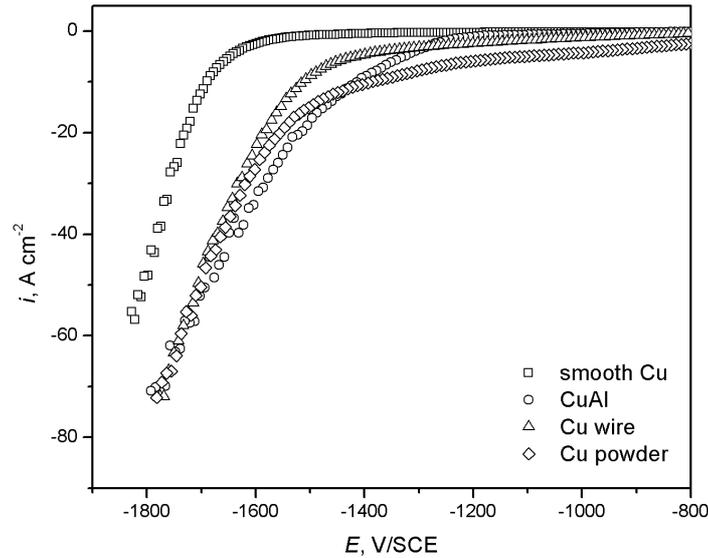

Figure 5. Current-potential curves in 1M NaOH solution at 21°C. Scan rate 1 mV/s.

EIS measurements were performed on the high surface area copper electrodes at electrode potentials located in the hydrogen evolution region. Complex plane plots for the smooth Cu, CuAl, Cu wire and Cu powder electrodes at −1.2 V are given in Figure 6.

In all four cases the shape of the impedance spectra corresponds to a depressed semicircle in the studied frequency range. The experimental impedance data were fitted to an electrical equivalent circuit consisting of the solution resistance R_S in series with a parallel connection between a constant phase element CPE and the charge transfer resistance R_{ct} [15,16]. The total impedance of this model is equal to:

$$Z = R_S + \left(R_{ct}^{-1} + T(j\omega)^{\Phi}\right)^{-1} \tag{1}$$

where T is a parameter related to the double layer capacitance and ϕ is the constant phase angle parameter. The double layer capacitance is given by [17]:

$$T = C_{dl}^{\phi}\left(R_S^{-1} + R_{ct}^{-1}\right)^{1-\phi} \tag{2}$$
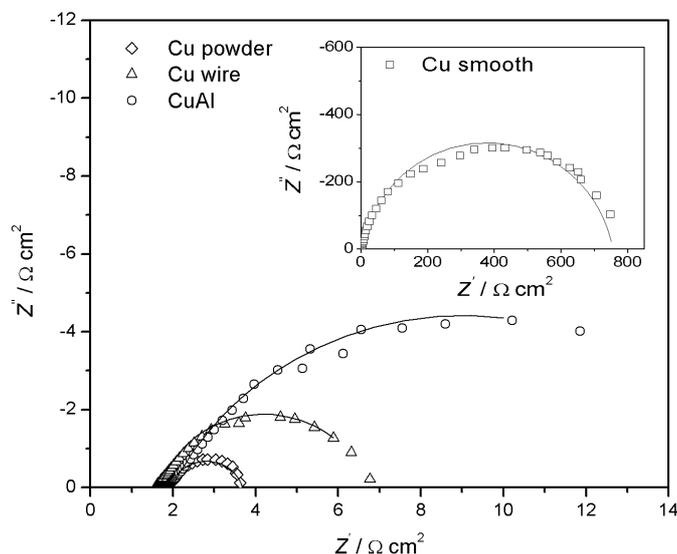
93

Figure 6. Nyquist plots obtained in 1M NaOH solution at 21°C. Symbols are experimental data and continuous lines are fitted data by the Levenberg-Marquardt procedure.

The values of the circuit elements obtained by modeling the experimental data are given in Table 2.

Tabel 2.

Impedance data obtained in 1 M NaOH solution for the studied copper electrodes.

Electrode	R_S [Ω cm^{-2}]	R_{ct} [Ω cm^{-2}]	C_{dl} [F cm^{-2}]	R_f
Cu smooth	1.88	753	$0.187 \cdot 10^{-3}$	7.5
CuAl	1.90	14.1	$13.8 \cdot 10^{-3}$	552
Cu wire	1.67	5.08	$14.7 \cdot 10^{-3}$	588
Cu powder	1.92	1.85	$17.2 \cdot 10^{-3}$	692

The surface roughness factor R_f of the prepared electrodes was determined from the ratio of the double layer capacitance values and the double layer capacitance of a smooth copper electrode. Assuming a value of $25 \cdot 10^{-6}$ F cm^{-2} suggested in the literature for the double layer capacity of a smooth electrode, the highest surface area has been obtained for the Cu powder electrode, followed by the Cu wire electrode.

CONCLUSIONS

Thermal spraying is a suitable method to obtain porous structures with high surface area. The CuAl electrodes present a rough surface with large pores, with a diameter between 70 – 200 µm. The Cu wire and Cu powder electrodes reveal also a porous structure but the pores are much smaller, i.e. between 50 – 70 µm for the wire sprayed electrodes and 10 – 30 µm for the powder sprayed electrodes.

The shift of the current-potential curves to lower overpotentials, comparatively to a smooth copper electrode, is to be attributed to the surface area enhancement effect.

The values of the roughness factor determined from the impedance data are in good agreement with the increase of the porosity observed from the SEM and OM micrographs. The decrease of the charge transfer resistance values is consistent with the increase of the current densities obtained by polarisation measurements.

Based on the steady-state polarisation and impedance measurements, improved electrocatalytic activities for the hydrogen evolution reaction are attributed to the increase of the real surface of the electrodes.

EXPERIMENTAL SECTION

Electrode preparation

The high surface area copper electrodes were prepared by thermal arc and combustion spraying of three different types of materials: CuAl alloy wire, Cu wire and Cu powder.

The CuAl electrode was prepared by thermal arc spraying of a CuAl wire (92% Cu, 8% Al) with a diameter of 1.6 mm. The operating parameters were set to: arc current 200 A, arc voltage 30 V and gas pressure 3 bars. After depositon the coating was activated by alkaline leaching of the Al in 1M NaOH at $80^{o}C$ for 120 min.

The Cu wire and Cu powder electrodes were obtained by combustion spraying of copper wire (Cu 99.8%) with the diameter of 1.6 mm and copper powder with the particle size -90 +45 µm (-170 +325 mesh) respectively. The deposition was performed with an oxyacetylene torch and with air as atomizing gas (pressure 3 bars).

In all cases, as a support for the electroactive coating a carbon steel plate with the dimensions of $100 \times 300 \times 3$ mm was used. Prior to the deposition the substrate was degreased and sanded with corundum in order to assure an adequate adherence.

Electrode characterization

The surface morphology of the electrodes was investigated by scanning electron microscopy (SEM) with a Philips XL 30 ESEM microscope operating at 20 kV and by optical microscopy (OM) using a LEICA D MR/M microscope. The elemental composition was determined by Energy dispersive X-Ray analysis (EDX) coupled with the scanning electron microscopy. For the phase composition X-Ray diffraction spectra were registered with a Philips X'pert diffractometer using the Cu-Kα radiation.

Electrochemical measurements

The electrocatalytic activity of the copper electrodes was investigated towards the hydrogen evolution reaction. Steady state current-potential curves were recorded with a VoltaLab 21 potentiostat in 1 mol L^{-1} NaOH solution with a scan rate of 1mV s^{-1}. A conventional three-electrode electrochemical cell was used with a platinum counterelectrode and a saturated calomel electrode as reference. The *iR* drop between the electrode surface and solution was minimized using a Haber-Luggin capillary, placed at about 1 mm of the surface. Electrochemical impedance spectroscopy (EIS) was applied to determine the surface roughness of the electrodes. Impedance spectra in the frequency range 1 kHz to 10 mHz were recorded using a Solartron Instruments 1287 Potentiostat and a 1255B Frequency Response Analyzer. The experimental data were fitted to the equivalent circuit by a complex non-linear least squares (CNLS) Levenberg-Marquard procedure using the ZView-Scribner Associates Inc. software.

REFERENCES

1. M. A. Matthews, *Pure and Applied Chemistry*, **2001**, *73*, 1305.

2. H. J. Miao, D. L. Piron, *Electrochimica Acta*, **1993**, *38*, 1079.

3. Y. Choquette, L. Brossard, A. Lasia, H. Menard, *Electrochimica Acta*, **1991**, *35*, 1251.

4. Y. Choquette, L. Brossard, A. Lasia, H, Menard, *Journal of the Electrochemical Society*, **1990**, *137*, 1723.

5. P. Los, A. Rami, A. Lasia, *Journal of Applied Electrochemistry,* **1993**, *23*, 135.

6. C. Hitz, A. Lasia, *Journal of Electroanalytical Chemistry*, **2001**, *500*, 213.

7. R. P. Simpraga; B. E. Conway, *Electrochimica Acta,* **1998**, *43*, 3045.

8. D. Miousse, A. Lasia, V. Borck, *Journal of Applied Electrochemistry*, **1995**, *25*, 592.

9. G. Schiller, R. Henne, V. Borck, *Journal of Thermal Spray Technology*, **1995**, *4*, 185.

10. J. Fournier, D. Miousse, J. G. Legoux, *International Journal of Hydrogen Energy*, **1999**, *24*, 519.

11. L. Birry, A. Lasia, *Journal of Applied Electrochemistry*, **2004**, *34*, 735.

12. T. Kenjo, *Electrochimica Acta*, **1988**, *33*, 41.

13. "*Fuel Cell Handbook*" by EG&G Technical Services *(Seventh Edition),* **2004**.

14. a) A. Kellenberger, N. Vaszilcsin, W. Brandl, N. Duteanu, *International Journal of Hydrogen Energy*, **2007**, *32*, 3258; b) A. Kellenberger, N. Vaszilcsin, W. Brandl, *Journal of Solid State Electrochemistry*, **2007**, *11,* 84; c) N. Vaszilcsin, W. Brandl, A. Kellenberger, D. Toma, *Chemical Bulletin of Polytechnic University Timişoara,* **1998**, *43*, 330.

15. L. Chen, A. Lasia, *Journal of the Electrochemical Society*, **1991**, *138*, 3321.

16. L. Birry, A. Lasia, *Journal of Applied Electrochemistry*, **2004**, *34*, 735.

17. G. J. Brug, A. L. G Van Der Eeden, M. Sluyters-Rehbach, J. H. Sluyters, *Journal of Electroanalytical Chemistry*, **1984**, *176*, 275.

In memoriam prof. dr. Liviu Oniciu

ELECTRODEPOSITION OF SOME HEAVY METALS ON RETICULATED VITREOUS CARBON ELECTRODE

SORIN-AUREL DORNEANU[*], BEKE FERENCZ-LÁSZLÓ, PETRU ILEA

ABSTRACT. Nowadays, the damage of the environment quality has reached alarming levels requiring severe measures for stopping this process. In order to harmonise with the maximum admitted concentrations (MAC) of heavy metal ions (HMIs) in the discharged effluents, the electrochemical procedures represent a clean, flexible and efficient alternative of decontamination. In this context, the present paper describes the results of our researches concerning the electroextraction of heavy metals from synthetic diluted solutions. Starting from simple or complex solutions with initial HMI contents of 10 ppm (parts per million), the MAC can be reached after 90 min. of electrolysis in a continuous flow electrochemical reactor equipped with a three-dimensional (3D) electrode made of reticulated vitreous carbon.

Keywords: *electrodeposition, heavy metal ions, reticulated vitreous carbon electrode, waste waters*

INTRODUCTION

Many manufacturing sectors like galvanotechnical, metallurgical, electronic or chemical industries produce huge quantities of high pollutant residual waste waters containing HMIs. At the end of the past century, the production of hazardous wastes was estimated, as described in Table 1, at about 7000 millions tons/year, from millions tons/year are generated only in the European Community [1].

Table 1.

Estimated global production of industrial wastes [1]

Manufacturing sectors	Contained metals	Quantity (tons/year)
Electronic	As, Cr, Hg, Se, Ni, Cu	1200000
Mineral oil and coal	As, Pb, V, Cd, Ni, Zn	1200000
Mining and metallurgy	Hg, Cr, Cu, As, Zn, Pb	390000
Agriculture	Mg, As, Cu	1400000
Metals' Processing	Cr, Co, Ni, Fe	240000
Others		720000

[*] *Department of Physical Chemistry, "Babes-Bolyai" University, 11 Arany Janos, 400028 Cluj-Napoca, Romania; dorneanu@chem.ubbcluj.ro*

The recycling of heavy metals represents an economical and ecological solution for the treatment of these huge quantities of wastes. The liquid effluents containing HMIs, resulted from the metals processing industry, can be electrochemically treated in order to extract the metals by means of the cathodic deposition: $M^{z+} + ze^- \rightarrow M$. The recovery of pure metals represents the main advantage of the electrodeposition.

Depending on the HMIs' concentrations, the heavy metals recovery from waste waters by electrodeposition can be done in different manners. For high concentrations (over few grams per litter), two-dimensional cathodes can be used and the content of HMIs can be reduced with one order of magnitude. The resulting effluent can be reused in the process or it can be introduced in a new stage of chemical or electrochemical decontamination. For low HMIs' concentrations, under hundreds milligrams per litter, 3D electrodes can be used and the content of HMIs can be reduced to levels that allow the discharge of the effluents in environment.

The 3D electrodes are generally made from carbonaceous materials, among witch the reticulated vitreous carbon (RVC), having the best performances, is the mainly used material. The RVC is made exclusively from vitreous carbon and has an open honeycomb-shaped structure, conferring to the material a small electric resistance, a high porosity and a high specifically surface area. It is produced at different degrees of porosity between 10 and 100 pores per inch (ppi), having a pores' fraction between 90 and 97% [2]. At pH = 7, the RVC electrochemical stability domain is ranged between -1.2 and +1.0 V *vs.* SCE. In the absence of Cl$^-$ ions and depending on the pH value, the anodic limit corresponds to the water decomposition to oxygen; the useful cathodic potential domain is limited by the reduction reaction of the hydrogen (rrH) and can be extended to more negative values by deposition of a Hg thin layer on the RVC surface [3].

Concerning the use of RVC for the heavy metals recovery from waste waters, the literature presents many studies [4-12], but, in the majority of them, the composition of the aqueous solutions was modified by adding of concentrated supporting electrolytes in order to increase the electrolyte conductivity.

In this paper, we present our results concerning the electroextraction of heavy metals from synthetic diluted solutions by using RVC. Simple or complex solutions with initial HMIs contents of 10 ppm were prepared using diluted HNO_3. The specific electrodeposition potentials were evaluated by cyclic voltametry (CV) and the prepared solutions were electrolysed potentiostatically in a continuous flow electrochemical reactor (ER), equipped with a 3D RVC electrode. The residual concentrations of HMIs were measured by atomic adsorption spectroscopy (AAS).

RESULTS AND DISCUSSION

CV studies

Arming to evaluate the possibilities of the HMIs' electroextraction from extremely diluted electrolytes, preliminary studies were completed by CV in mono-elemental solutions. The measurements were performed at a scan rate of 50 mV/s, all the solutions being deaerated by nitrogen bubbling in order to eliminate the interferences due to the oxygen electroreduction. For each studied HMI, the working electrode compartment was firstly filled with 5 mL of 10 mM HNO_3 and the voltamogram of the supporting electrolyte was recorded. After this, 1, 1, and respectively 3 mL of 10 mg/L dissolved metal solutions in 10 mM HNO_3 were added successively (resulting HMI's concentrations of 1.66, 2.85 and 5 ppm, respectively) and the corresponding voltamograms were recorded. Two examples of the acquired curves in 1.66 and 5 ppm HMIs' solutions during the cathodic scan are presented in Figure 1.
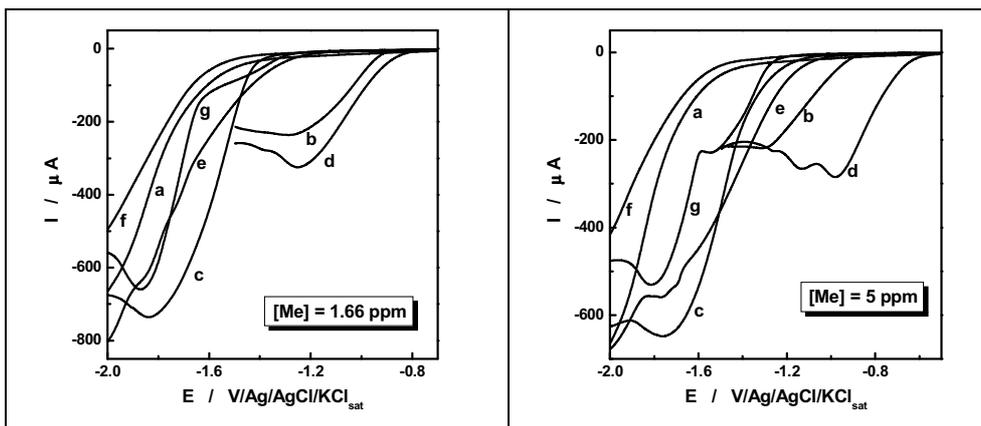

Figure 1. Recorded curves by CV in 1.66 and 5 ppm of corresponding HMIs solutions during the cathodic scan: a – supporting electrolyte only; b – Cd; c – Co; d – Cu; e – Ni; f – Pb; g – Zn. (anodic polarization curves are not presented)

As it can be seen from Figure 1, excepting the Pb case, where the electrodeposited metal blokes the rrH, the HMIs' additions induce increases of the cathodic currents even at the 1.66 ppm concentration level. Moreover, the increase of the HMIs' concentrations shifts the start of the net cathodic current to more positive potential values, suggesting that the heavy metal electrodeposition process starts before the rrH. Unfortunately, an optimal electrodeposition potential cannot be evaluated by CV studies due the fact that the rrH occurs simultaneously with the heavy metal electrodeposition process.

Electrodeposition studies

  The studies concerning the heavy metal electrodeposition from mono-elemental or complex solutions were performed using electrolyte volumes of 250 or 350 mL, respectively. At 5, 10, 15, 20, 25, 30, 35, 40, 45, 50, 55, 60, 70 and 90 minutes after the experiments' begin, aliquots of 3 or 10 mL respectively, were sampled from the overflow outlet and were analysed by AAS. During the experiments, the working electrode current ($I_{W.E.}$), the counter-electrode potential ($E_{C.E.}$) and the cell voltage (E_C) were also recorded, allowing us to estimate the current efficiency (η_C) and the specific electricity consumption (W_S).

Single metal electrodeposition results

  Figure 2 presents two examples of recorded signals during the electroextraction of Cu and Ni from the corresponding mono-elemental solutions at working electrode potentials ($E_{W.E.}$) of – 200 mV and -1200 mV respectively, in rapport with the previously mentioned reference electrode. Based on the recorded data and the AAS results, the final parameters (as presented in Table 2) were evaluated after 90 min. of electrolysis

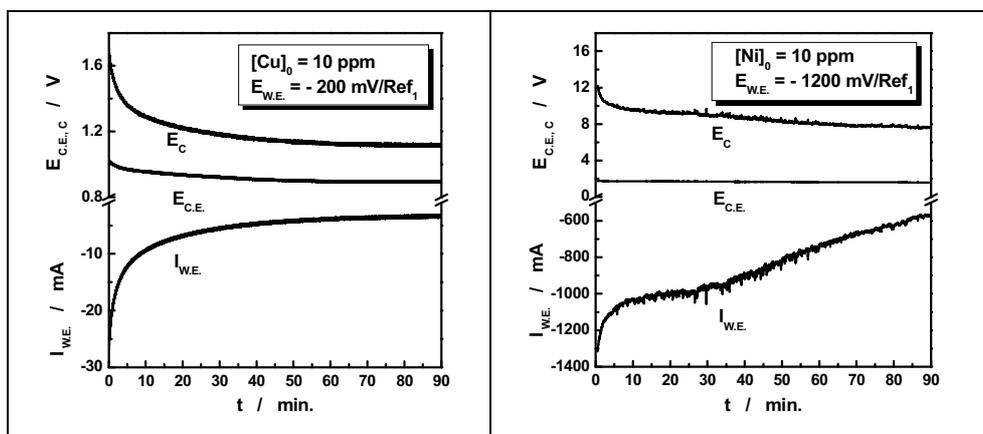**Figure 2.** Recorded signals during the electroextraction of Cu and Ni from the corresponding mono-elemental solutions.

Table 2.

Estimated final parameters after 90 min. of electrolysis

Metal	Residual concentration	η_C	W_S
Cu	0.09 ppm	24.2 %	0.043 kWh m^{-3}
Ni	0.29 ppm	0.16 %	44.2 kWh m^{-3}

As it can be seen from Figure 2 and Table 2, the recorded signals and also the η_C and the W_S present acceptable values in the case of Cu, but degrade significantly for the Ni electrodepositions due to the parallel rrH process. The evolution of HMIs' concentrations during their electroextraction from the corresponding mono-elemental solutions is presented in Figure 3.
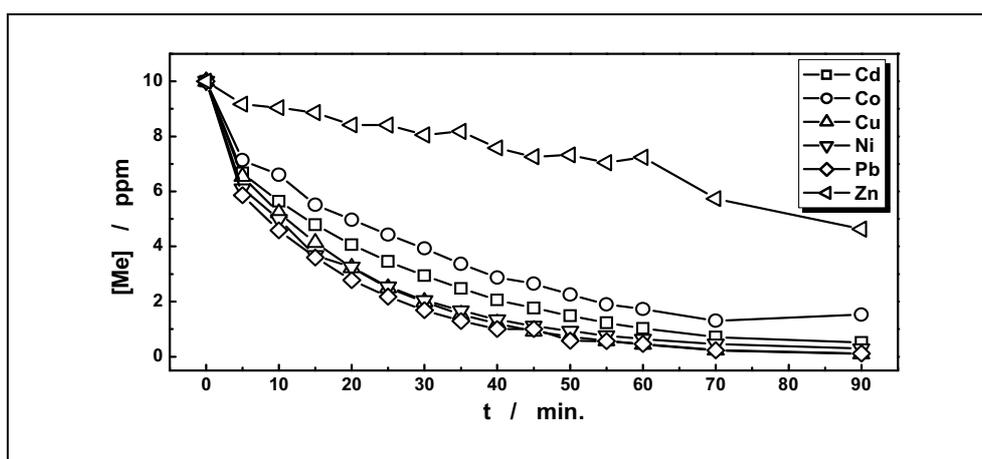

Figure 3. The evolution of studied HMIs' concentrations during their electroextraction from the corresponding mono-elemental solutions

As it can be see from Figure 3, excepting the Zn case, all the concentrations of the studied HMIs quickly decrease during the first hour of their electroextraction from the corresponding mono-elemental solutions. The residual concentrations values ([Me]$_{Res. Mono}$, presented in Table 3, together with the values of the applied working electrode potentials, $E_{W.E. Mono}$) are similar with the MAC levels [13].

Simultaneous metals electrodeposition results

The evolution of studied HMIs' concentrations during their electroextraction from the complex multi-elemental solution is presented in Figure 4 and the residual HMIs' concentration values ([Me]$_{Res. Multi}$) are presented in Table 3.

Table 3.

Comparison of the HMIs' electrodeposition parameters from mono and multi-elemental solutions

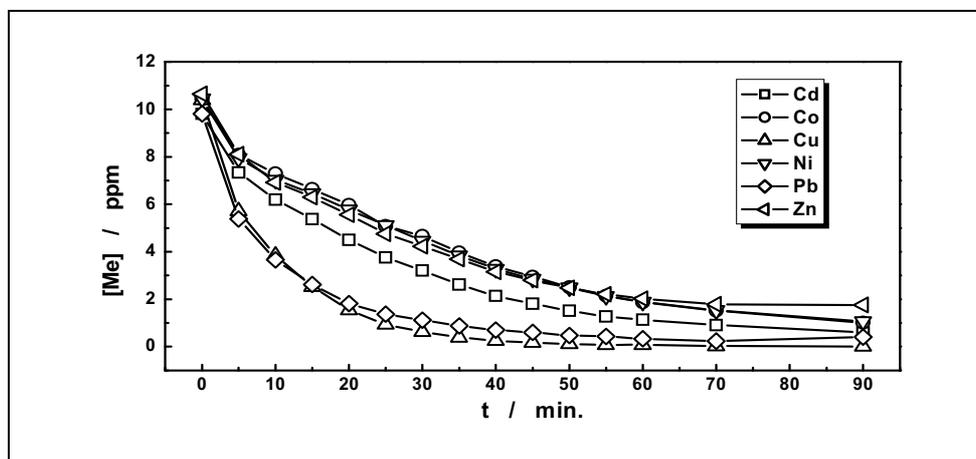| Metal	Cd	Co	Cu	Ni	Pb	Zn
$E_{W.E. Mono}$ / V	- 0.8	- 1.1	- 0.2	- 1.2	-0.6	-1.2
[Me]$_{Res. Mono}$ / ppm	0.51	1.52	0.09	0.29	0.12	4.63
[Me]$_{Res. Multi}$ / ppm	0.60	1.01	0.006	1.06	0.40	1.76
MAC / ppm	0.30	-	0.20	1.00	0.50	1.00

Figure 4. The concentrations evolution of studied HMIs during their electro-extraction from the complex multi-elemental solution on RVC electrode polarised at -1100 mV *vs.* Ag/AgCl/KCl$_{sat}$ reference electrodes

As it can be observed from Figure 4 and Table 3, the [Me]$_{Res. Multi}$ evaluated after the HMIs electrodeposition from multi-elemental solutions decrease for Co, Cu and Zn and increase for Cd, Ni and Pb. Moreover, it is worth to note that the [Me]$_{Res. Multi}$ values for Cu, Ni and Pb are very similar with the MAC levels.

CONCLUSIONS

The results of our researches concerning the electroextraction of some heavy metals (Cu, Co, Cd, Ni, Pb and Zn) from diluted solutions allow us to formulate the following conclusions:

• the electroextraction of Cu, Ni and Pb from extremely diluted solutions allows to achieve directly the MAC levels;

• for Cd and Zn, the obtained residual concentrations are in close proximity to the MAC levels;

• the mixture of studied HMIs doesn't obstruct the components electrodeposition, the individual residual concentrations being similar with the obtained ones in mono-elemental solutions;

• surprisingly, for Zn, the residual concentration after the electro-deposition from multi-elemental solution is smaller that the obtained one after the electrodeposition from mono-elemental solution;

• this preliminary results prove the feasibility of the electrochemical decontamination of the heavy metal polluted waste waters, but, in the same time, they require further researches in order to optimise the experimental parameters and also to validate the results using real waste waters.

102

EXPERIMENTAL SECTION

Reagents

The all solutions were prepared starting from mono-elemental AAS standard solutions (Merck) of Cd, Co, Cu, Ni, Pb and Zn, each one containing 1 g/L of dissolved metal and 0.5 M HNO_3. All prepared mono-elemental solutions contained 10 mg/L of the corresponding dissolved metal and 10 mM HNO_3. The tested complex solution contained 10 mg/L of each mentioned metal and 30 mM HNO_3. In order to achieve the desired compositions, 63 % HNO_3 solution (Merck, p.a.) and double-distilled water were also used.

Experimental setups

For CV measurements, a three-compartment glass electrochemical cell was used. A vitreous carbon disc (Φ = 3 mm), an Ag/AgCl/KCl$_{sat}$ system and a Pt wire (Φ = 0.8 mm, L = 15 mm) were utilized as working, reference and counter electrode, respectively. The LabView 6.1 software and a PCI 6024 E data acquisition board (National Instruments, USA) were also used for driving a computer controlled home-made potentiostat.

The electrodeposition measurements were completed using the experimental setup described in Figure 5.
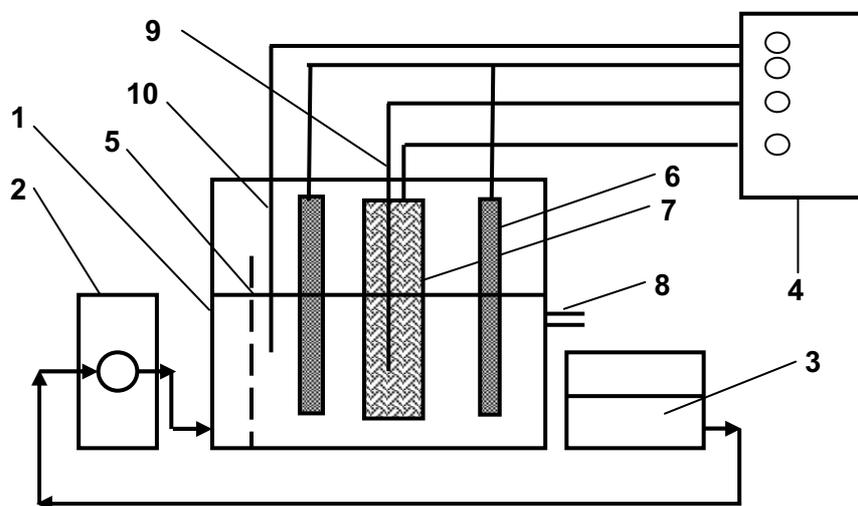

Figure 5. Experimental setup for the heavy metals electrodeposition:
1 – uncompartmented ER; 2 - peristaltic pump; 3 – electrolyte tank;
4 – computer controlled potentiostat; 5 – drilled diaphragm for flow
uniforming; 6 – graphite bar anodes; 7 – RVC cathode; 8 – overflow
outlet; 9 – cathode reference electrode; 10 – anode reference electrode.

The second experimental setup includes a home-made plexiglas uncompartmented ER, a Reglo-Digital peristaltic pump (Ismatec, Switzerland) and a HP72 potentiostat (Wenking, Germany). A 100 ppi RVC parallelepiped (L x W x H = 48 mm x 24 mm x 30 mm) was used as cathode and four graphite cylindrical bars (Φ = 12 mm, L = 30 mm) were utilised as counter-electrodes. Two Ag/AgCl/KCl$_{sat}$ reference electrodes were used to record the cathode's and anode's potentials during the electrodeposition. In order to assure a laminar and uniform electrolyte flow, a drilled PVC diaphragm was fixed between the inlet port and the electrodes compartment. The overflow outlet maintains a constant electrolyte level inside of the ER, allowing also periodical electrolyte sampling for the HMIs' content analysis.

The AAS measurements were completed with an Avanta PM spectrometer (GBC, Australia). The LabView 6.1 software and a PCI 6024 E board (National Instruments, USA) were used to drive the HP72 potentiostat and for data acquisition. During the heavy metals electrodeposition experiments, the peristaltic pump assures a constant electrolyte flow rate of 46 mL/min.

REFERENCES

1. F. Veglio, R. Quaresima, P. Fornari, *Waste Mangement*, **2003**, *23*, 245.
2. J.M. Friedrich, C. Ponce-de-Leon, G.W. Reade, F.C. Walsh, *Journal of Electroanalytical Chemistry*, **2004**, *561*, 203.
3. J. Wang, *Electrochimica Acta,* **1981**, *26*, 1721.
4. M. Lee, J.-G. Ahn, J.-W. Ahn, *Hydrometallurgy,* **2003**, *70*, 23.
5. I. Whyte, *PhD Thesis*, Southampton University, **1991**.
6. D. Pletcher, I. Whyte, F.C. Walsh, *Journal of Applied Electrochemistry,* **1991**, *21*, 667.
7. D. Pletcher, I. Whyte, F.C. Walsh, *Journal of Applied Electrochemistry,* **1993**, *23*, 82.
8. C. Ponce de Leoon, D. Pletcher, *Electrochimica Acta,* **1996**, *41*, 533.
9. J.Y. Choi, D.S. Kim, *Journal of Hazardous Materials,* **2003**, *B99*, 147.
10. C. Lupi, M. Pasquali, A. Dell'Era, *Minerals Engineering,* **2006**, *19*, 1246.
11. M. Lanza, V. Bertazzoli, *Journal of Applied Electrochemistry,* **2000**, *30*, 61.
12. A. Dutra, A. Espiinola, P. Borges, *Minerals Engineering*, **2000**, *13*, 1139.
13. Romanian Government Decision no. 352 from 11.05.2005.

In memoriam prof. dr. Liviu Oniciu

ELECTROCHEMISTRY OF IRON (III) PROTOPORPHYRIN (IX) SOLUTION AT GRAPHITE ELECTRODE

GRAZIELLA LIANA TURDEAN[a], CAMELIA FĂRCAŞ[b], AMELIA F. PALCU[c], MARINELLA S. TURDEAN[d]

ABSTRACT. Cyclic voltammmetry was used to investigate the electrochemical properties of iron (III) protoporphyrin (IX) (hemin, Fe(III)P) dissolved in TRIS buffer at a graphite electrode. A quasi-reversible single electron transfer attributed to the Fe(III)P/Fe(II)P redox process controlled by diffusion was identified. The pH influence on the electrochemical activity of hemin and its electrocatalytic behaviour towards nitrite reduction was also investigated and demonstrated.

Keywords: iron (III) protoporphyrin (IX), nitrite, cyclic voltammetry.

INTRODUCTION

Nitrite is an important source of nitrogen in green plants and its complete reduction to ammonia involves the overall transfer of six electrons [1]. The reduction of nitrate and nitrite has gained renewed attention in view of its relevance to pollution control due to excessive use in fertilizers, detergents, industrial processes and food technologies. Also, the control of water quality is important to avoid contamination of food produced when water is used as a raw material. Electrochemical reduction catalysis can be advantageously applied to the treatment of industrial wastewater, whereby nitrate species are transformed into harmless reduction products from various cathodic materials and solutions of different compositions. Generally, however, the electrochemical reactions of interest have been found to proceed at potentials substantially more negative than their thermodynamic values with low current density, providing evidence that their energies of activation are very high [2].

Organo-iron derivatives have been identified as intermediates in several biological processes. The main motivation for the investigation of iron-porphyrins' redox properties has been to establish their correlation with

[a] *Babes-Bolyai" University, Faculty of chemistry and chemical engineering, Department of Physical Chemistry, Arany Janos St. 11, 400028 Cluj-Napoca, Romania, gturdean@chem.ubbcluj.ro*
[b] *Colegiul tehnic "Napoca", str. Taberei nr. 3, 400512 Cluj-Napoca, Romania*
[c] *Liceul Teoretic "Mihai Veliciu" Chisineu-Cris, str. Primaverii nr. 3-5, 315100 Chisineu-Cris, jud. Arad*
[d] *"Dimitrie Cantemir" Christian University, Splaiul Unirii no. 176, 050099 Bucharest, Romania*

structure–function relationships of complex homoproteins. Due to electrochemical reversibility of iron-porphyrin derivatives, they can be used as electron transfer mediator for modification of different electrode materials, and preparations of chemically modified electrodes with these compounds have received great interest in the field of electroanalysis. Different supporting carbon materials have been used to disperse and stabilize electron transfer mediators, due to their low background currents, wide potential windows, chemical inertness and low costs [3]. Iron-porphyrins are also well recognized for their excellent electrocatalytic properties toward the detection of many important analytes, such as nitric oxide [4], neurotransmitters [5], O_2 [6], hydrogen peroxide [7], nitrite [8], superoxide [9], sulfur oxoanions [10], tryptophan and its derivatives [11 - 12].

Hemin (iron protoporphyrin IX) (Fe(III)P) is a naturally occurring iron-porphyrin complex possessing catalytic function [7] and as consequence is the active center of the family of heme-proteins, such as b-type cytochromes, peroxidase, myoglobin and hemoglobin [9, 13]. Its capacity to mimics the catalytic properties of enzymes lead to an intensive research activity of this small molecule. Hemin dissolved in an aqueous solution, adsorbed on an electrode surface [14] or immobilized on ion-exchange resins, zeolites, silica, clays, in polymer or lipid film on an electrode surface was studied from electrochemically point of view [15, 16]. Also, it was used as catalyst for dioxigen [6, 17 - 18], nitrite [1], hydrogen peroxide [19].

The aim of this paper was a fully electrochemically characterization of the hemin in solution and the identification of its capacity to electrocatalyse the nitrite reduction.

RESULTS AND DISCUSSION

Electrochemical behaviour of hemin on graphite electrode

Figure 1A shows a set of cyclic voltammograms obtained at different scan rates, when the graphite electrode was immersed in the hemin solution. A well formed and similarly shaped pairs of peaks corresponding to the single electron transfer into the Fe(III)P/Fe(II)P redox couple is observed at $E_{p,a} = E_{p,c} = -0.42$ V *vs*. Ag/AgCl, KCl$_{sat}$ ($\Delta E_p = 0$), only at 10 mVs^{-1} as in the case of the reversible processes. The variation of the scan rate between 100 and 1000 mVs^{-1} leads to an exponentially increasing of peak separation ΔE_p (calculated as E_{pa} - E_{pc}), as it is observed for the quasi-reversible systems controlled by diffusion (figure 1B).

At scan rates ranging from 100 - 1000 mVs^{-1} the peaks currents (I_p) increase linearly with the scan rate (v) and not with $v^{1/2}$ (slope of log I_p *vs.* log v between 0.85 and 1). This indicates that the redox reaction is a surface process, due to the slow adsorption of the hemin on the electrode surface during the measurements.
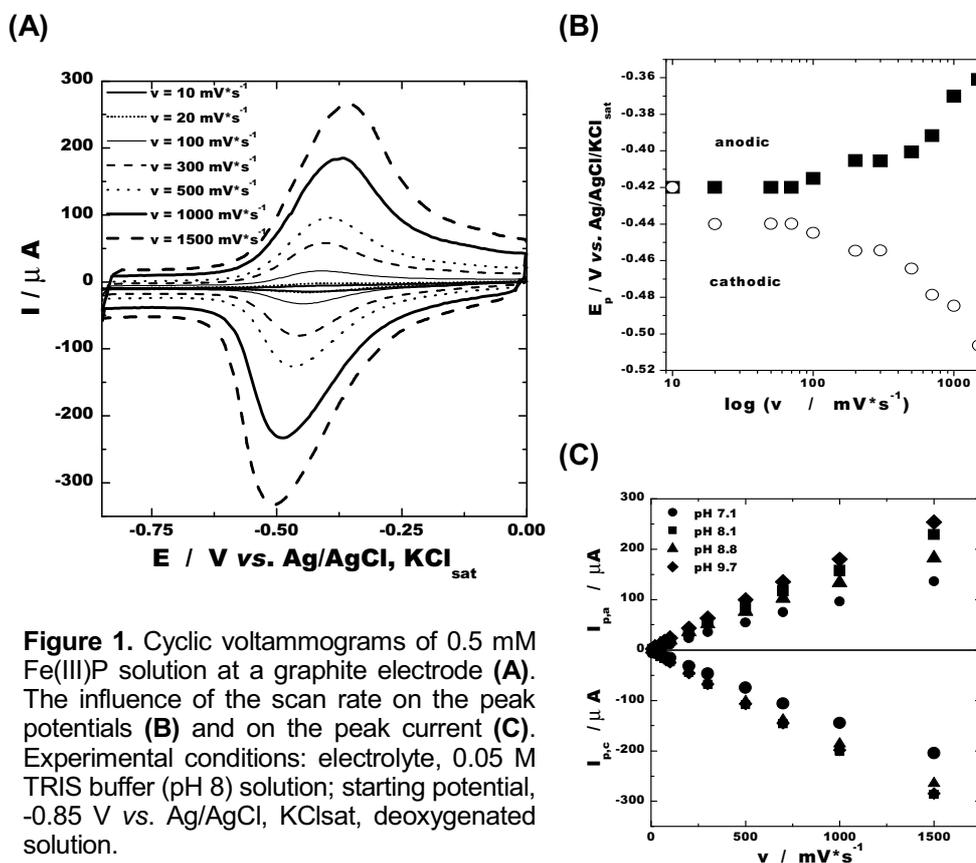
106

(A)

(B)

(C)

Figure 1. Cyclic voltammograms of 0.5 mM Fe(III)P solution at a graphite electrode **(A)**. The influence of the scan rate on the peak potentials **(B)** and on the peak current **(C)**. Experimental conditions: electrolyte, 0.05 M TRIS buffer (pH 8) solution; starting potential, -0.85 V *vs*. Ag/AgCl, KClsat, deoxygenated solution.

The effect of pH on the electrochemical behavior of hemin on graphite electrode was studied in different buffer solutions (pH 6.5 - 10) in the absence of oxygen. The pairs of well-defined redox peaks of hemin are strong pH dependent. The current intensity of peaks has a maximum value in the range pH 8-8.5, in spite of the potential scan rate (Figure 2).

Both reduction and oxidation peak potentials of Fe(III)P/Fe(II)P redox couple shifted negatively with an increase in pH (results not shown). The pH dependencies of the formal peak potentials in the studied pH range can be expressed as follows: $E^{0'} = -38{,}55 - 47.95pH$ (R = 0.995, n = 7, v = 300 mVs^{-1}) or $E^{0'} = -70.82 - 44.27pH$ (R = 0.995, n = 8, v = 500 mVs^{-1}). (The formal potential is the mean between E_{pa} and E_{pc}).

As observed in similar cases [12, 16] the slopes of $E^{0'}$ - pH dependence are reasonably close to the theoretical value of -59.1 mV pH^{-1} at 25 ^{0}C for a reversible one proton coupled with one electron redox reaction process in accordance with the following equation:

$$(H_2O)(OH)Fe(III)P + H^+ + e^- \rightleftharpoons (H_2O)_2Fe(II)P \qquad (1)$$
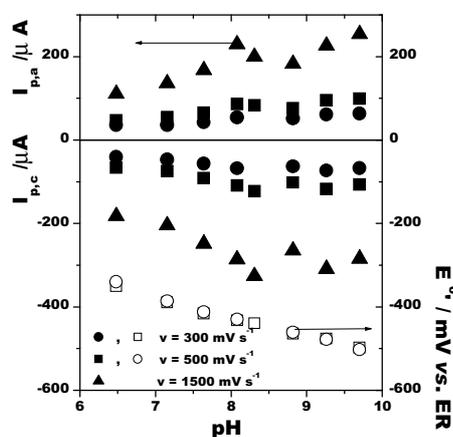
107

Figure 2. The current peak and the formal peak potential dependences on the pH of Fe(III)P solution. Experimental conditions: see figure 1.

It is possible that the pH dependency of $E^{o'}$ of Fe(III)P is due to changes in the ligation of the metal. In weak acidic and neutral pH range, the iron is coordinated to water molecules and hydroxyl ions. At basic pH, it is difficult to assign a mechanism for the proton/electron transfer coupling. If we consider a low surface coverage of the Fe(III)P on the electrode, we can assume that there is small interaction between adjacent porphyrins. In this case the formation of monomeric Fe(III)P(OH)$_2$ would explain the coupling between electron and proton transfer [16].

Due to stability, electrochemical reversibility and high electron transfer rate constant of Fe(III)/Fe(II) redox couple at graphite electrode, it can be used as a mediator to shuttle electrons between electrodes and analyte molecules. To assess the electrocatalytic properties of hemin, its electrocatalytic activity towards nitrite reduction was examinated. In order to test this ability of the studied molecule, cyclic voltammograms were obtained in the presence and absence of nitrite and/or hemin in Tris buffer solution (pH 8).

As shown in figure 3, in the presence of hemin and different concentrations of nitrite, a cathodic peak at ~ -0.8 V accompanied by a current increasing, indicates a strong catalytic activity of hemin toward these analyte. At the bare surface of the graphite electrode, in the absence of hemin and in the presence of nitrite no response was observed. The same behavior was observed for the electroreduction of chlorate and iodate at multi-walled carbon nanotubes (MWCNTs) and Fe(III)P-MWCNTs-modified electrodes [12].

Casella and al. [2] have demonstrated that a positive value of the switch potential (~ 0.5 V) is important for the appearance of the nitrite reduction peak. So it can be considered that the over all reduction process involves a preliminary adsorption process of analyte on the electrode surface, and the adsorbed complex undergoes a subsequent multi-step reduction process in the negative region of potentials between –0.3 and –1.3 V.
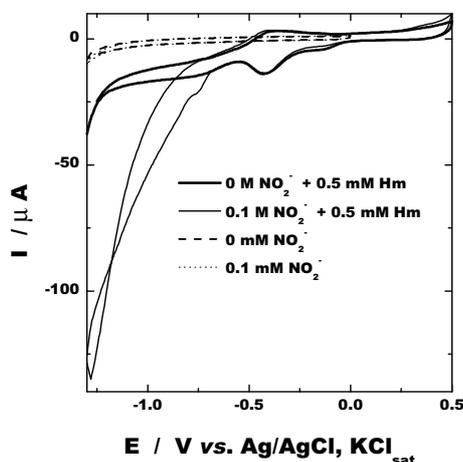
Figure 3. Electrocatalytic effect of 0.5 mM Fe(III)P on the nitrite reduction. Experimental conditions: electrolyte, 0.05 M TRIS buffer (pH 8) solution; scan rate, 20 mVs^{-1}; starting potential, -1.3 V *vs.* Ag/AgCl, KCl$_{sat}$; deoxygenated solution.

These fore, in all the reported studies [20 -22], it was suggested that the first step of the catalytic process at pH 7.4, involves the formation of an iron-nitrosyl complex as a consequence of the metal-centered Fe(III)P/Fe(II)P reduction followed by nitrite binding, according to equations 2-3:

$$Fe(III)P + e^- \rightarrow Fe(II)P \tag{2}$$
$$Fe(II)P + HONO + H^+ \rightarrow [Fe(II)P(NO^+)]^+ + H_2O \tag{3}$$

These steps are then followed by the reduction of the iron-nitrosyl adduct, according to equation 4:

$$[Fe(II)P(NO^+)]^+ + e^- \rightarrow [Fe(II)P(NO\bullet)] \tag{4}$$
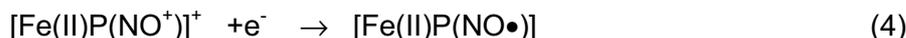
It should be noted that no clear evidence to fully characterize the above-cited reduction process and no accurate overall catalytic process was established in the literature. Only a few attempts were reported to model a probable mechanism of reduction of nitrite to ammonia by iron porphyrins [1].

CONCLUSIONS

The electrochemical investigation by cyclic voltammetry of the iron (III) protoporphyrin (IX) reveals a quasi-reversible behaviour, corresponding to a one-electron transfer redox process at a graphite electrode. The influence of the buffer pH on the peak current and $E^{o'}$ of hemin was also, investigated.

The electrocatalytic ability of hemin towards nitrite reduction was evidenced by recording cyclic voltammograms on graphite electrode in the presence and absence of nitrite in buffer solution. A decrease in overpotential and enhancement of peak current for nitrite reduction indicates strong catalytic activity of porphyrin toward these analyte.

EXPERIMENTAL SECTION

Reagent and materials

Iron (III) protoporphyrin (IX) chloride, $NaNO_2$, HCl, NaOH and TRIS chloride were purchase from Sigma. All reagents were of analytical grade and were used as received, without further purification.

A 0.5 mM stock solution was prepared by dissolving the appropriate amount of hemin in 0.05 M TRIS chloride buffer (pH 10.5). A 1M nitrite solution was prepared in above 0.05 M TRIS. The pH adjustment of solution was achieved by using HCl and NaOH. Deionized water was used for preparing all solutions.

Apparatus

Cyclic voltammetric investigations were carried out on a computer controlled AMEL 433 trace analyser (*AMEL, Milan, Italy*).

All measurements were done using a standard single-compartment three electrode cell equipped with a platinum counter electrode, an Ag/AgCl, KCl_{sat} reference electrode (*Radiometer*, *France*) and a spectral graphite (3 mm diameter) (*Ringsdorff-Werke, Gmbh, Bonn-Bad Godesberg, Germany*) working electrode. The surface of the graphite electrode was polished with 600, 1000, and 2000, grit SiC emery paper, washed with water and then sonicated in water. All experiments were performed at room temperature. The oxygen was purged from the electrolyte solutions by bubbling with high purified argon and all experiments are done under this inert atmosphere.

ACKNOWLEDGEMENTS

REFERENCES

1. D. Mimica, J. H. Zagal, F. Bedioui, *Journal of Electroanalytical Chemistry*, **2001**, *497*, 106.
2. I. G. Casella, M. Gatta, *Journal of Electroanalytical Chemistry*, **2004**, *568*, 183.
3. F. Valentini, A. Amine, S. Olanducci, M.L. Terranova, G. Palleschi, *Analytical Chemistry,* **2003**, *75*, 5413.
4. Y. Chi, J. Chen, M. Miyake, *Electrochemical Communications,* **2005**, *7*, 1205.
5. B. Duong, R. Arechabaleta, N.J. Tao, *Journal of Electroanalytical Chemistry,* **1998**, *447*, 63.
6. N. Zheng, Y. Zeng, P.G. Osborne, Y. Li, W. Chang, Z. Wang, *Journal of Applied Electrochemistry,* **2002**, *32,* 129.

7. Y.-L. Zhang, C.-X. Zhang, H.-X. Shen, *Electroanalysis,* **2001**, *13*, 1431.

8. W. J. R. Santos, A. L. Sousa, R. C. S. Luz, F. S. Damos, L. T. Kubota, A. A. Tanaka, S. M. C. N. Tanaka, *Talanta,* **2006**, *70*, 588.

9. J. Chen, U. Wollenberger, F. Lisdat, B. Ge, F.W. Scheller, *Sensors & Actuators B,* **2000**, *70*, 115.

10. S. M. Chen, *Inorganica Chimica Acta,* **1996**, *244*, 155.

11. C. G. Nan, Z. Z. Fena, W. X. Li, D. J. Ping, C. H. Qin, *Analytica Chimica Acta,* **2002**, *452*, 245.

12. A. Salimi, H. MamKhezri, R. Hallaj, S. Zandi, *Electrochimica Acta*, **2007**, *52*, 6097.

13 J.-S. Ye, Y. Wen, W. D. Zhang, H.-F. Cui, L. M. Gan, G. Q. Xu, F.-S. Sheu, *Journal of Electroanalytical Chemistry*, **2004**, *562*, 241.

14. P. Bianco, J. Haladjian, K. Draoui, *Journal of Electroanalytical Chemistry,* **1990**, *279*, 305.

15. T. Sagara, S. Takeuchi, K-i. Kumazaki, N. Nakashima, *Journal of Electroanalytical Chemistry*, **1995**, *396*, 525.

16. D. L. Pilloud, X. Chen, P.L. Dutton, C. C. Moser, *Journal of Physical Chemistry*, **2000**, *104*, 2868.

17. J.-S. Ye, Y. Wen, W. D. Zhang, H.-F. Cui, L. M. Gan, G. Q. Xu, F.-S. Sheu, *Journal of Electroanalytical Chemistry*, **2004**, *562*, 241.

18. L. Zhang, G.-C. Zhao, X.-W. Wei, Z.-S. Yang, *Chemical Letters*, **2004**, *33*, 86.

19. T. Lotzbeyer, W. Schuhmann, H-L. Schmidt, *Bioelectrochemistry & Bioenergetics*, **1997**, *42*, 1.

20. S. Trevin, F. Bedioui, J. Devynck, *Journal of Electroanalytical Chemistry*, **1996**, *408*, 261.

21. S. Trevin, F. Bedioui, J. Devynck, *Talanta*, **1996**, *43*, 303.

22. D. Mimica, J.H. Zagal, F. Bedioui, *Electrochemical Communications*, **2001**, *3,* 435.

In memoriam prof. dr. Liviu Oniciu

NEW [4.4.4.4]CYCLOPHANE AS IONOPHORE FOR ION-SELECTIVE ELECTRODES

LIDIA VARVARI, IONEL CATALIN POPESCU[*], SORIN AUREL DORNEANU

ABSTRACT. A new cyclophane derivative (M7F2) was tested as ionophore for ion-selective electrodes (ISE), based on PVC membrane. Two types of ISE membranes were prepared and compared: one with, and one without potassium tetrakis(4-clorophenyl)borate as ionic additive. Potentiometric tests were performed in calcium, magnesium, sodium and potassium standard solutions. The best response was obtained for calcium, i.e., lowest detection limit, highest linear range and a quasi-nernstian slope. The investigated cyclophane ISE showed comparable analytical performances.

Keywords: cyclophane, PVC-based ISE, calcium ISE

INTRODUCTION

Ion-selective electrodes (ISE) are well-known for their wide applications in important fields such as clinical, food and environmental chemistry [1]. For example, it is estimated that over a billion clinical analyses are performed annually in laboratories all over the world using ISE [2].
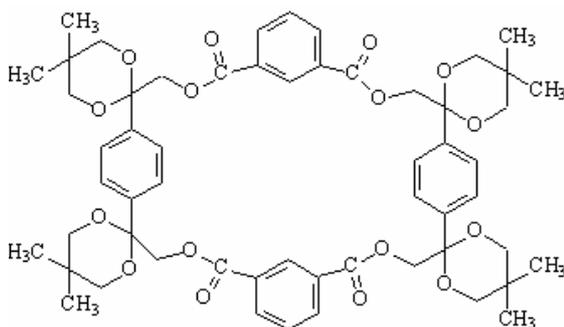

Figure 1. The structure of M7F2 ionophore

ISE are usually made of a polymer matrix incorporating an ionophore. Macrocyclic compounds are the most frequently used ionophores; they selectively bind different ions by entrapping them in their cavity. The selectivity of the membrane is thus strongly influenced by the size match between the ion and the host cavity. Many cyclophane derivatives are successfully used as ionophores [3, 4].

[*] *Department of Physical Chemistry, Babes-Bolyai University, 400028 Cluj-Napoca, Romania, cpopescu@chem.ubbcluj.ro*

This paper aims at testing a newly synthesized [4.4.4.4]cyclophane as ionophore for cation-selective membranes. Its name, 5,5,10,10,22,22,27,27-tetrakis[3',3'-dimethyl-1',5'-dioxapentan-1',5'-diyl]-2, 13,19,30-tetraoxo-3,12,20,29-tetraoxapenta-cyclo[29.3.2^{6,9}.2^{23,26}.1^{14,18}.1^{1,31}]tetracontan-1^{40},6,8,14,16,18^{37},23^{38}, 24,26^{39},31,33-dodecaene is abbreviated as M7F2. The structure of the ionophore is shown in Figure 1.

RESULTS AND DISCUSSION

I. Calibration curves for Ca^{2+}, Mg^{2+}, Na$^+$, K$^+$

An example of calibration curves obtained for both types of prepared membranes, in presence of different concentrations of calcium ion, is shown in Figure 2. The calculated values of the corresponding slopes and detection limits (DL) are presented in Table 1. All values represent the average of three measurements, performed successively with three electrodes, in the same working conditions.
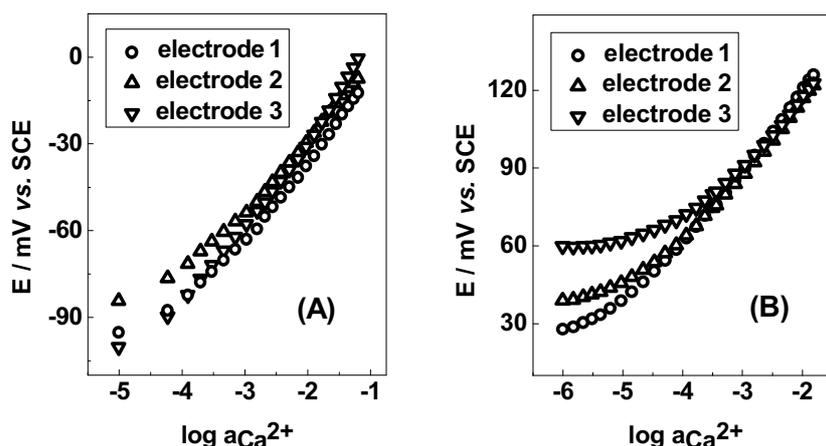

Figure 2. Calibration curves obtained in presence of Ca^{2+} solution for the membrane with (A) and without ionic additive (B)

Table 1.

Values of slope and DL for the membranes with and without ionic additive

Ion Membrane type	Slope (mV/Δp$_{ion}$)				DL (mM)			
	Ca^{2+}	Mg^{2+}	Na$^+$	K$^+$	Ca^{2+}	Mg^{2+}	Na$^+$	K$^+$
With ionic additive	26.8 ± 1.1	32.6 ± 5.2	39.8 ± 5.4	39.3 ± 4.9	1.92* *10^{-2}	5.42	8.62	1.23* *10^{-1}
Without ionic additive	29.0 ± 2.0	5.2 ± 0.4	57.7 ± 7.0	37.0 ± 5.1	2.22* *10^{-2}	-	3.02* 10^{-1}	4.00

From Table 1 it can be noticed that both prepared membranes presented potentiometric response to the tested cations. For calcium, both membranes present a nernstian slope (S) of about 28 mV/decade, the lowest DL ($\approx 2{*}10^{-5}$ M) and a large linear range ($\approx$ 4 decades). For all other tested ions, significantly higher DL were obtained. In presence of K^+, both membranes presented undernernstian response. A nernstian response was also obtained for Mg^{2+} and Na^+ using the membrane with, and without ionic additive, respectively.

II. Study of the ionic interference

Based on DL and sensitivity results, calcium was chosen as primary ion. Concentrations of interfering ion (Mg^{2+}, Na^+, and K^+) varied up to 0.5 M, while calcium was kept at a constant concentration of 5 mM.

Figure 3 shows an example of calibration curve obtained during the interference study carried out in presence of variable sodium concentration. Table 2 lists the average values of the potentiometric selectivity coefficients.
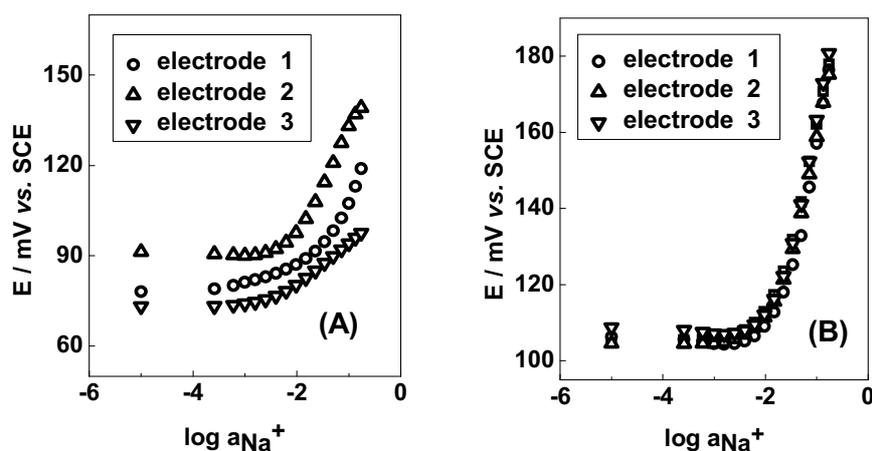

Figure 3. Calibration curves obtained for Na^+ in presence of constant Ca^{2+} concentration (5 mM), for the membrane with (A) and without ionic additive (B)

Table 2.

Values of selectivity coefficients for the two membranes, with Ca^{2+} as primary ion (5 mM) and Mg^{2+}, Na^+, K^+ as interfering ions

Interferent Membrane type	$logK^{pot}_{A, B}$		
	Mg^{2+}	Na^+	K^+
With ionic additive	-0.38 ± 0.05	2.23 ± 0.24	4.64 ± 0.48
Without ionic additive	-0.32 ± 0.14	1. 43 ± 0.04	1.34 ± 0.02

The lowest interference with respect to Ca^{2+} is observed in the case of Mg^{2+}, which is a remarkable fact, taking into account the usually high interference between the two ions [8]. For the ionic additive-free membrane, $logK^{pot}_{Ca,Mg}$ was -0.32, and for the other one it was -0.38.

The positive values of $logK^{pot}_{Ca,Na}$ and $logK^{pot}_{Ca,K}$ suggest a high sensitivity towards Na^+ and K^+ at the chosen concentration of Ca^{2+}. In the case of the membrane with ionic additive, the high value $logK^{pot}_{Ca,K}$ can be due to the high amount of potassium ions introduced in the membrane through the ionic additive. In order to improve the estimated selectivity, additional tests should be performed at different concentrations of primary and/or interfering ions, depending on the prospective applications of the ISE. For example, in some mineral waters where sodium and magnesium are ten times less concentrated than calcium, the concentration of the last one can be successfully measured using ISE based on the M7F2 compound.

III. Study of repeatability

Both the inter-electrode and inter-measurements repeatability were estimated and two examples of representative results are presented in Figure 4. The first case shows the mean values of the response recorded with the same electrode (based on ionic additive-free membrane) during three successive tests performed for Ca^{2+} in the same working conditions. The second figure shows the mean value of the responses for three similar electrodes (with additive-free membrane), recorded simultaneously in Na^+ solutions. In both cases, a good repeatability was obtained, in spite of a relatively high dispersion observed at low concentrations. This dispersion is due to the high level of the electric noise caused by the absence of supporting electrolyte.
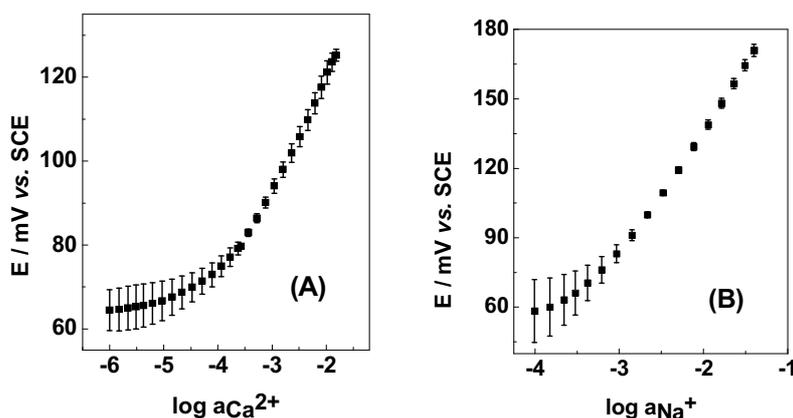

Figure 4. Mean value and standard deviation of three measurements successively performed in Ca^{2+} solution with the same electrode (based on the additive-free membrane) and in the same working conditions (A), and for simultaneous measurements performed with three similar electrodes in Na^+ solution (B)

CONCLUSIONS

This study aimed at characterizing the M7F2 cyclophane as ionophore for ISE based on two types of PVC membranes prepared with and without an ionic additive, respectively. A good detection limit ($\approx 2*10^{-5}$ M), a wide linear range (about four decades) and a quasi-nernstian slope (≈ 28 mV/decade) were obtained for Ca^{2+} in the case of both types of investigated membranes. The electrodes also showed potentiometric response to other ions (Mg^{2+}, Na^+, K^+) but their analytical parameters were poorer than those obtained for calcium.

It is worth to mention that the best selectivity against Ca^{2+} was obtained for Mg^{2+}, the values of the logarithm of the selectivity coefficient being -0.38 and -0.32 for the membrane with, and without ionic additive, respectively.

A good repeatability was obtained both for inter-measurements and inter-electrode tests.

EXPERIMENTAL SECTION

Materials

The M7F2 ionophore was synthesized [5, 6] in the research team of prof. Ion Grosu from the OCD of our faculty. All reagents used were of analytical grade. Calcium chloride, lithium acetate, 2-nitrophenyloctylether (NPOE), high molecular weight polyvinyl chloride (PVC), tetrahydrofurane (THF) and potassium tetrakis(4-clorophenyl)borate (KTkClPB) were purchased from Fluka (Darmstadt, Germany). Potassium chloride was from Riedel-deHaën (Darmstadt, Germany), magnesium chloride was purchased from Chimopar (Bucharest, Romania) and sodium chloride was from Merck (Darmstadt, Germany).

Membrane preparation

Two types of membranes were investigated: (i) the first contained 0.7% (w/w) M7F2 as ionophore, 0.3% (w/w) KTkClPB as ionic additive, 33% (w/w) PVC as polymer matrix and 66% (w/w) NPOE as plasticizer; (ii) the second membrane had the same composition excepting that it was prepared without ionic additive and the percent of ionophore was 1% (w/w). Each membrane weighted 0.3 g.

Membranes were prepared according to the following procedure. The ionophore, ionic additive, plasticizer and polymer matrix were successively dissolved in THF, under stirring. After dissolution, the mixture was poured into a glass cylinder, in THF atmosphere, in order to avoid pores formation. The membranes were dried and stored in dark. Before use they were conditioned for at least 24 hours in the solution containing the cation to be determined.

Experimental setup

Measurements were performed using a PC-controlled setup [7]. The system control, as well as data acquisition were performed using LabView 5.1. Data treatment was done by using the Origin 5.0 software.

117

Two lots of three electrodes (based on the two types of investigated membranes) were prepared by fixing an 8 mm diameter disc membrane at the bottom end of a plastic syringe body. As internal reference, a Ag/AgCl system was used. The inner electrolytes contained the same ion as the test solution, at a concentration of 5 mM. The similar electrodes were tested simultaneously, and each measurement was repeated three times in the same working conditions. A double-junction saturated calomel electrode was used as external reference. The external liquid junction was filled with CH_3COOLi 0.1 M.

Experimental procedure

The experimental consisted in two main parts: in the first one, the potentiometric response of the two types of the prepared membranes was recorded for Ca^{2+}, Mg^{2+}, Na^+, and K^+ using separate solutions, and the corresponding calibration curves were drawn. In the second part, the ionic interference between Ca^{2+} and different common cations was examined.

Potentiometric measurements were performed in batch mode, using the standard addition method for the preparation of standard solutions. For the interference study, the method of constant primary ion concentration was used: the primary ion concentration was constant, while increasing concentrations of the interfering ion were added.

ACKNOWLEDGEMENTS

REFERENCES

1. E. Bakker, D. Diamond, A. Lewenstam, E. Pretsch, *Analytica Chimica Acta,* **1999**, *393,* 11.

2. E. Bakker, P. Buhlmann, E. Pretsch, *Chemical Reviews*, **1997**, *97*, 3083.

3. E. M. Vazquez, J. Bobacka, A. Ivaska, *J. Solid State Electrochemistry*, **2005**, *9,* 865.

4. R. Ludwig, N. Dzung, *Sensors,* **2002**, *2*, 397.

5. N. Bogdan, I. Grosu, E. Condamine, L. Toupet, Y. Ramondenc, I. Silaghi-Dumitrescu, G. Ple, E. Bogdan, *European Journal of Organic Chemistry,* **2007**, *28,* 4674.

6. N. Bogdan, PhD Thesis, **2006**.

7. S. A. Dorneanu, V. Coman, I. C. Popescu, P. Fabry, *Sensors and Actuators B*, **2005**, *105,* 521.

8. K. Suzuki, K. Watanabe, Y. Matsumoto, M. Kobayashi, S. Sato, D. Siswanta, H. Hisamoto, *Analytical Chemistry,* **1995**, *67*, 324.

In memoriam prof. dr. Liviu Oniciu

ELECTROCHEMICAL INVESTIGATION OF SILVER / SILVER ION COUPLE REVERSIBILITY IN CHOLINE CHLORIDE - UREA BASED IONIC LIQUID

LIANA ANICAI[a], ANCA COJOCARU[b], ANDREEA FLOREA[a], TEODOR VISAN[b]

ABSTRACT. Cyclic voltammetry and electrochemical impedance spectroscopy were used for studying both cathodic and anodic processes on Pt electrode in an ionic liquid as electrolyte support at 70^0C temperature. Air and water stable solutions containing Ag^+ ion (0.14M, 0.282M and 0.565M $AgNO_3$) are based on choline chloride (ChCl) and urea (1: 2) mixtures. Voltammograms were recorded using scan rates in 10-200 mV/s range. It is shown that the Ag^+/Ag couple on Pt electrode exhibits almost reversible behavior in ChCl-urea electrolyte support at 70^0C, with diffusion control of cathodic process and a stripping anodic process. The diffusion coefficient of Ag^+ ion was estimated. Impedance of Pt electrode has been measured as a function of frequency for different overpotential values in the region of beginning and current peak Ag deposition. The non-uniformity of Ag deposited surface is one of the main factors determining the depressed shape of the impedance semicircle in Nyquist spectra. The values of fitting parameters for impedance data were calculated and the simulated curves have agreed with the experimental ones. Considerations regarding the use of Ag/Ag^+ ion couple as reference electrode in electrochemical experiments with ChCl based ionic liquids are made.

INTRODUCTION

Room temperature (or ambient temperature) ionic liquids based on choline chloride (ChCl) are of interest for last years. The preparation and applications of this new class of ionic liquids containing a quaternary ammonium salt (ChCl chemical compound is 2 hydroxy-ethyl-trimethyl-ammonium) mixed with hydrogen bond donor species, as amides, carboxylic acids, ethylene glycol etc., were described first by Abbott *et al*. [1-3]. Among the electrochemical applications, these ionic liquids can be used for the deposition of a range of metal coatings [4-6] including Zn, Cr, Sn, Cu, Ag at high current efficiency; also, they are well suited for metal electropolishing [7].

---

[a] *Petromservice SA, Division of Ecological Technologies Development, Bucharest, Romania*
[b] *Department of Applied Physical Chemistry and Electrochemistry, University Politehnica Bucharest, Calea Grivitei 132, 010737-Bucharest, Romania*

Recently, we reported some data [8] about cyclic voltammetry experiments and demonstrated that the Ni electrodeposition process in ChCl - urea and ChCl - malonic acid systems as ionic liquids represents an environmentally friendly alternative for the classic electrodeposition techniques in aqueous solutions which are used in present at industrial scale. The new proposed technique is an ecological procedure because the ionic liquid is air and moisture stable and its components are both common chemical compounds: chloride choline, which is used for chicken feed as vitamin B4 and urea, which is a common fertilizer.

The electrodeposition of silver as pure metal or its alloys is a technological process involved in a variety of finishing processes, an example being in electronics for the manufacture of printed circuit boards. Also, the electrodeposition and electrodissolution of silver in aqueous solutions were extensively studied in the past years in relation to silver recovery from photographic wastes. Silver deposits can be obtained from aqueous solutions in various conditions regarding composition, structure, aesthetic aspect, thickness and deposition rate. Obviously, a better approach of the silver electrodeposition kinetics was achieved by determining the diffusion and kinetic parameters and also establishing the mechanism of electrode process. The study of the mechanism of cathodic process of silver ion in thiosulphate aqueous solution performed by Gonnissen *et al.* [9] is an example. However, regarding the electrochemistry of silver in ionic liquids we found out that it is a lack of information about the electrode process kinetics and diffusion.

The present paper aimed to illustrate the electrochemical reversibility of Ag/Ag$^+$ ion couple in choline chloride - urea mixture as ionic liquid by showing the similar electrochemical behavior as in aqueous solutions or molten salts. To the authors knowledge, cyclic voltammetry and electrochemical impedance spectroscopy for Ag deposition and dissolution on Pt inert electrode in such ionic liquids have not been applied, yet. The obtained value of diffusion coefficient of Ag$^+$ ion may also be compared with other similar values in different electrolytes. Moreover, since we have used a quasi-reference electrode consisting in a silver wire immersed in the investigated ionic liquid, the results may allow us to make some considerations regarding the use of Ag / Ag$^+$ ion couple as reference electrode in ionic liquids.

RESULTS AND DISCUSSION

The electrochemical experiments were carried out firstly in supporting electrolyte consisting in choline chloride - urea mixtures (1: 2, in moles) as binary ionic liquids, in order to know the potential window and potentially electrochemical reactions occurring on Pt electrode. Also, in our preliminary determinations with gradually additions of AgNO$_3$ in the above ionic liquid

we found out a decrease in the specific electrical conductivity at a constant temperature for concentrated solutions, whereas the increase of temperature leads in all systems to an important increase in conductivity.

Cyclic voltammetry measurements

Cyclic voltammetry curves were recorded for studying both cathodic and anodic processes on Pt electrode in pure ionic liquid as electrolyte support at 70^0C constant temperature using scan rates in 10-200mV/s range.

An example of typical cyclic voltammogram recorded in choline chloride – urea mixture (1: 2, in moles) at 70^0C is shown in Fig. 1, indicating a potential window on Pt electrode from about +1.4 V to –1.2 V (electrode potentials *vs.* Ag quasi reference). During the cathodic scan the current density was lower than 0.5 mAcm^{-2}. It is worth to mention that on the cathodic branch of voltammograms two consecutive reduction waves appear at potentials around –0.35 V and –0.8 V, respectively, with a current amplitude that increases at faster scan rates.
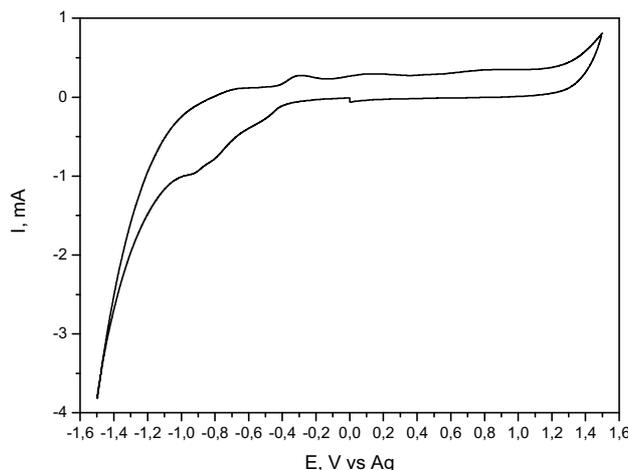

Figure 1. Cyclic voltammogram for Pt electrode (0.5 cm^2) in choline chloride - urea mixture (1: 2, in moles) at 70^0C; 10 mV/s scan rate.

It was considered that the existence of such waves with limiting currents less than 1 mAcm^{-2} is due to the presence of small amounts of H$^+$ ion in binary ionic liquid, resulted by dissociation of water molecules that surely are present in our experiments. In anodic direction, the current is almost zero in -0.9 ÷ +1.2 V potential range, with a continuous increasing at more positive values.

We performed voltammetric measurements in air and water stable solutions containing concentrations of Ag^+ ion of 0.14M, 0.282M, 0.565M $AgNO_3$, respectively, and choline chloride (ChCl) with urea (1: 2) mixture as electrolyte. Figures 2-4 show cyclic voltammograms recorded with various scan rates at 70^0C constant temperature, in the same potential range. Starting from the stationary potential (0V *vs.* Ag quasi reference electrode), all figures show clearly the beginning of cathodic deposition process with a current peak located at electrode potentials in the range -0.1 ÷ -0.3V, followed by a quite large potential region of limiting currents.
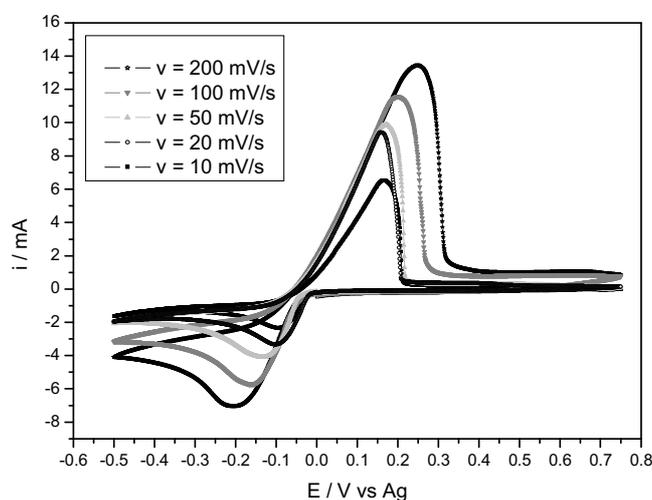

Figure 2. Cyclic voltammogram for 0.14M $AgNO_3$ in ChCl+urea (1:2) with Pt electrode (0.5 cm^2) at various scan rates, 70^0C.

In experiments with a further polarizing the Pt electrode (not shown), a continuous increasing of cathodic current at more negative potentials, generally more negative than -1.2V, was recorded, proving a supplementary process of ionic liquid solvent together with the massive deposition of Ag on working electrode. In all voltammograms, by returning the electrode potential in the anodic direction, a single well pronounced peak was obtained, with a peak potential situated at +0.2 ÷ +0.4V. This clearly seen anodic peak having the increasing amplitude for higher concentrations and scan rates is surely due to the silver stripping process onto the platinum electrode. Next increasing of current at potentials more positively than +1.2V (not shown, too) was attributed to the anodic process of supporting electrolyte, being probably the chlorine evolution.
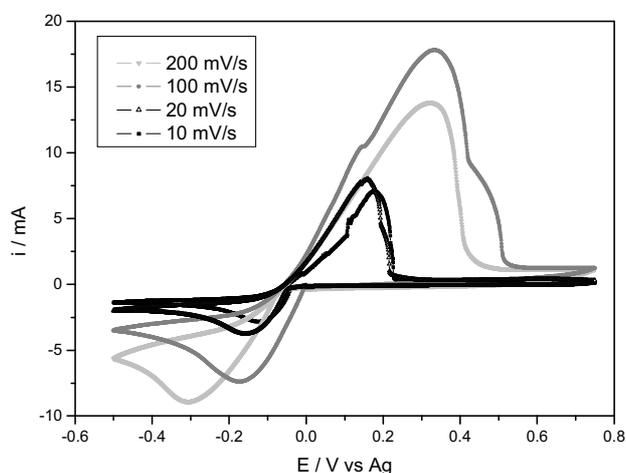
Figure 3. Cyclic voltammogram for 0.282M AgNO$_3$ in ChCl+urea (1:2)
with Pt electrode (0.5 cm^2) at various scan rates, 70^{0}C.

Referring to the silver electrodeposition and electrodissolution, it is worth to note that for each silver ion concentration, the increase of scan rate entails the increase of both cathodic and anodic peak currents. However, it was remarked the gradual shift of peak potentials in cathodic and anodic direction, respectively (*ie* an increase of ΔE$_p$ difference by increasing scan rate). An explanation would be the IR ohmic drop owing to the gradually diminishing of electrical conductivity of ionic media by adding AgNO$_3$ amounts in ChCl+urea ionic liquid.
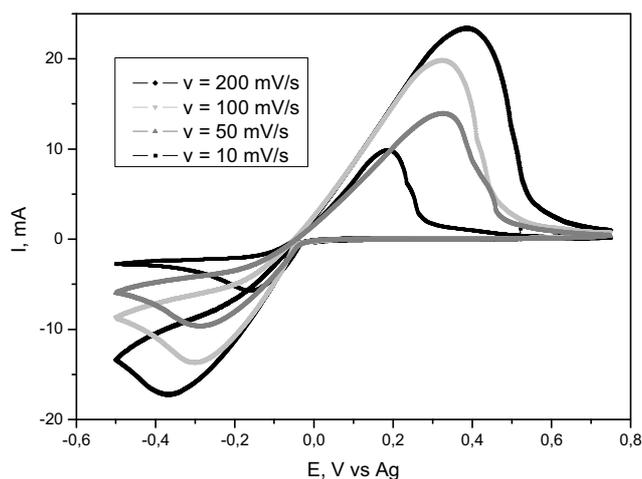

Figure 4. Cyclic voltammogram for 0.565M AgNO$_3$ in ChCl+urea (1:2)
with Pt electrode (0.5 cm^2) at various scan rates, 70^{0}C.

This phenomenon, already noticed in our conductivity measurements, is related to the existence of ionic complexes (in form of chloride complex ions) between choline chloride and urea as components of ionic electrolyte. We consider new bonds formation with introduced silver ions, which become chloride ionic complexes. According to the mechanism suggested by Gonnissen [9], the silver deposition involves these complexated silver ions, with the following scheme:

$$AgL_n \Leftrightarrow AgL + (n-1) L \qquad (1)$$
$$AgL + e^- \Leftrightarrow Ag + L \qquad (2)$$

The symbol L means the ligand present in the electrolyte, *ie* choline chloride as component in our system.

Thus, the reaction follows a chemical-electrochemical (CE) mechanism. The first chemical reaction is a rapid process, so that it does not affect the overall reaction rate. It involves the partial decomplexation of AgL_n species in the bulk of solution, considered as an equilibrium reaction, this being too fast to be detected. Then, AgL intermediate species are reduced at the electrode in the electrochemical step with a reversible single electron transfer. The results of our investigations suggest for the cathodic process to be diffusion controlled, especially for more diluted ionic liquids and for small scan rates, where the IR ohmic contribution in ΔE_p separation may be not important.
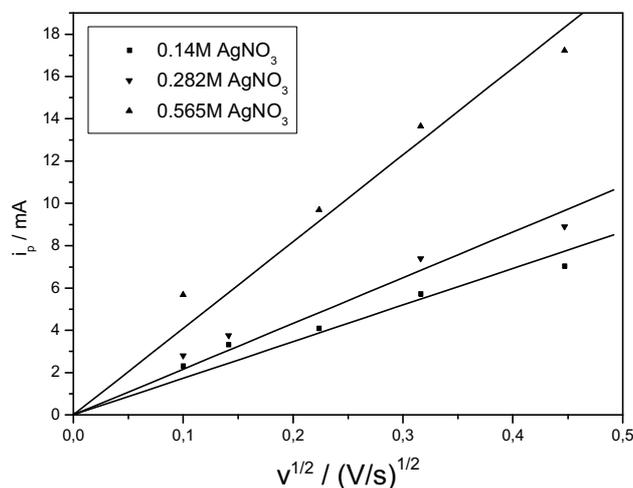

Figure 5. Cathodic peak current (i_p) *vs.* square root of the scan rate ($v^{1/2}$) for the three Ag^+ concentrations in ChCl+urea (1:2); Pt electrode ($0.5cm^2$), 70^0C.
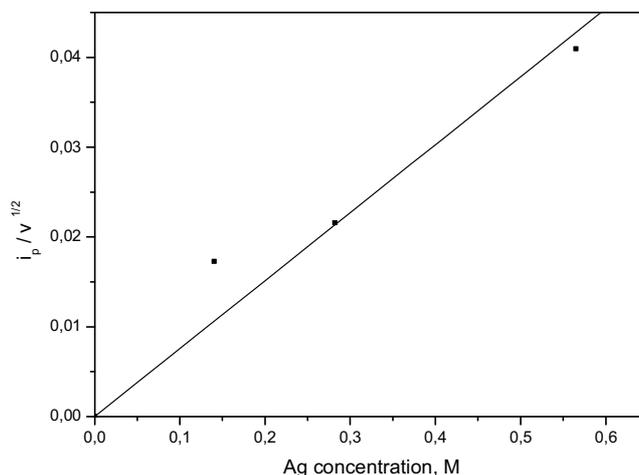
Figure 6. The $i_p / v^{1/2}$-c dependence for cathodic silver deposition in ChCl+urea ionic liquid; Pt electrode (0.5cm^2), 70^{0}C.

A quantitative analysis of the CVs varying both scan rate (v) and Ag$^+$ concentration (c) is presented in Figs 5 and 6. These figures show that the cathodic peak current (i_p) is almost linearly proportional to square root of the scan rate ($v^{1/2}$); this invariance of current function $i_p/v^{1/2}$ with scan rate accompanied by a linear $i_p / v^{1/2}$ - c dependence allowed us to calculate the diffusion coefficient using the well-known Randles-Sevcik equation for reversible processes. A value of diffusion coefficient for complexed silver ion of 0.36×10^{-6} cm^2/s was estimated from Fig. 6, whereas a higher value, of 0.92×10^{-6} cm^2/s, was computed considering the data of diluted solution (0.14M), only (Fig. 5). Taking into account the lack of information about the diffusion data in ionic liquid media, we have compared the diffusion coefficient obtained in diluted solution with similar measurements in aqueous solutions and found out them being quite close to the previous data reported for silver ion in thiosulphate solutions from photographic wastes (D=0.5×10^{-5} cm^2/s at room temperature [10,11]).

It also resulted that the Ag$^+$/Ag couple on Pt exhibits almost reversible behavior in ChCl-urea electrolyte support at 70^{0}C, with diffusion control of cathodic process and a rapid charge transfer.

The a.c. impedance measurements

The *a.c.* frequency response of the supporting electrolyte system (pure ChCl+urea ionic liquid) was investigated at different electrode potentials, where some increases of current were observed. Figure 7 presents the Nyquist

and Bode spectra, illustrating the absence of any cathodic process in the region of less negative potentials. Here, the *a.c.* frequency response is almost totally capacitive (for instance, the phase angle of 70^0 is closed to theoretical value, 90^0). However, due to water impurities, probably, the cathodic process has modified drastically the a.c. response at −1V potential, where the phase angle is around 10^0 and the charge transfer resistance (diameter of semicircle) decreases with three orders of magnitude.
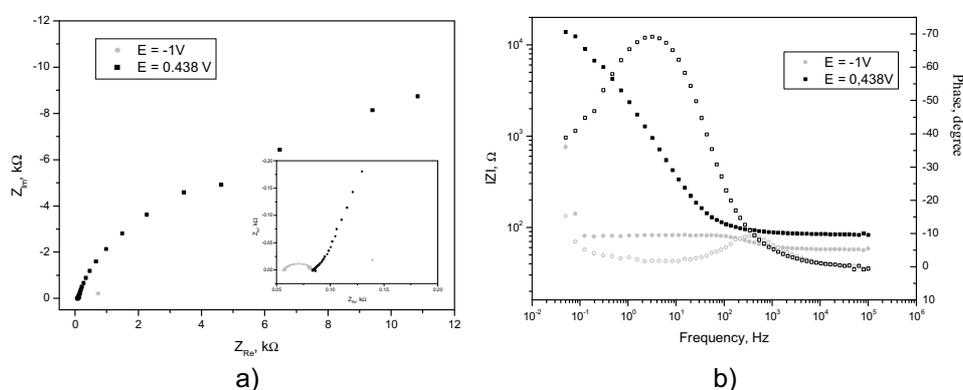

a)   b)

Figure 7. Nyquist (a) and Bode (b) diagrams of ChCl+urea (1:2) with Pt electrode (0.5 cm^2) at two potentials: 0.438V and −1V.

Impedance investigations in solutions containing choline chloride (ChCl) with urea (1: 2) mixture as electrolyte and 0.14M, 0.282M, 0.565M AgNO$_3$, respectively, are also performed at different electrode potentials, *ie* at the beginning of silver deposition and within the potential region of peak current or limiting current. As in CV experiments, a quite different behavior of the a.c. impedance was noticed in the region near equilibrium potentials (E=0 V *vs*. Ag pseudo-reference electrode), compared to the region of a massive Ag deposition. The impedance spectra as Nyquist diagrams (Figs. 8a-10a) show clearly at less cathodic polarization the capacitive semi-circles in the region of high frequences, followed by a linear dependence of imaginary part of impedance against the real part. The values of charge transfer resistance (the diameters) drastically decreased with 2-3 orders of magnitude in the potential region of continuous deposition. The shape of depressed semi-circles may be attributed to the non-uniformity of silver deposit onto platinum surface, especially after the first nuclei of electrocrystallised silver occur forming a monolayer. Thus, during *a.c.* measurements at higher negative overpotentials a roughness of cathode surface has continuously increased. Generally, the value of the real part of impedance determined by

126

extrapolation of capacitive arc to zero frequency decreases with an increase of cathodic overpotential (indicating a diminution of the charge transfer resistance), and increases with a decrease of Ag^+ ion concentration.

Figure 8. Nyquist (a) and Bode (b) diagrams of silver electrodeposition from 0.14M $AgNO_3$ in ChCl+urea (1:2) with Pt electrode (0.5 cm^2) at two potentials: 0V and -0.1V
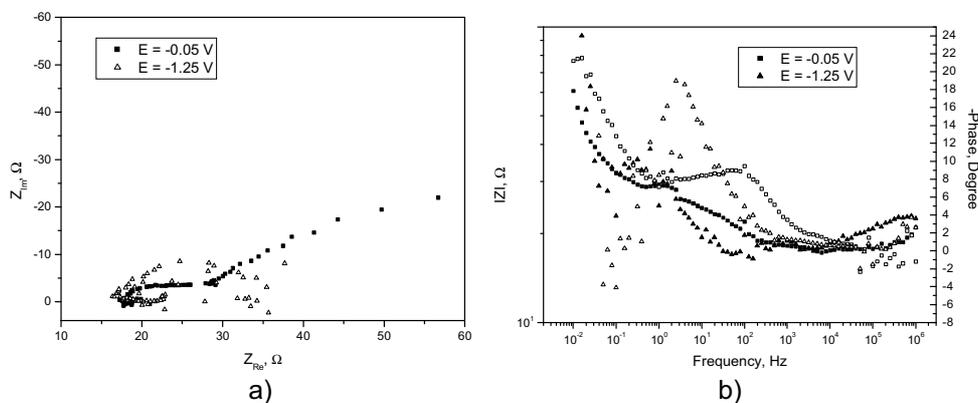
Figure 9. Nyquist (a) and Bode (b) diagrams of silver electrodeposition from 0.282M $AgNO_3$ in ChCl+urea (1:2) with Pt electrode (0.5 cm^2) at two potentials: -0.05V and -1.25V

The same behavior is evidenced in all Bode diagrams (Figs. 8b-10b). The capacitive response at potentials near 0V is illustrated by a phase angle of about 60^0 and large values of impedance. In the potential region of continuous silver deposition, the phase angle decreases at values around

20^0 and less. Moreover, the large linear portions of impedance variation with frequency for more negatively polarised samples are correlated with the thickening of silver film onto platinum electrode. Corespondingly, at lower frequencies a Warburg impedance appears.
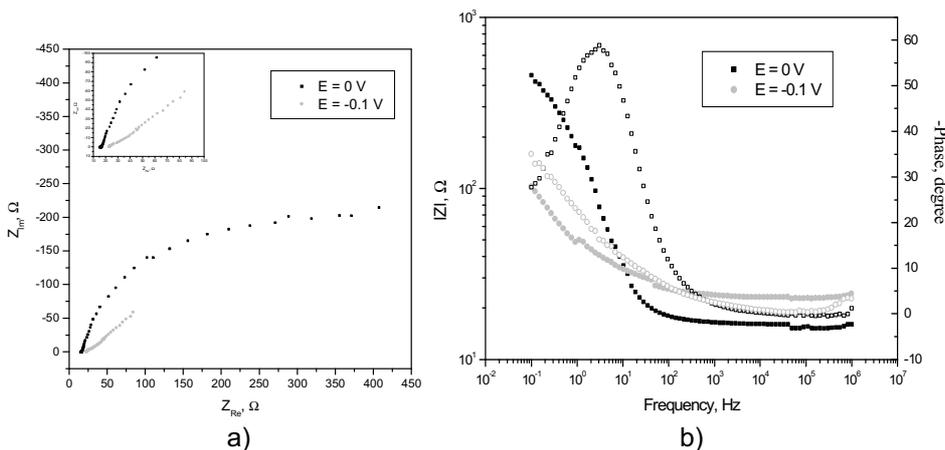

Figure 10. Nyquist (a) and Bode (b) diagrams of silver electrodeposition from 0.565M AgNO$_3$ in ChCl+urea (1:2) with Pt electrode (0.5 cm^2) at two potentials: 0V and -0.16V
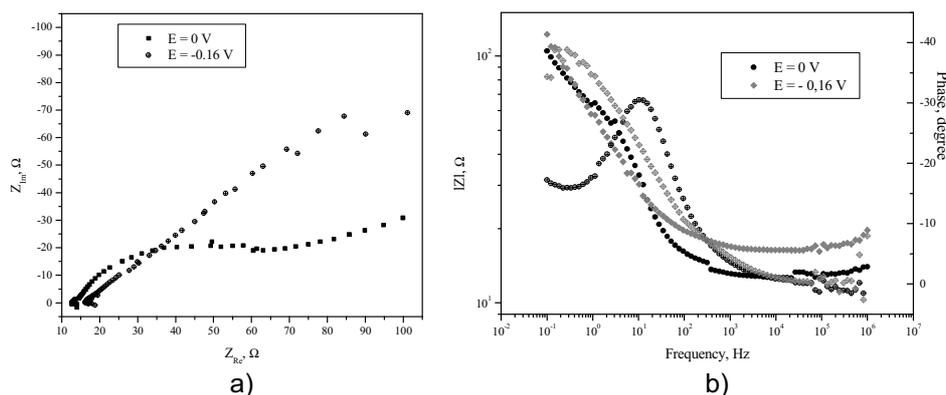
We consider that the above interpretation of impedance of Pt electrode in Ag$^+$ ion containing electrolyte measured at different overpotentials and for different silver concentrations was consistent to the above described reaction mechanism.

Impedance data were simulated by proposing an equivalent electric circuit (Fig. 11). This model of interface is composed of the electrolyte resistance, R$_s$, connected with a constant phase element, CPE (which is a non-ideal capacitor), in parallel with the charge transfer resistance, R$_{ct}$, which describes the electrochemical reaction under activation control; finally, a Warburg element (W) which represents a diffusion controlling step was added in series with the charge transfer resistance.

The constant phase element CPE replaces the capacity of the electric double layer for a better fitting; it takes into account the deviation from pure capacitive behavior, having the impedance given by the expression:

$$\text{CPE} = \frac{1}{T}\left(\frac{1}{j\omega}\right)^{p} \tag{3}$$

where for the exponent value p=1, CPE reduces to a ideal capacitor with a capacitance T and, for p=0 value, to a simple resistor. In the above expression the other significations are: ω – the angular frequency of *ac* voltage and j – the imaginary vector unit ($j=\sqrt{-1}$).

128

The Warburg impedance has a resistive part (W-R) and a capacitive part (W-CPE), for this last component (capacitive part) considering an expression similar with eq. (3). However, since W represents the diffusive component of equivalent circuit the exponent p was considered around a constant value, p=0.5. The values of circuit parameters resulted from fitting procedure are given in Table I. An example of both experimental and fitted data is represented in Figure 12.
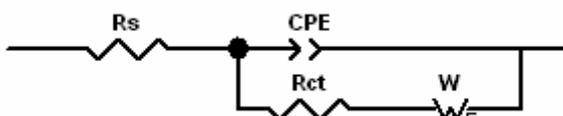

Figure 11. The proposed equivalent electrical circuit used for fitting impedance data. The significances of circuit parameters are given in text.

a)   b)
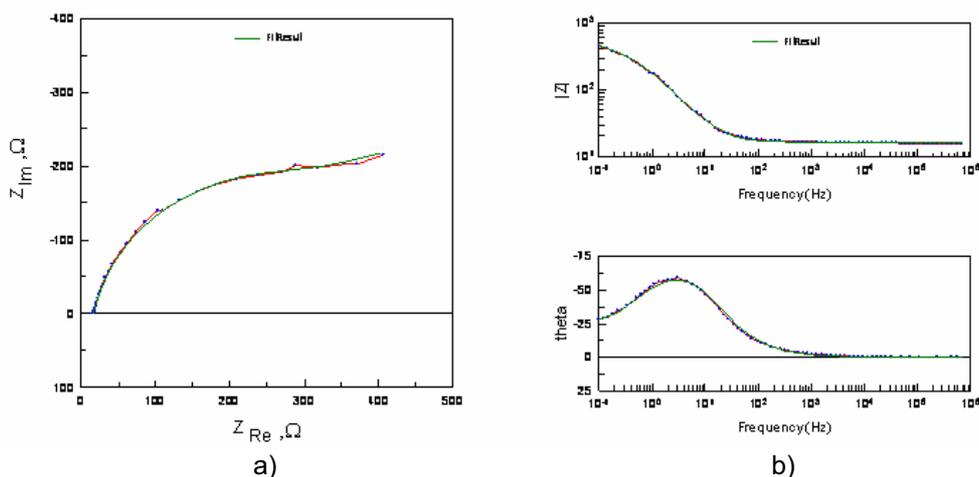
Figure 12. Nyquist and Bode diagrams of silver electrodeposition from 0.14M AgNO$_3$ in ChCl+urea (1:2) with Pt electrode (0.5 cm^2) at 0V electrode potential. Dotted lines represent the experimental data; the continuous lines show the fitted points using the model circuit from Figure 11.

As can be seen from Table I, the ohmic resistance of electrolyte has almost a constant value, of around 10Ωcm^2. We have noticed that for relatively diluted solutions the charge transfer resistance, R$_{ct}$, decreases with shift of the electrode potential towards negative direction. This behavior corresponds to a more intensive rate of charge transfer after the first silver layer was deposited on Pt, leading to the increasing the exchange currents.

Table 1 shows that at near equilibrium potentials (zero values of E), with increasing silver concentration in binary ionic liquid there is also a continuous decreasing in diffusion resistance (W-R). On contrary, in the

129

region of intense silver deposition (-0.1V to -0.2V) W-R has a slightly increase. This constitutes an evidence for a diffusion control of cathodic process. As a consequence, we confirm the chemical step (1) as a rapid one, the diffusion of complexated Ag ion to the electrode surface being the rate-determining step. Taking into account an approximately constant value of CPE-p exponent (p is mostly in the 0.6-0.86 range) we can compare the values of CPE-T at each potential; the increasing of double layer capacitance with cathodic overpotential would be explained by an increasing in the surface area of electrode, which is due to the further silver deposition on the electrode.

Table 1.

Fitted parameters for silver electrodeposition on Pt electrode ($0.5 cm^2$) in ChCl+urea (1: 2) ionic liquid at 70^0C

Circuit parameter	0.14M AgNO$_3$		0.282M AgNO$_3$			0.565M AgNO$_3$	
Potential	0V	-0.1V	-0.05V	-0.12V	-1.25V	0V	-0.16V
R$_s$, Ω	16.12	23.05	17.94	11.17	19.19	12.96	16.55
CPE-T, µF	1019	4009	2827	498	1563	1834	5931
CPE-P	0.86	0.60	0.70	0.81	1.24	0.73	0.57
R$_{ct}$, Ω	409.4	20.0	9.4	5.0	8.0	49.9	148.2
W-R, Ω	280.4	411.7	45.8	589.8	5.8	21.0	626.9
W-T, µF	5340	21290	37330	45400	480	500	6140
W-P	0.55	0.54	0.53	0.5	0.74	0.001	0.84

About the using of Ag/Ag+ ion couple as the reference electrode in ionic liquid media

In our experiments we have arbitrarily chosen a quasi-reference electrode consisting in a silver wire immersed in the ionic liquid containing Ag$^+$ ion (ChCl + urea + AgNO$_3$ (or AgCl)). This convenience of use has led to the frequent employment. It has advantage of achieving quickly its equilibrium potential and reproducibility and of maintaining its potential well with time, making it particularly well suited to act as a comparison. The results about reversible behavior of silver/silver ion couple may lead to some interpretations regarding the use of this couple as reference electrode in ChCl based ionic liquids.

It is well known that a reference electrode ideally provides a fixed reference potential against which the potential of the working electrode is measured. Conventionally, its Galvani electric potential is set equal to zero. One of the most common used reference electrodes in electrochemical studies undertaken in aqueous media is the silver/silver chloride (Ag/AgCl) electrode with NaCl or KCl aqueous solutions in concentration ranging from 1M to saturation. Sometimes, this electrode is also used in experiments in non-aqueous media being easier to construct and with potentials established rapidly and reproducibly.

However, the electrode potential difference between two electrodes immersed in electrolytes in contact with each other involves supplementary potentials, apart from ohmic potential drop term (IR). Thus, a salt bridge may give rise to a liquid junction potential which may alter the imposed potential of working electrode from potentiostat. For good results, the liquid junction potentials at the reference electrode/salt bridge and salt bridge/working solution interfaces must have similar magnitudes but opposite polarities and will, therefore, cancel each other. The complexity of problem is related to knowledge of the free energies of solvation for charged (cation) or neutral particles transferred between the aqueous and organic solvent; for minimizing errors these transfer free energies should be the same from solvent to solvent. It follows that in electrochemical measurements using non-aqueous solutions an electrochemical series can be established for each solvent [12]. The problem is how the potentials of such a series would compare with the corresponding potentials in water.

In conditions where AgCl is soluble in a non-aqueous solvent, the working electrode potential is measured against Ag/non-aqueous solution containing Ag^+ ion (commonly as $AgNO_3$) reference couple. For example, we have used a nonaqueous Ag/Ag^+ system (10^{-2}M $AgNO_3$ + 0.1M tetra-n-butylammonium perchlorate, CH_3CN) as reference electrode in acetonitrile [13]. In cyclic voltammetry experiments carried out in molten nitrates (300-600^{0}C), we also employed a silver wire immersed in a melt containing $AgNO_3$ with a concentration about 10^{-2}M in the studied molten nitrate electrolyte [14,15].

Working in medium and high temperature molten halides or carbonates, within 450-1000^{0}C range, the choosing of an appropriate reference electrode is much more difficult. Using LiCl-KCl melts, the reference electrode was a Ag wire immersed in silver ion containing melt (1M AgCl in LiCl-KCl eutectic) placed in a separated compartment [16]. Usually, especially at high temperatures, a metal electrode (Pt, Al, W, Ni etc.) simply immersed in the melt is frequently used as quasi-reference electrode in molten electrolytes where no established reference electrode couple exists [17].

The use of such quasi-reference electrodes for experiments in ionic liquids was reported by many authors. For example, Bakkar and Neubert [18] employed a Pt wire directly placed in the electrochemical cell during corrosion studies carried out in ChCl binary mixtures (with urea, ethylene glycol, glycerol, malonic acid). A silver wire as quasi-reference electrode was used recently by Abbott *et al.* during studies of either stainless steel electropolishing [7] or deposition of metals and alloys [19-21] in deep eutectic solvents based on choline chloride. We consider that employing a Ag wire immersed in an ionic liquid with a certain content in chloride ions such as ChCl ionic complex species, a half-cell reaction of AgCl film formation occurs:

$$Ag(solid) + Cl^-(ionic\ liquid) \Leftrightarrow AgCl(solid) + e^- \qquad (4)$$

This process of film formation on Ag quasi-reference electrode has advantages of achieving the equilibrium potential in short time, reproducibility and maintaining electrode potential with time, making it particularly well suited to act as a comparison.

CONCLUSIONS

Both voltammetric and electrochemical impedance measurements showed a quite reversible and diffusion controlled process of silver deposition in choline chloride + urea mixture at 70^0C, where one electron transfer process is preceded by a chemical step of delivering of electroactive species. Thus, the diffusion of complexated silver ion with choline chloride was considered as rate-determining step.

Additionally, the EIS data exhibit a non-uniformity of electrodeposited silver layer onto platinum substrate as well as change in behavior of cathodic process at more negative potentials. The experimental impedance data were fitted using a single electric circuit as model, with the values of circuit parameters in good agreement with the experimental data. The use of Ag/Ag^+ reference electrodes for experiments in ionic liquids was finally discussed.

EXPERIMENTAL SECTION

Cyclic voltammetry and electrochemical impedance spectroscopy investigations were conducted in ChCl-urea-AgNO$_3$ ionic liquid media. The binary ChCl-urea system as supporting electrolyte was separately prepared with analytical grade choline chloride (Merck) and urea (Fluka) in the corresponding amounts for 1: 2 (in moles) mixtures. AgNO$_3$ was dissolved as precursor of Ag^+ ion in concentrations in the range of 0.14 - 0.565 M, the molarity values being calculated using own experimental data of ionic liquid density (work in progress). The electrochemical cell (50 cm^3) contained a Pt foil (0.5 cm^2) as working electrode, a large platinum plate (4 cm^2) as auxiliary electrode, and a Ag wire placed in the same electrolyte (a quasi reference electrode). In the experiments a computer driven Autolab PGSTAT 302 potentiostat was used. Voltammograms were recorded using scan rates in 10 -200mV/s range. The impedance was measured in the potentiostatic conditions with a sinusoidal potential perturbation of the peak to peak amplitude equal to 10 mV at frequency sweep from 1 MHz to 0.01 Hz at different electrode potentials. Zview 2.80 software (Scribner Assoc. Inc.) was used for fitting impedance data. All electrochemical tests were carried out in a quiescent aerated ionic liquid at 70^0C.

ACKNOWLEDGEMENT

REFERENCES

1. A. P. Abbott, G. Capper, D. L. Davies, H. Munro, R. K. Rasheed, V. Tambyrajah, *Chemical Communications,* **2001**, 2010.
2. A. P. Abbott, G. Capper, D. L. Davies, R. K. Rasheed, V. Tambyrajah, *Chemical Communications,* **2003**, 70.
3. A. P. Abbott, D. Boothby, G. Capper, D. L. Davies, R. K. Rasheed, *Journal of American Chemical Society,* **2004**, *126*, 9142.
4. K. J. McKenzie, A. P. Abbott, *Physical Chemistry Chemical Physics,* **2006**, *8*, 4265.
5. W. Freyland, C. A. Zell, S. Zein El Abedin, F. Endres, *Electrochimica Acta,* **2003**, *48*, 3053.
6. A. P. Abbott, G. Capper, D. L. Davies, H. L. Munro, R. K. Rasheed, V. Tambyrajah, in: Ionic liquids as green solvents: progress and prospects, R. D. Rodgers, K. R.Seddom, Eds., ACS Symposium Series, **2003**, 439.
7. A. P. Abbott, G. Capper, K. J. McKenzie, K. S. Ryder, *Electrochimica Acta,* **2006**, *51*, 4420.
8. L. Anicai, M. Duțu, A. Perțache, T. Visan, *Coroziune si Protectie Anticoroziva (Cluj-Napoca),* **2007**, *2*, 10.
9. D. Gonnissen, S. Vandeputte, A. Hubin, J. Vereecken, *Electrochimica Acta,* **1996**, *41*, 1051.
10. D. Bistriteanu, T. Visan, M. Buda, N. Ibris, *Chemical Bulletin of Politehnica University Timisoara*, **1998**, *43*, 67.
11. N. Ibris, M. Buda, D. Bistriteanu, T. Visan, *Annals West Univ. Timisoara,* 15, **2006**, 109.
12. R. G. Compton, G. H. W. Sanders, Electrode Potentials, Oxford Univ. Press, Oxford, **1996**.
13. E. Saint-Aman, M. Ungureanu, T. Visan, J. C. Moutet, *Electrochimica Acta,* **1997**, *42*, 1829.
14. S. Sternberg, T. Visan, *Electrochimica Acta,* **1981**, *26*, 75.
15. D. Tkalenko, N. Chmilenko, T. Visan, M. Tkalenko, C. Ghiga, *Studia Universitatis Babes-Bolyai, Chemia,* **1996**, *41*, 158.
16. S. Sternberg, I. Lingvay, T. Visan, *Electrochimica Acta,* **1985**, *30*, 283.
17. M. Chemla, D. Devilliers Eds, Molten Salts Chemistry and Technology, Materials Science Forum, Vol.73-75, Trans.Tech.Publ., Switzerland, **1991**.
18. A. Bakkar, V. Neubert, *Electrochemical Communications,* **2007**, *9*, 2428.
19. A. P. Abbott, G. Capper, K. J. McKenzie, K. S. Ryder, *Journal of Electroanalytical Chemistry,* **2007**, *599*, 288.
20. A. P. Abbott, J. Griffith, S. Nandhra, C. O'Connor, S. Postlethwaite, K. S. Ryder, E. L. Smith, *Surface and Coatings Technology,* **2008**, *202*, 2033.
21. A. P. Abbott, D. L. Davies, G. Capper, R. K. Rasheed, V. Tambyrajah, US Patent **2004** / 0097755.

In memoriam prof. dr. Liviu Oniciu

ELECTROREDUCTION OF CARBON DIOXIDE TO FORMATE ON BRONZE ELECTRODE

MARIA JITARU[*], MARIANA TOMA

ABSTRACT. This paper presents our data on the electrochemical reduction of carbon dioxide, on bronze electrode ($Sn_{85}Cu_{15}$) in aqueous medium (0.2 M K_2CO_3), under CO_2 atmosphere, $(12-25)^0C$. The current efficiency for main product (formate) depends on the current density and was found to be up to 74% at high negative potential (> - 1.6 V/SCE), decreasing with operating time and with temperature increase (72-74% at 12 ^{0}C and 60-65% at 25 ^{0}C).

Keywords: carbon dioxide, electroreduction, formate, bronze electrode.

INTRODUCTION

The electrochemistry of CO_2 is a continuously growing field because it is a remarkable process with respect to at least two reasons. Firstly, CO_2 is the ultimate by-product of all processes involving oxidation of carbon compounds. Secondly, CO_2 represents a possible potential source for C-feedstock for the manufacture of chemicals.

The electroreduction of CO_2 at various metal electrodes yields many kinds of organic substances, namely CO, CH_4, C_2H_6, EtOH, other alcohols, formic acid, etc. Sánchez-Sánchez et al. [1] summarized representative results for the direct electrochemical CO_2 reduction at solid electrodes. The various types of electrocatalytic behavior among metals can be related to their electronic configuration and can be grouped into sp and d metals [2, 3]. The electroreduction techniques had to overcome the difficulty of finding electrodes with both high electrocatalytic activity and satisfactory lifetime [3].

The thermodynamic requirements for various CO_2-reduction reactions should be considered, because of the stability and chemical inertness of CO_2. The necessary energy to carry out carbon dioxide transformations for the processing and recovery of the air carbon-based sources can be generated by high temperatures, extremely reactive reagents, electricity, or by light irradiation [1]. However, because of the close proximity of the hydrogen

---

[*] *Faculty of Chemistry and Chemical Engineering, Babes-Bolyai University, 11, Arany Janos, 400028, Cluj-Napoca, Romania, mjitaru@chem.ubbcluj.ro*

potential, hydrogen evolution may also occur, as a concurrent reaction, depending on the operating system. The electroreduction of carbon dioxide needs substantial overpotentials due to the kinetic barrier and the large difference in the HOMO and LUMO energies. Moreover, the cathodic reduction of carbon dioxide is normally accompanied by hydrogen evolution and often mixtures of reaction products are obtained.

The main competitive reactions (1-5) involve electrosorbed species with hydrogen atom participation. Thus, in the electrochemical reduction of CO_2 in water, the hydrogen formation competes with the CO_2 reduction reaction. Therefore, the suppression of hydrogen formation is very important because the applied energy is wasted on hydrogen evolution instead of being used for the reduction of CO_2.

$$H^+ + e^- \longrightarrow H_{ad} \tag{1}$$

$$CO_2 + H_{ad} \longrightarrow HCOO_{ad} \tag{2}$$

$$HCOO_{ad} + H_{ad} \longrightarrow HCOOH \tag{3}$$

$$HCOO_{ad} + CH_3OH \longrightarrow CH_3COOH + OH_{ad} \tag{4}$$

$$OH_{ad} + H_{ad} \longrightarrow H_2O \tag{5}$$

The large number of recent papers, published during the last ten years on electrochemical reduction of carbon dioxide are both fundamental and preparative interest [4-19].

According to the recent review of Gattrell and Gupta [4] the reaction product distribution strongly depends on conditions at which data has been reported. When used in the aqueous solution, most flat metallic electrodes yielded carbon monoxide and formic acid [5, 6-10]. Hori et al. [11] with regard to the hydrocarbons formation on copper cathode revealed extended aspects on the deactivation of copper. Many workers reported "poisoning" or "deactivation" of the copper electrode in 10-30 min after the start of the CO_2 electroreduction [11].

CO_2 can be reduced on the surface of Pd-Pt-Rh alloys in the potential range of hydrogen electrosorption [12, 13]. The presence of the adsorbed product of the electroreduction of CO_2 on the electrode surface does not block hydrogen absorption [1, 3, 13].

The electrocatalytic activity of bronze cathode for the electrochemical reduction of stable inorganic molecules (nitrates and NO) has been reported [14, 15]. An enhancement of the electrocatalytic activity of Cu by alloying with Sn was observed only in the composition region up to 15% (wt.) Sn. A further increase in Sn content results in a rapid decline of the electrocatalytic activity caused by changes in the phase structure of the alloy material [14].

136

The current efficiency for formate depends on the electrode nature [1,5], current density and CO_2 pressure. Other factors such the hydrogen overpotential [2] and mass transfer capacity of the cathode are important and depend on the operating time. During the experiments the tin was lost from the cathode surface [11,13] and this fact decreased the current efficiency for carbon electroreduction.

Several papers related to the electrochemistry of CO_2 are of technological interest [16-19]. Copper tube electrodes have been employed for the production of methanol and formic acid [16].

The idea of this work is to enhance the electrocatalytic activity of copper for reduction of carbon dioxide to formate, diminishing the competitive hydrogen formation in the presence of tin in Cu-Sn alloy cathode.

RESULTS AND DISCUSSIONS

Voltamperommetric response of system

The potential was scanned at a sweep rate of 25 - 250 mVs^{-1}. Typical current-potential curves are illustrated in Fig. 1. The starting potential of the cathodic current was observed at approximately -1.1 V. No voltammetric peak was observed in potential range down to – 2.0 V. Further CO_2 reduction may proceed with increasingly negative potentials, inhibiting the hydrogen evolution.
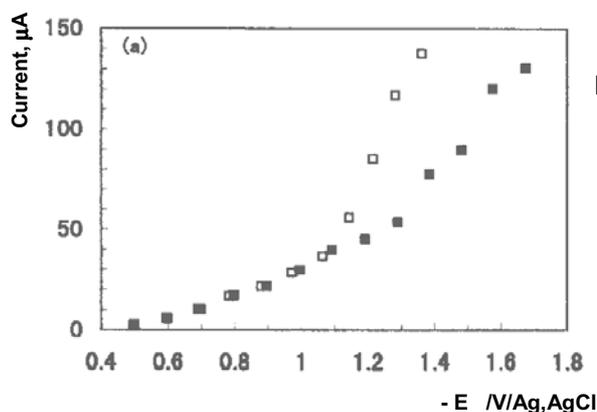

Figure 1. Current-potential curves for CO_2 reduction on bronze ($Sn_{85}Cu_{15}$) in 0.2 M K_2CO_3, saturated with CO_2 under CO_2 atmosphere at ambient temperature (20±0.4) ^0C.
€- Ar gas; ■ – CO_2 gas.

From the polarization curves it was observed that the CO_2 reduction presented a Tafel slope corresponding to $n_e=1$, indicating that the first electronation of the CO_2 molecule to form the radical anion (CO_2^{-}), is the rate-controlling step.

Factors influencing the current efficiency

In absence of CO_2 in the cell, the current was used only for hydrogen evolution; no other reaction products were detected both in electrolyte and in cell atmosphere. In presence of CO_2, the main product detected (by HPLC Perkin-Elmer LC 200, ODS-18 column) and by gas chromatography (Hewlett-Packard 6890, TCD, FID, Porapac QS columns) was formic acid (formate and methyl formate, in the presence of methanol). Accordingly, only the formate has been determinated during our experiments. The influence of applied potential and temperature on the current efficiency for formic acid formation has been determinated.
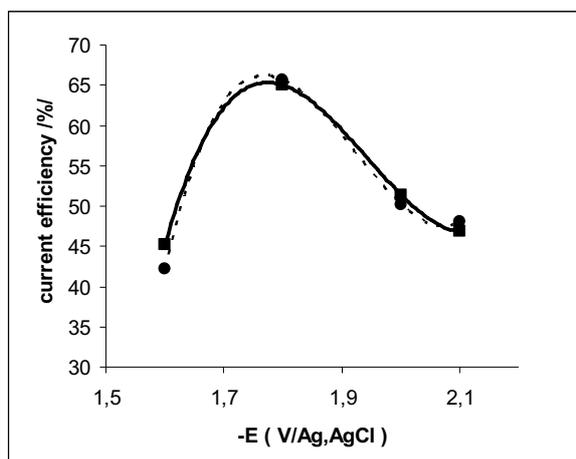
Influence of applied potential

Figure 2. Current efficiency - potential diagrams for CO_2 reduction on bronze ($Sn_{85}Cu_{15}$) in 0.2 M K_2CO_3, saturated with CO_2, under CO_2 atmosphere at ambient temperature $(20\pm0.4)\ ^0C.$(● and ■) – two series of experiments

The maximum of the partial current density for the formation of formic acid on bronze electrode is 80-100 $mAcm^{-2}$, larger that with other reported electrode materials [1, 3].

Influence of temperature

The results of the temperature studies show (Fig. 3) that current efficiency achieved is in the range of 74% after 30 min. of electrolysis, carried out at the optimum reduction potential of -1.8 V (Fig.2).

It is well known that in aqueous electrolytes, the electroreduction of CO_2 not only to HCOOH is in competition with the H_2 evolution permanently [13].

138
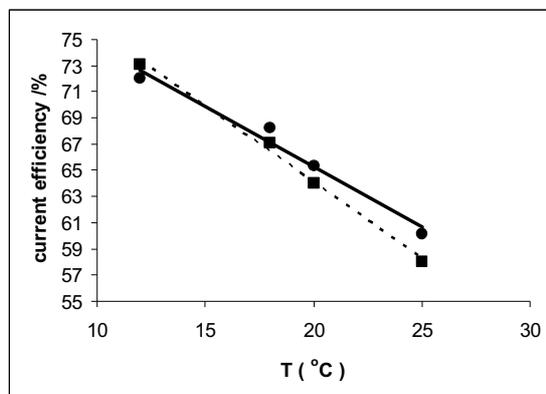
Figure 3. Current efficiency - temperature diagrams for CO_2 reduction on bronze ($Sn_{85}Cu_{15}$) in 0.2 M K_2CO_3, under CO_2 atmosphere, at 120 mA.cm^{-2}, (● and ■) – two series of experiments

The increase in the temperature under ambient conditions leads to a decrease of the current efficiencies for the HCOOH formation because of the decreasing CO_2 concentration in the electrolyte; thus the H_2 evolution becomes more dominant. In this small temperature range ($\Delta=13^0C$), the decrease was demonstrated. Probably, with the decrease of temperature under 12^0C, the competitive hydrogen evolution could be further diminished.

The preliminary data were obtained on the influence of electrolysis time and of the presence of methanol, on the current efficiency for formate formation (Table 1).

After 40-50 minutes of electrolysis, a cathode deactivation was observed (the corresponding current efficiencies decreased with 10-30%). A further increase in electrolysis time leads to a rapid decline in activity.

On the other hand, the presence of methanol up to 50% in volume leads to a smaller selectivity for formate formation, which becomes only (54-58) % at -1.8 V and low temperature (12 ^0C), comparing with (72-74) % in aqueous electrolyte.

The preliminary data in Table 1 are according to bibliographical information and with the supposed beneficial effect of Sn on the electro-catalytic activity of copper cathode, in bronze. Thus, when aqueous solution was used, copper was reported to be a suitable electrode for the formation of hydrocarbons. The electrochemical reduction of CO_2 with a Cu electrode in methanol-based electrolyte was investigated by other authors [6]. The main products from CO_2 were methane, ethylene, ethane, carbon monoxide and formic acid. On the other hand, very recent paper demonstrated the influence of added Sn on the electrocatalytic activity of copper, as the basic cathode material, on the electrocatalytic activity of the resulting material for nitrate (NO_3^-) reduction [15].

Table 1.

Current – efficiencies on bronze cathode depending on
electrolysis time and presence of methanol

Composition of electrolyte	Time of electrolysis (min)	Current Efficiency (%)
Aqueous 0.2 M K_2CO_3	30	72-74
	60	62-65
MeOH/water (1/2) + 0.2 M K_2CO_3	30	59-63
	60	49-52
MeOH/water (1/1) + 0.2 M K_2CO_3	30	54-58
	60	42-43

The current efficiency for HCOOH production increased after hydrogen was absorbed on the electrode surface. This fact was demonstrated using the bronze electrode after activation by H_2 evolution (10 minutes before the electrolysis in the presence of carbon dioxide). The participation of absorbed hydrogen in the reduction of CO_2 and the possibility of direct attack on the reaction intermediates by absorbed hydrogen could be involved.

CONCLUSIONS

The present paper demonstrated for the first time, up to our knowledge, that the bronze electrode is suitable for selective electroreduction of CO_2 to formate, especially in aqueous bicarbonate solution. The selectivity diminishes in the presence of methanol.

The important current efficiency for formic acid formation (up to 74%) have been obtained at reduction potential of -1.8 V and 12 ^{0}C, during the first 30 minutes of electrolysis.

According to our preliminary observations on the increase of current efficiency after the saturation of the electrode with adsorbed hydrogen (H_{ad}) the electrochemical hydrogenation can be also involved in the electroreduction mechanism.

The most important result of this work is the enhancing of the electrocatalytic activity of copper for reduction of carbon dioxide to formate, diminishing the competitive hydrogen formation, in the presence of tin of the Cu-Sn alloy cathode.

As perspectives, it is envisaged to use this procedure as a suitable alternative for testing other cathodes including modified materials, like nanocopper cathodes, modified with underpotential deposited stanium.

EXPERIMENTAL SECTION

Reagents and solution preparation

All reagents (potassium permanganate, potassium carbonate, potassium hydroxide, methanol, formic acid) were reagent grade from Fluka. The electrolytes were prepared from MiilQ water. To saturate the potassium bicarbonate the carbon dioxide (Fluka, quality sign 48) free of organics has been used.

Formate determination

The solution of the sample is treated with excess of standard potassium permanganate in alkaline conditions to form manganese dioxide. The manganese dioxide and excess potassium permanganate were determined iodometrically in acid conditions and the concentration of oxidizable impurities were calculated and expressed as formic acid.

Apparatus

Voltammetric measurements were made using a potentiostat-galvanostat system – BAS 100B (Bioanalytical Systems, USA) with the specific software BAS 100W and a classic three-electrode electrochemical cell. The electrochemical cell is comprised of a cell bottom of 20 mL capacity. A working electrode of ($Sn_{85}Cu_{15}$) (2 mm diameter) and a platinum plate auxiliary electrode were inserted through the cell top into the cell. During the voltammetry determination, a salt bridge for the protection of the reference electrode Ag/AgCl was used. The pH measurements were made with a pH-meter Basic 20 (Crison).

Procedure

Cyclic voltammetry and linear sweep potential voltammetry were performed in the usual way with a potential sweep rate of 5 mV/s at 25º C. The sensitivity is 10 µA/V and the domain of potential was established after several determinations: -400 to 400 mV vs. Ag/AgCl.

The electroreduction of CO_2 was made in a laboratory divided bench-scale reactor (V= 200 ml; Nafion 424 membrane), equipped with bronze cathode (S= 2.2 cm^2) and Pt anode. The electrolyte was aqueous or hydro-alcoholic 0.2 M K_2CO_3 saturated with carbon dioxide. The catholyte was stirred magnetically. The faradic efficiency of formation for the main products were calculated from the total charge passed during batch electrolyses, which was set to 50 coulombs.

During the preparative electrolysis, samples were taken (in 30-min periods) with a volume of 5 mL from the electrolyte. The samples from the electrolyte were studied with respect to formate formation.

REFERENCES

1. C. M. Sánchez-Sánchez, V. Montiel, D. A. Tryk, A. Aldaz, A. Fujishima, *Pure Applied Chemistry*, **2001**, *20,*1917.

2. M. Jitaru, D. A. Lowy, M. Toma, B. C. Toma, L. Oniciu, *Journal of Applied Electrochemistry,* **1997**, *27*, 875.

3. M. Jitaru, *Journal of the University of Chemical Technology and Metallurgy*, **2007**, *42,* 333.

4. M. Gattrell, N. Gupta, *Journal of Electroanalytical Chemistry***, 2006**, *594*, 1.

5. S. Kaneco, N. Hiei, Y. Xing, H. Katsumata, H. Ohnishi, T. Suzuki, K. Ohta, *Electrochimica Acta*, **2002**, *48,* 51.

6. G. M. Brisard, A. P. M. Camargo, F. C. Nart and T. Iwasita, *Electrochemistry Communications*, **2001**, *3,* 603.

7. H. Yano, T. Tanaka, M. Nakayama and K. Ogura, *Journal of Electroanalytical Chemistry*, **2004**, *565,* 287.

8. R. Aydin and F. Köleli, *Journal of Electroanalytical Chemistry*, **2002**, *535,* 107.

9. T. Kuniko, T. Fudeko, K. Masahiro, A. Yoshio, A. Makoto*, Bulletin of the Faculty of Human Environmental Science*, **2005**, *(36),*13.

10. L. Jaeyoung, Tak Yongsug, *Electrochimica Acta*, **2001,** *46,* 3015.

11. Y. Hori, H. Konishi, T. Futamura, A. Murata, O. Koga, H. Sakurai and K. Oguma, *Electrochimica Acta,* **2005**, *50,* 5354.

12. R. Aydin and F. Köleli*, Synthetic Metals*, **2004**, *144,* 75.

13. M. Lukaszewski, M. Grden and A. Czerwinski, *Electrochimica Acta*, **2004**, *49,* 3161.

14. C. Polatides, G. Kyriacou, *Journal of Applied Electrochemistry***, 2005**, *35*, 421.

15. Z. Mácová , K. Bouzek and J. Šerák, *Journal of Applied Electrochemistry,* **2007**, 37, 557.

16. K. Ohta, A. Hashimoto and T. Mizuno, *Energy Conversion and Management,* **1995**, *36,* 625.

17. Sh. Ikeda, T. Ito, K. Azuma, N. Nishi, K. Ito and H. Noda, *Denki Kagaku*, **1996***, 64*, 625.

18. T. Mizuno, K. Ohta, A. Sasaki, T. Akai, M. Hirano and A. Kawabe, *Energy Sources,* **1995**, 17, 503.

19. H. Noda, Sh. Ikeda, A. Yamamoto, H. Einaga and K. Ito, *Bulletin of the Chemical Society of Japan*, **1995**, *68*, 1889*.*

In memoriam prof. dr. Liviu Oniciu

KINETIC AND THERMODYNAMIC CHARACTERIZATION OF PROTEIN ADSORPTION AT FLUID INTERFACES

MARIA TOMOAIA-COTISEL[a], OSSI HOROVITZ[a], OLIMPIA BOROSTEAN[a], LIVIU-DOREL BOBOS[a], GHEORGHE TOMOAIA[b], AURORA MOCANU[a] AND TRAIANOS YUPSANIS[c]

ABSTRACT. The formation and characterization of nanostructured polyfunctional layers (films) based on protein adsorption at different fluid interfaces, such as air/water or oil/water interfaces, in the absence or in the presence of stearic acid are investigated. For instance, kinetics and thermodynamics of protein adsorption at the air/aqueous solutions were studied, thereby evidencing the protein surface active properties. The investigated protein was a globulin extracted and purified from aleurone cells of barley. The conjugated effect of protein and stearic acid simultaneous adsorption was also investigated, at the benzene/aqueous solutions interface. A stable mixed lipid and protein film has been formed by the co-adsorption of these biomolecules at liquid-liquid interface showing that the interaction between stearic acid and the protein is significant.

Keywords: adsorption, fluid interfaces, protein, stearic acid

INTRODUCTION

A great number of problems in interface science deal with the adsorption [1-15] and relaxation [5, 16-20] of surface active compounds (in short, surfactants) at fluid interfaces. In fact, the modern soft-matter physical chemistry has opened a great number of questions dealing with the dynamics of soft surfaces, particularly with protein or lipid dynamics at interfaces. Among these systems, adsorbed protein films are frequently considered as model systems to explore the surface behavior of proteins or their interaction with lipids at fluid interfaces. In vivo, the control over protein functional behavior is often mediated by the formation of supramolecular assemblies with lipids that frequently play a crucial role in the molecular organization of biological systems.

[a] *Babes-Bolyai University of Cluj-Napoca, Faculty of Chemistry and Chemical Engineering, Arany J. Str., no 11, 400028 Cluj-Napoca, Romania, mcotisel@chem.ubbcluj.ro*
[b] *Iuliu Hatieganu University of Medicine and Pharmacy, Department of Orthopedic Surgery, Mosoiu Str., no. 47, 400132 Cluj-Napoca, Romania*
[c] *Aristotelian University, School of Chemistry, Laboratory of Biochemistry, 54006 Thessaloniki, Greece*

Protein adsorption at interfaces is also an important subject of investigations, in many artificial systems encountered in industrial applications, particularly because many alimentary emulsions are stabilized by proteins. The understanding of protein behavior and its interactions with other biomolecules might bring strong information for a desired performance.

Usually protein adsorption at fluid interfaces is studied by measurements of the interfacial tension between the two phases (*e.g.,* oil and water) [21-23]. By protein adsorption, the interfacial tension is reduced in time, for a particular concentration in protein, and as a function of protein concentration. From interfacial tension isotherms, information is gained upon the processes taking place in the early stage of adsorption [24]. Generally, the interfacial phenomena and adsorption kinetics are essential in determining chemical and physical properties of such systems [25]. Thus, the adsorption kinetics of egg yolk was studied at the triacylglycerol / water interface and the effect of pH was assessed [26]. The role of the charged protein surface in the adsorption dynamics was studied on L-glutamic acid copolymers [27].

Model for protein adsorption at interfaces

Experimentally, it was found that the dynamics of surface tension presents three regimes [24], specific for diluted solutions of different proteins (Fig. 1):

- an induction regime, noted regime I, where the interfacial tension remains relatively constant, at the values characteristic for the pure liquid phase (e.g., the air/water interface)
- the second regime, noted regime II, is distinguished by a sudden drop of interfacial tension from its initial value
- the last regime, named regime III, corresponds to a quasi-linear decrease of interfacial tension, with a less abrupt slope than for the second regime.
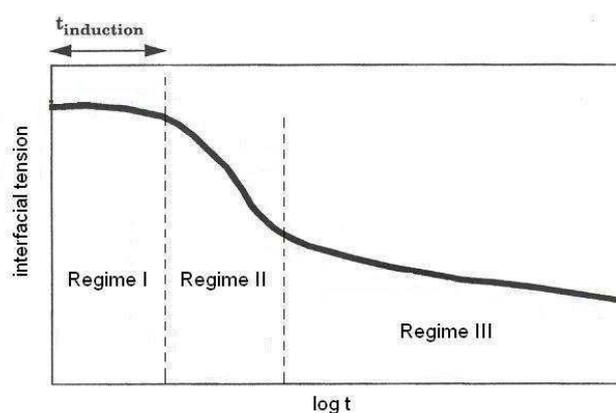

Figure 1. Plot in semilogarithmic coordinates corresponding to the three adsorption regimes of proteins at fluid interfaces.

144

An induction time, as in the first regime, is frequently observed in protein solutions at low concentrations, at the air/water interface [28, 29]. Protein molecules are present at the interface, but they do not reduce considerably the interfacial tension. In this period, the diffusion of protein molecules to the surface is important in controlling the adsorption, and is followed by modifications of the protein configuration (denaturation). An induction period is observed only for much diluted protein solutions. In more concentrated solutions, regime III is directly attained.

In the regime II, there is already a saturated protein monolayer at the interface, but the relaxation in the conformation of proteins makes possible both the adsorption of more inner segments, of the protein molecules at the interface, and the diffusion of more protein molecules from the bulk to the interface. Both effects contribute to the decrease of interfacial tension in time. Conformational modifications and denaturation of proteins are therefore more important in reducing interfacial tension than the initial diffusion and adsorption of protein molecules. It is recognized that the protein adsorption corresponding to the regime II can give indications on the protein conformational stability of adsorbed proteins.

In the regime III, there is only a slight decrease of interfacial tension, ascribed to conformational modifications in the adsorption layer with the formation of multilayers and consequently building of o continuous protein gel lattice at the interface.

In many cases, the time dependence of interfacial tension is a logarithmic one, $\sigma(t) \sim k \log t$, for the protein adsorption at the air/water interface.

Among proteins, the plant proteins are particularly important because they are largely used as ingredients in human alimentation and in other fields, such as cosmetics or drugs delivery systems. Adsorption properties of plant proteins (such as α-gliadins or pea protein) were investigated at the oil / water interface [30] and compared with the corresponding properties of gelatin.

Recently, we studied the adsorption of a plant protein, namely the major globular protein extracted from aleurone cells of barley [31], on various surfaces, such as glass or mica [32, 33], the surface of citrate anions capped gold nanoparticles in colloidal aqueous solutions [34, 35], and on gold nanoparticles auto-assembled as an interfacial film on a solid surface [36], using UV-Vis spectroscopy, TEM and AFM observations.

In the present paper we investigate the adsorption of the same globular protein at fluid interfaces, such as the air/water and oil/water interfaces, as well as the simultaneous adsorption of the protein and stearic acid at the interface between the aqueous and benzene solutions.

RESULTS AND DISCUSSION

Protein adsorption at the air/water interface

Interfacial tension, σ, at the air/aqueous 0.5 M NaCl solution interface, at 20 $^{\circ}$C, for different bulk protein concentrations, C_p, in the aqueous phase, at different times, t, of adsorption

C_p = 5 mg/L		C_p = 4 mg/L		C_p = 3 mg/L		C_p = 2 mg/L		C_p = 1 mg/L		C_p = 0.5 mg/L	
t, min	σ, mN/m	t, min	σ, mN/m	t, min	σ, mN/m	t, min	σ, mN/m	t, min	σ, mN/m	t, min	σ, mN/m
0	67.77	0	72.3	0	72.25	0	72.07	0	72.19	0	72.13
5	66.51	5	71.85	5	72.08	5	72.02	5	72.11	5	72.10
10	65.8	10	71.01	10	71.99	10	71.87	10	72.08	10	72.08
15	65.3	15	70.52	15	71.91	15	71.73	15	72.02	15	72.05
20	64.93	20	70.01	20	71.65	20	71.62	20	71.99	20	72.02
25	64.73	25	69.32	25	71.59	25	71.50	25	71.93	25	72.02
30	64.44	30	69.09	30	71.42	30	71.39	30	71.88	30	71.99
40	64.16	40	68.45	40	70.98	40	71.10	40	71.82	40	71.96
50	63.59	50	67.99	50	70.69	50	70.87	50	71.73	50	71.93
60	63.33	60	67.48	60	70.06	60	70.55	60	71.59	60	71.90
80	62.84	80	66.84	80	69.25	80	69.92	80	71.36	80	71.87
100	62.66	100	65.98	100	68.74	100	69.32	100	71.16	100	71.85
120	62.56	120	65.35	120	67.99	120	69.11	120	70.93	120	71.79
150	62.44	150	64.31	150	67.12	150	68.34	150	70.44	150	71.73
180	62.32	180	63.85	180	66.31	180	67.76	180	70.06	180	71.64
210	62.26	210	63.39	210	65.97	210	67.30	210	69.69	210	71.50
240	62.26	240	63.28	240	65.45	240	66.96	240	69.49	240	71.39
		270	63.05	270	65.03	270	66.44	270	69.28	270	71.30
		300	62.97	300	64.93	300	66.27	300	68.94	300	71.13
		330	62.87	330	64.73	330	66.12	330	68.77	330	70.93
		360	62.83	360	64.56	360	65.81	360	68.54	360	70.75
		410	62.79	390	64.38	390	65.64	390	68.48	390	70.70
		450	62.8	420	64.15	420	65.26	480	68.23	420	70.61
		480	62.65	450	64.01	450	65.06	570	68.06	450	70.58
		510	62.56	480	63.81	480	65.06	600	68.02	480	70.55
		540	62.56	510	63.69	510	65.03			510	70.52
		570	62.64	540	63.60	540	64.97			540	70.52
				570	63.43	570	64.78				
						600	64.60				
						630	64.51				

The values of the interfacial tension measured at different times of protein adsorption, for each of the investigated protein concentrations, at the air/aqueous (0.5 M NaCl) solution interface, are given in Table 1.

From this table, it can be observed that the interfacial tension varies strongly with time, the adsorption equilibrium being reached in more than 10 hours for some protein concentrations. The equilibrium is indicated by the almost constant value of the interfacial tension.

Further, using semilogarithmic coordinates, the representation of interfacial tension against the logarithm of the adsorption time, $\sigma = f(\log t)$, is given in Fig. 2. The general aspect of the plots is similar to that resulting from the model of the three adsorption regimes of proteins (Fig.1). While regime I (induction period) and II (monolayer saturation) are clearly evidenced in the plots, for regime III the beginning is barely outlined for the highest concentration (5 mg/L). On the other hand, the induction period is clearly delimited only for the lower protein concentrations (below 4 mg/L).
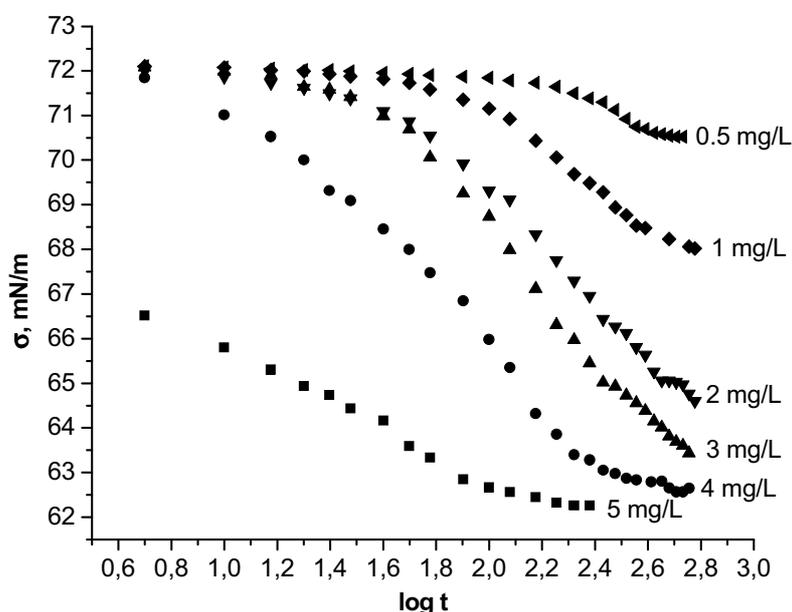

Figure 2. Representation in semilogarithmic coordinates of dynamic interfacial tension (mN/m) against time (min) for protein adsorption from the aqueous phase (with various protein concentrations), at the interface with air, at a temperature of 20 $^{\circ}$C.

The limiting values of the interfacial tensions, those corresponding to the maximum time of protein adsorption for each protein concentration can be considered for the establishing of thermodynamic adsorption equilibrium that is given by the static interfacial tension. The representation of these static interfacial tensions versus C_p concentration (Figure 3) shows the typical appearance of a surface tension isotherm, in presence of a surface active substance. The surface activity of the protein at the air / aqueous solution interface is thus confirmed.

147

The adsorption equilibrium and the final adsorption regime III occur upon protein adsorbed monolayer coverage, and is attributed to continued relaxation of the adsorbed layer and possible build-up of protein multilayers, as depicted in Figure 4.
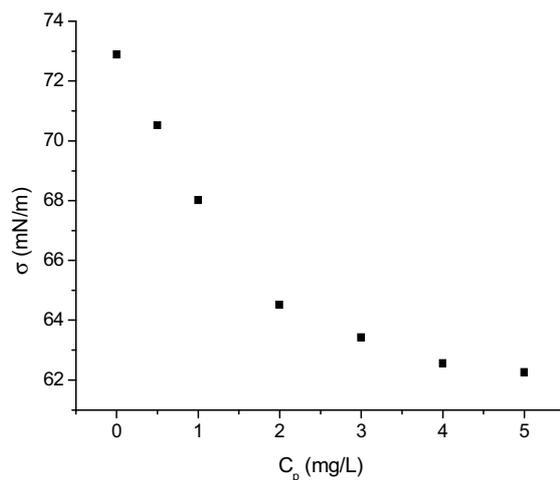

Figure 3. Variation of the static interfacial tension at the interface with air, for protein adsorption from the aqueous phase, against the protein concentration at 20 °C temperature.
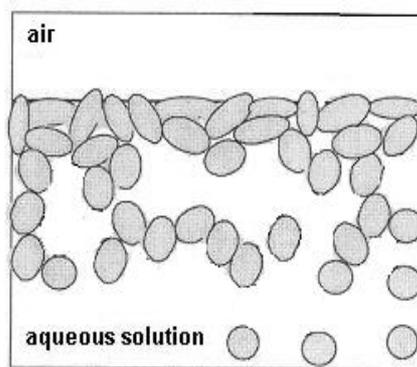

Figure 4. Schematic representation of protein adsorption at interface (regime III)

Protein and stearic acid co-adsorption at the oil/water interface
Furthermore, we studied the lipid and protein layers at the benzene/ aqueous (0.5 M NaCl) solutions interface. To explore the interaction between lipid and protein, we have chosen a fatty acid (stearic acid) as a simple

148

model for lipids. For the beginning we studied the adsorption of protein and separately the adsorption of stearic acid at the same interface oil/water for two distinct temperatures, 20 and 36 ^{O}C.

The dynamics of protein adsorption at benzene/water (0.5 M NaCl) interface is examined over the time scales ranging from seconds to several hours by measuring the interfacial tension at the benzene/aqueous solutions interface for the chosen constant temperature. The adsorption of protein at the benzene/aqueous solution interface leads to an interfacial tension versus time profile that presents common characteristics with the adsorption of bovine serum album at the benzene/water interface [40, 41]. For oil/water interface the induction period for protein adsorption was not detected. The adsorption equilibrium of protein appears to be established in about 60 min at the oil/water interface. The equilibrium data for pure protein adsorbed at the benzene/aqueous interface are given in Tables 2 and 3 at 20 and 36 ^{O}C, respectively.

The protein diffusion and protein interfacial affinity determine the duration of early stages of adsorption period at fluid interfaces. Continued protein rearrangement leads to the final interfacial tension reduction resulting in various interfacial contacts per protein molecule.

Independently, the adsorption of stearic acid at the benzene/aqueous (0.5 M NaCl, pH 5.5) solution interface was investigated. The adsorption behavior of stearic acid is similar with its adsorption at the interface benzene/ water (pH 2) interface. At pH 2, stearic acid (pK_a = 5.63 [42] is neutral and at pH 5.5 it is almost 50% ionized. The static adsorption is reached at about 100 min depending on the stearic acid bulk concentration in substantial agreement with data published by us earlier [39]. The equilibrium data for the adsorption of stearic acid at benzene/water interface are given in Table 2 (for 20 ^{o}C) and in Table 3 (for 36 ^{o}C).

For co-adsorption of stearic acid and protein at benzene/water interface it was observed that the adsorption equilibrium is apparently reached in about 60 min. Therefore, for mixed layers of protein and stearic acid, the equilibrium (static) interfacial intension is recorded at an adsorption time of 60 min. It is to be mentioned that for very long adsorption times (several hours) some aging effects are noticed.

For comparison, the co-adsorption of protein and stearic acid at the oil/water interface was recorded by interfacial tension measurements executed at 60 min after the oil/water interface was formed, for both temperatures investigated, 20 and 36°C. The results are also given in Tables 2 and 3.

To avoid the superposition of a strongly time dependent effect, due to the protein adsorption over the one generated by the adsorption of stearic acid from the benzene phase, we have chosen the 2.9 mg/L concentration of protein in the aqueous solutions. The concentration of stearic acid was varied in the range of 0.025 to 0.4 M stearic acid in benzene.

149

Table 2.

Interfacial tensions (σ) and interfacial pressures (Π) for the simultaneous adsorption of stearic acid (SA) and protein (P) at the benzene/aqueous solution interface, at a constant temperature of 20 ^{o}C.

C_{SA} (mol/L)	σ (mN/m)		Π (mN/m)	
	$C_p = 0$	$C_p = 2.9$ mg/L	SA	P
1	2	3	4	5
0.000	34.70	24.90	0.00	9.80
0.030	29.25	24.40	5.45	4.85
0.039	28.43	23.64	6.27	4.79
0.050	27.24	22.58	7.46	4.66
0.064	25.25	21.82	9.45	3.43
0.082	23.82	21.23	10.88	2.59
0.105	22.13	20.14	12.57	1.99
0.136	20.49	19.32	14.21	1.17
0.174	19.15	18.20	15.55	0.95
0.223	17.57	17.15	17.13	0.42
0.287	16.60	16.28	18.10	0.32
0.368	15.81	15.51	18.89	0.30

Table 3.

Interfacial tensions (σ) and interfacial pressures (Π) for the simultaneous adsorption of stearic acid (SA) and protein (P) at the benzene/aqueous solution interface, at constant temperature of 36 ^{o}C.

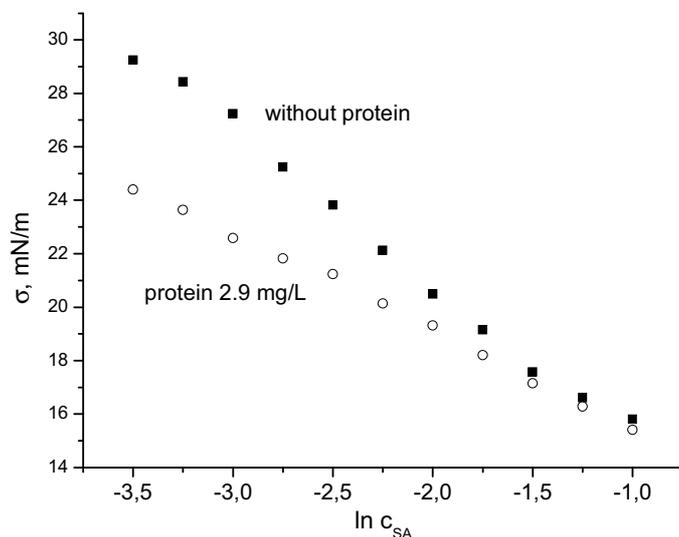| C_{SA} (mol/L) | σ (mN/m) | | Π (mN/m) | |
	$C_p = 0$	$C_p = 2.9$ mg/L	SA	P
1	2	3	4	5
0.000	35.10	25.17	0.00	9.93
0.025	31.22	22.31	3.88	8.91
0.034	30.05	21.91	5.05	8.14
0.040	29.80	21.63	5.30	8.17
0.050	29.47	21.47	5.63	8.00
0.065	28.78	20.93	6.32	7.85
0.083	28.20	20.44	6.90	7.76
0.109	26.88	19.58	8.22	7.30
0.135	25.84	18.88	9.26	6.96
0.176	24.74	18.59	10.36	6.15
0.225	23.92	17.78	11.18	6.14
0.287	22.60	17.14	12.50	5.46
0.368	20.98	16.13	14.12	4.85

Figure 5. Equilibrium interfacial tension, σ, against the logarithm of stearic acid molar concentration, c_{SA}, in the organic phase, for the interface aqueous 0.5 M NaCl solution / benzene, in absence and presence of protein in the aqueous phase at 20 ^{o}C

Figure 6. Equilibrium interfacial tension, σ, against the logarithm of stearic acid molar concentration, c_{SA}, in the organic phase, for the interface aqueous 0.5 M NaCl solution / benzene, in absence and presence of protein in the aqueous phase at 36 ^{o}C.
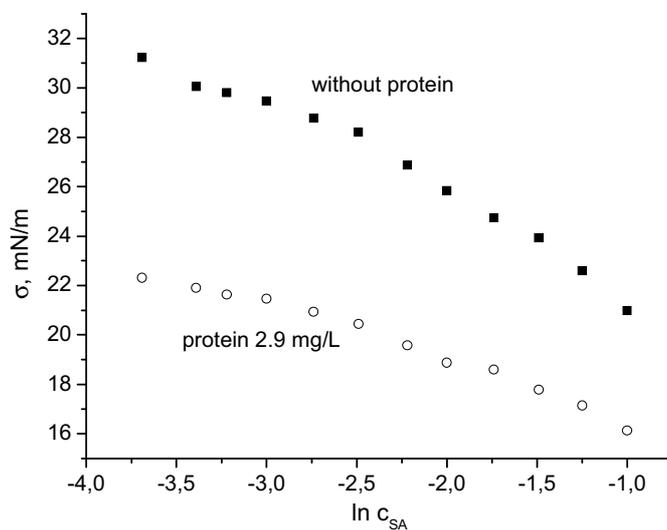
In Figs 5 and 6 the static interfacial tension isotherms versus stearic acid concentration (C_{SA}) are given for the situation without and with protein (2.9 mg/L concentration) in aqueous solutions. From the adsorption isotherm, it is to be noted that the stearic acid is surface active at the benzene/water interfaces.

The processing of the isotherms according to Gibbs equation:

$$\left(\frac{\partial \sigma}{\partial \ln c_{SA}} \right)_T = -RT\Gamma$$

allows for the determination of the SA surface concentration (Γ) for a certain interfacial tension and the corresponding molecular area: $A = \dfrac{1}{\Gamma N_A}$,

N_A being the Avogadro's constant; R and T having their usual meanings. For the saturation of the interface with adsorbed SA, the limiting molecular areas are determined for stearic acid adsorbed at the oil/water interface with or without protein at two temperatures, 20 and 36 ^{o}C, see Table 4.

Table 4.

Limiting molecular areas, A_0, and the correlation coefficients, r, for adsorbed stearic acid film at the benzene/water interfaces, in the absence and the presence of protein, for two temperatures.

Adsorbed layers	20 ^{o}C		36 ^{o}C	
	A_0, Å^2/molecule	Standard error	A_0, Å^2/molecule	Standard error
SA	79.6	±4.9	87.0	±4.7
SA and protein	111.5	±1.8	124	±7

The comparison of the limiting molecular areas for stearic acid in the absence of protein leads us to the conclusion that the SA film at the benzene/water interface is more expanded than the pure SA film at the air/water interface, A_o = 20 Å^2 [39]. The area increase in adsorbed SA as compared to spread film is due to the benzene molecules which penetrate between the hydrocarbon chains of the SA interfacial film, tending to reduce the attraction among the SA chains.

Also, the limiting molecular areas, A_0, for stearic acid in the presence of protein is much greater than the area of pure SA oriented at one and the same interface at constant temperature. The protein effect is related with the penetration of protein among the hydrocarbon chains of SA film adsorbed at the oil/water interfaces. The increase in temperature brings also an expanding effect upon SA adsorbed film at benzene/water interface.

The equilibrium interfacial tensions are apparently established in about 60 min in contrast with 100 min for pure stearic acid adsorbed film at the oil/water interfaces. The more rapid attainment of the adsorption equilibrium

of SA at the benzene/water interface in the presence of protein is probably due to the interaction between SA and protein in the interfacial adsorbed mixed film.

In order to get a better image of the possible interactions in the mixed SA and P film, data regarding the variation of the equilibrium interfacial tension with SA concentration in the absence (column 2) and in the presence of protein (column 3) in Tables 3 and 4, for 20 and 36 ^{o}C, respectively were compared. It is evident that the presence of protein leads to an additional decrease of interfacial tension, respectively to an increase of the pressure in the adsorbed SA film for all concentrations of SA. Column 4 lists the interfacial pressures of pure SA. The last column shows the contribution of protein to the interfacial pressure of the mixed SA and P film, the contributions of SA (column 4) being assumed as constant. The contribution of protein was evaluated from the difference of the values in columns 2 and 3 for each individual concentration of SA. It is noted that the interfacial pressure due to the protein decreases with the increasing of SA concentration. In other words, the contribution of each component to the interfacial pressure of the mixed adsorbed film is not independent. This fact also suggests the interaction between SA and protein.

Similar cases are reported in the literature on mixed lipid and protein films obtained by penetration of lipid monolayers spread at the air/water interface by an injected protein in the aqueous phase under the lipid monolayer. The penetration of the protein in the lipid layer leads to an increase of its surface pressure at constant area, and the pressure increment was considered a measure of the lipid and protein interaction [43]. This situation corresponds to a sequentially adsorbed lipid and protein mixed film.

In our case, in the complex process of adsorption and penetration of SA and protein at the oil/water interface, the interaction between the stearic acid and the protein is revealed by the decrease of interfacial tension, respectively the increase of the interfacial pressure at the benzene/water interfaces. The increment of interfacial pressure is attributed to the mutual penetration of the two adsorbed films. The interaction between carboxyl groups or the negatively charged carboxylate of SA molecules and the peptide bridges of protein or with protein positively charged regions may be suggested, as well as the interaction among their hydrocarbon chains, which is not to be completely neglected even at the oil/water interface.

Moreover, in our case, the simultaneously adsorbed stearic acid and protein mixed films are formed where the molecular associations can be generated at the interfaces, such as negatively charged complexes when stearate molecules (negatively charged at pH 5.5) are involved in associations and neutral complexes when stearic acid not charged is involved in the interaction within mixed adsorbed layers at oil/water interfaces, as recently emphasized for β-lactoglobulin and pectin in adsorbed layers at fluid interfaces [2].

153

CONCLUSIONS

Our previous studies on the adsorption of the globular storage protein, extracted and purified from aleurone cells of barley, at the solid interface of gold nanoparticles is completed by the investigation of the adsorption of the same protein at gas/liquid and liquid/liquid interfaces. The evolution in time of the protein adsorption at the air/aqueous solution interface evidenced a kinetic behavior compatible with the three steps model, induction regime, conformational change regime and relaxation regime coupled with a possible build-up of multilayers, proposed for various proteins [24]. On the other hand, the values at thermodynamic equilibrium of interfacial tensions are situated on a typical adsorption isotherm, thus evidencing the surface-active character of the investigated protein. The same character is manifested at liquid – liquid interfaces, studied on the model system, such as an aqueous NaCl solution with protein and stearic acid solution in benzene. Here the effect of both surface-active substances is conjugated.

EXPERIMENTAL SECTION

Materials

The protein solution used is that of the major globular storage protein from aleurone cells of barley (*Hordeum vulgare* L.) extracted and purified as shown elsewhere [31]. The protein was dissolved in ultra pure water and diluted to the working concentrations. The pH of the major aleurone protein solution was about 5.6. The protein is related to 7S globulins present in other cereals and to the vicilin-type 7S globulins of legumes and cottonseed. It contains 4 subunits of about 20, 25, 40 and 50 kDa molecular weights [31]. The N-terminal sequence of 16 amino acids in the protein [14] is given as follows: ^1X ^2Glu ^3Gln ^4Gly ^5Asp ^6Ser ^{7}***Arg*** ^{8}***Arg*** ^9Pro ^{10}Tyr ^{11}Val ^{12}Phe ^{13}Gly ^{14}Pro ^{15}***Arg*** ^{16}(*Ser* or *His*) ^{17}Phe, where *X* stands for the first amino acid of the N-terminal of aleurone protein which was not identified. The secondary structure of this protein was recently investigated by advanced spectroscopy [37, 38]. Deionized water of ultra high purity was used in all experiments and it was obtained from an Elgastat water purification system. Benzene, stearic acid and NaCl were of high purity, purchased from Merck and used without further purification.

Methods

The adsorption of the protein at the air/water interface was investigated by measurements of the dynamic interfacial tension of aqueous solutions with variable protein concentrations, in the range from 0.5 to 5 mg/L, by means of the ring method (Le Compte du Nouy) and the plate method (Wilhelmy method), described elsewhere [16-18, 39-41]. In order to maintain constant

the ionic strength of the aqueous phase and full solubility of globular protein, this aqueous phase was a 0.5 M NaCl solution [31]. The temperature was maintained constant at about 20 °C.

The influence of protein adsorption on interfacial tension at a water/ oil interface was studied using the following phases:

- benzene solutions of stearic acid (SA), having different SA concentrations in the range from 0.4 to 0.025 M
- an aqueous 0.5 M NaCl solution without protein and separately with a constant protein content of 2.9 mg/L.

The measurements of interfacial tension were executed by the ring method (Le Compte du Nouy) and the plate method (Wilhelmy) at two different temperatures (20°C and 36°C) for the oil/water interfacial systems.

ACKNOWLEDGEMENTS

REFERENCES

1. R. A. Ganzevles, R. Fokkink, T. van Vliet, M. A. Cohen Stuart, H. H. J. de Jongh, *Journal of Colloid and Interface Science,* **2008**, *317*, 137.

2. E. V. Kudryashova, H. H. J. de Jongh, *Journal of Colloid and Interface Science,* **2008**, *318*, 430.

3. J. Minones Conde, J. M. Rodriguez Patino, *Journal of Food Engineering*, **2007**, *78*, 1001.

4. Y. Zhang, Z. An, G. Cui, J. Li, *Colloids and Surfaces A*, *Physicochemical and Engineering Aspects,* **2003**, *223*, 11.

5. F. Monroy, F. Ortega, R. G. Rubio and M. G. Velarde, *Advances in Colloid and Interface Science,* **2007**, *134-135*, 175.

6. J. Gualbert, P. Shahgaldian, A. W. Coleman, *International Journal of Pharmaceutics*, **2003**, *257*, 69-73.

7. T. Xu, R. Fu, L. Yan, *Journal of Colloid and Interface Science,* **2003**, *262*, 342.

8. S. V. Dorozhkin, E. I. Dorozhkina, *Colloids and Surfaces A*, *Physicochemical and Engineering Aspects*, **2003**, *215*, 191.

9. A. N. Lazar, P. Shahgaldian, A. W. Coleman, *Journal of Supramolecular Chemistry*, **2001**, *1*, 193.

10. Y. Wang, X. Yin, M. Shi, W. Li, L. Zhang, J. Kong, *Talanta*, **2006**, *69*, 1240.

11. W. Lu, Y. Zhang, Y. -Z. Tan, K.-L. Hu, X.-G. Jiang, S.-K. Fu, *Journal of Controlled Release*, **2005**, *107*, 428.

12. T. Maruyama, S. Katoh, M. Nakajima, H. Nabetani, T. P. Abbott, A. Shono, K. Satoh, *Journal of Membrane Science,* **2001**, *192*, 201.

13. S. Salgin, S. Takac, T. H. Ozdamar, *Journal of Membrane Science*, **2006**, *278*, 251.

14. J. Tian, J. Liu, X. Tian, Z. Hu and X. Chen, *Journal of Molecular Structure*, **2004**, *691*, 197.

15. F. Wang, Z. Yang, Y. Zhou, S. Weng, L. Zhang, J. Wu, *Journal of Molecular Structure*, **2006**, *794*, 1.

16. P. Joos, A. Tomoaia-Cotisel, A. J. Sellers, M. Tomoaia-Cotisel, *Colloids and Surfaces B: Biointerfaces*, **2004**, *37*, 83.

17. M. Tomoaia-Cotisel, P. Joos, *Studia Universitatis Babes-Bolyai, Chemia*, **2004**, *49* (1), 35.

18. M. Tomoaia-Cotisel, D. A. Cadenhead, *Langmuir*, **1991**, *7*, 964.

19. M. Tomoaia-Cotisel, J. Zsakó, E. Chifu, D. A. Cadenhead, *Langmuir*, **1990**, *6* (1), 191.

20. M. Tomoaia-Cotisel, *Progress in Colloid and Polymer Scence.,* **1990**, *83*, 155.

21. E. Dickinson, B.S. Murray, G. Stainsby, *Journal of the Chemical Society, Faraday Transactions, 1,* **1988**, *84*, 871.

22. A. -P. Wei, J. N. Herron, J.D. Andrade, in "From Clone to Clinic" (D.J.A. Crommelin, H. Schellekens, Editors.), Kluwe Academic Publishers, Dordrecht, **1990**, pp. 305.

23. W. Van der Vegt, H.C. Van der Mei, H.J.Busscher, *Journal of Colloid and Interface Science,* **1993**, *156*, 129.

24 C. J. Beverung, C.J.Radke, H.W.Blanch, *Biophysical Chemistry*, **1999**, *81*, 59.

25. G. Lu, H.Chen, J.Li, *Colloids and Surfaces A, Physicochemical and Engineering Aspects*, **2003**, *215*, 25.

26. S. M. Mel'nikov, *Colloids and Surfaces B: Biointerfaces*, **2003**, *27*, 265.

27. C. J. Beverung, C. J. Radke, H. W. Blanch, *Biophysical Chemistry*, **1998**, *70*, 121.

28. K. B. Song, S. Damodaran, *Langmuir*, **1991**, *7*, 2737.

29. M. G. Ivanova, R. Verger, A. G. Bois, I. Panaiotov, *Colloids and Surfaces*, **1991**, *54*, 279.

30. V. Ducel, J. Richard, Y. Popineau, F. Boury, *Biomacromolecules*, **2004**, *5*, 2088.

31. T. Yupsanis, S. R. Burgess, P. J. Jackson. P. R. Shewry, *Journal of Experimental Botany.,* **1990**, *41*, 385.

32. M. Tomoaia-Cotisel, in "Convergence of Micro-Nano-Biotechnologies, Series in Micro and Nanoengineering" Vol. 9 (Editors: M. Zaharescu, E. Burzo, L. Dumitru, I. Kleps, D. Dascalu), Romanian Academy Press, Bucharest, **2006**, pp. 147-161.

33. M. Tomoaia-Cotisel, A. Tomoaia-Cotisel, T. Yupsanis, Gh. Tomoaia, I. Balea, A. Mocanu, Cs. Racz, *Revue Roumaine de Chimie,* **2006**, *51*, 1181.

34. O. Horovitz, A. Mocanu, Gh. Tomoaia, L. Olenic, Gg. Mihăilescu, O. Boroştean, A. Popoviciu, C. Crăciun, T. Yupsanis, M.Tomoaia-Cotişel, In: "Convergence of micro-nano-biotechnologies, Series in Micro and Nanoengineering", Vol.9, Ed. Academiei, Bucureşti, **2006**, pp. 133-147.

35. O. Horovitz, Gh. Tomoaia, A. Mocanu, T. Yupsanis, Tomoaia-Cotisel, *Gold Bulletin*, **2007**, *40*, 213.
36. O. Horovitz, Gh. Tomoaia, A. Mocanu, T. Yupsanis, Tomoaia-Cotisel, *Gold Bulletin*, **2007**, *40*, 295.
37. I. Bratu**,** M. Tomoaia–Cotisel**,** G. Damian, A. Mocanu, *Journal of Optoelectronics and Advanced Materials,* **2007**, *9*, 672.
38. M. Tomoaia-Cotişel, A. Mocanu, N. Leopold, M. Vasilescu, V. Chiş, O. Cozar, *Journal of Optoelectronics and Advanced Materials,* **2007**, *9*, 637.
39. E. Chifu, M. Sălăjan, I. Demeter-Vodnár, M. Tomoaia-Cotişel, *Revue Roumaine de Chimie*, **1987**, *32* (7), 683.
40. M. Tomoaia-Cotisel, E. Chifu, in "*IUPAC Macro'83, Section IV: Structure and Properties"*, Bucharest, **1983**, pp. 636-639.
41. E. Chifu, M. Tomoaia-Cotisel, *Studia Universitatis Babes-Bolyai, Chemia*, **1987**, *26* (2), 3.
42. M. Tomoaia-Cotisel, D.A. Cadenhead, *Langmuir*, **1991**, *7*, 964.
43. G. Colacicco, *Journal of Colloid and Interface Science,* **1969**, *29*, 345.